Special Issue: The Apidima Legacy Collections: New Analyses and Interpretations

New Bioanthropological Insights on the Possible Early Upper Paleolithic Cranial and Postcranial Human Remains from Apidima Cave C (Peloponnese)

DAVID NAUMANN*
Paleoanthropology, Institute for Archaeological Sciences, Department of Geosciences, Eberhard Karls University of Tübingen, 72070 Tübingen, GERMANY; david.naumann@ifu.uni-tuebingen.de

VASSILIS G. GORGOULIS
Department of Histology and Embryology, Medical School, National and Kapodistrian University of Athens, Athens; Biomedical Research Foundation of the Academy of Athens, Athens, GREECE; Faculty Institute for Cancer Sciences, Manchester Academic Health Sciences Center, University of Manchester, Manchester M20 4GJ; and, Division of Cancer Research, Ninewells Hospital and Medical School, University of Dundee, DD19SY Dundee, UNITED KINGDOM; vgorg@med.uoa.gr

KONSTANTINOS EVANGELOU
Department of Histology and Embryology, and Museum of Anthropology, Medical School, National and Kapodistrian University of Athens, Athens; GREECE; cnevagel@med.uoa.gr

KATERINA HARVATI
Paleoanthropology, Institute for Archaeological Sciences and Senckenberg Center for Human Evolution and Paleoenvironments, Eberhard Karls Universität Tübingen; DFG Center for Advanced Studies 'Words, Bones, Genes, Tools', Eberhard Karls Universität Tübingen; HUMAN ORIGINS – Cluster of Excellence for Integrative Human Origins Studies (EXC 3101), Eberhard Karls University of Tübingen, GERMANY; Centre for Early Sapiens Behaviour (SapienCE), University of Bergen, NORWAY; and, Museum of Anthropology, Medical School, National and Kapodistrian University of Athens, Athens, GREECE; katerina.harvati@ifu.uni-tuebingen.de

*corresponding author: David Naumann; *david.naumann@ifu.uni-tuebingen.de*

submitted: 20 January 2026; revised 27 March 2026; accepted: 8 April 2026

Guest Editors: Katerina Harvati (Eberhard Karls Universität Tübingen), Effrosyni Roditi (Eberhard Karls Universität Tübingen), and Serena Lombardo (Eberhard Karls Universität Tübingen)

Handling Editor in Chief: Karen Ruebens

ABSTRACT

The Apidima cave complex was investigated by a team from the Museum of Anthropology, School of Medicine of the National and Kapodistrian University of Athens, during the late 1970s–80s, and yielded Paleolithic remains from the Middle and Late Pleistocene. Among the important findings were human remains excavated from Cave C, including a mostly complete and associated skeleton (Apidima 3) and a few additional isolated elements. The human remains were recovered from the same context as a Protoaurignacian lithic assemblage. Recently, three shell beads, possibly from the same context, produced calibrated radiocarbon dates ranging from 24.5 to 31.8 ka cal BP, suggesting the possible presence of an intrusive, potentially Gravettian burial context.

Despite the rarity of Upper Paleolithic human remains in the known Greek fossil record, the remains from Apidima Cave C have remained largely unknown, with only preliminary descriptions and assessments published to date. Here, we revisit this legacy material and conduct a comprehensive bioanthropological reinvestigation of the human remains from Cave C. Our study adds important new biological data to the literature, including measurements of the entire Apidima 3 skeleton and a re-evaluation of the burial context based on bone-preservation characteristics. Our findings support the initial assignment of this skeleton to the female sex. In contrast to the earlier interpretation of a young age at death (20–25 years), we show that she died during advanced adulthood, most likely between 40 and 60 years of age. This agrees with our observations of progressive stages of joint degeneration, including inflammatory osteoarthritic conditions in different skeletal elements, as well as severe occlusal

wear and signs of periodontitis in her dentition. Comparisons of stature, body mass, and limb osteometry with data from Upper Paleolithic individuals across Europe show that her body proportions best align with those of pre-Last Glacial Maximum females, consistent with her potential chronological attribution. Our study presents the most comprehensive and up-to-date inventory of human remains from Apidima Cave C, along with new bio-anthropological data and detailed anatomical descriptions.

INTRODUCTION

Apidima is a complex of five caves (Cave A-Cave E) situated on a coastal limestone cliff face in the Mani peninsula (southern Greece). The site was investigated in the late 1970s–80s by a team from the Museum of Anthropology, School of Medicine, National and Kapodistrian University of Athens, led by Professor T. Pitsios. It is primarily known for two Middle Pleistocene human crania, Apidima 1 and 2, found on the ceiling of Cave A (Harvati et al. 2009; 2011; 2019; 2026a [this issue]; Pitsios 1995). However, Pitsios also conducted excavations in the other caves, which yielded less well-known but significant findings. These include the Late Pleistocene human remains excavated from Cave C.

Cave C is located 19m above sea level (asl) and is thus situated about 15m higher than Cave A, with which it has no visible connection. The first excavations in Cave C were conducted as part of the fieldwork that began in 1978 (Mompherratou and Pitsios 1995; Pitsios 1985, 1999). The cultural assemblage excavated at the time was tentatively assigned to the Aurignacian based on a preliminary study of a subset of the assemblage (n=61; Darlas 1995). A recent comprehensive reevaluation of the complete assemblage of 915 specimens by our team confirmed its early Upper Paleolithic character and concluded that it is best considered as Protoaurignacian (Lombardo et al. 2026b [this issue]). The cultural remains from Cave C also comprised perforated shells, at the time assigned to *Nassa neritea* and considered to potentially represent Paleolithic shell beads (Karali-Giannakopoulou 1995; Mompheratou and Pitsios 1995). The human remains from Cave C were discovered and excavated from July 11 to 17, 1984 (Mompherratou and Pitsios 1995). Most of them were associated with one individual —Apidima 3 (originally named "LAO 1/S3")—but also scattered, isolated skeletal elements of additional individuals, whose chronological and anatomical associations could not be ascertained (Pitsios 1995, 1999), were found. Apidima 3 was reportedly found at a depth of 25–50cm below the past cave floor (surface level unknown) of the 1984 excavation in proximity to the cave entrance (Mompherratou and Pitsios 1995). The approximate position of Apidima 3's burial in Apidima Cave C is shown in Figure 1 and could be inferred from information about the excavation units and depths of human bones provided in Mompherratou and Pitsios (1995) and Pitsios and Liebhaber (1995). The approximate position of Pitsios' datum, also shown in Figure 1, was estimated from the positions of markings on the cave wall left by the previous excavators and that could be brought into association with descriptions of the excavation grid in Pitsios and Liebhaber (1995).

The authors described Apidima 3 as a partially disturbed ritual burial, including the arrangement of Apidima 3's body and potential grave goods. According to the excavators, the skeleton was found oriented perpendicular to the long axis of the cave with the cranium to the East and facing the exterior of the cave (South) (Mompherratou and Pitsios 1995; Pitsios 1999). The skeleton was reported to have been lying on its left side, with the thorax facing down and the legs in hyperflexion close to the chest (Mompherratou and Pitsios 1995; Pitsios 1999). The upper limbs and thorax region were said to be found more or less undisturbed, while other skeletal parts had been moved or were destroyed by erosion of sediment or animal activity (Mompherratou and Pitsios 1995; Pitsios 1999). The lack of photographs and detailed spatial information also poses problems for assessing the burial taphonomy. Interestingly, only an artistic drawing of a reconstruction of the original burial is provided in Mompherratou and Pitsios (1995) and Pitsios (1999); however, as far as can be ascertained, this drawing was not based on well-documented data and taphonomic observations, and therefore should not be taken at face value as an accurate representation of the find.

Although the presence of skeletal remains of multiple individuals in Cave C is briefly mentioned in most original publications, no information is available on their anatomy or exact provenance, and no explanation is provided for why they were not assigned to Apidima 3 (Pitsios 1995, 1999). This is because the spatial distribution of the skeletal remains and the site's stratigraphy were poorly documented. To our knowledge, no excavation notes or records exist, and only a few photographs or drawings of the excavated area have been published. One photograph was published in Pitsios (1999: 5: Figure 4), which illustrates the isolated left tibia S9.1 but provides no spatial information. Furthermore, no comprehensive database of finds with information on their spatial distribution is available, other than what is presented in the limited publications. As it is no longer possible to investigate the depositional environment from which the human remains originated, there is uncertainty about the anatomical association of some bones in the Apidima Cave C assemblage. For the same reasons, it is also not possible at present to confirm the presumed association between the human remains and the cultural assemblages excavated in the cave.

A date of ca. 30 ka, reported by Pitsios (1999) for Apidima Cave C, is, according to Pitsios 'an approximation,' mainly derived from the perceived association of the skel-

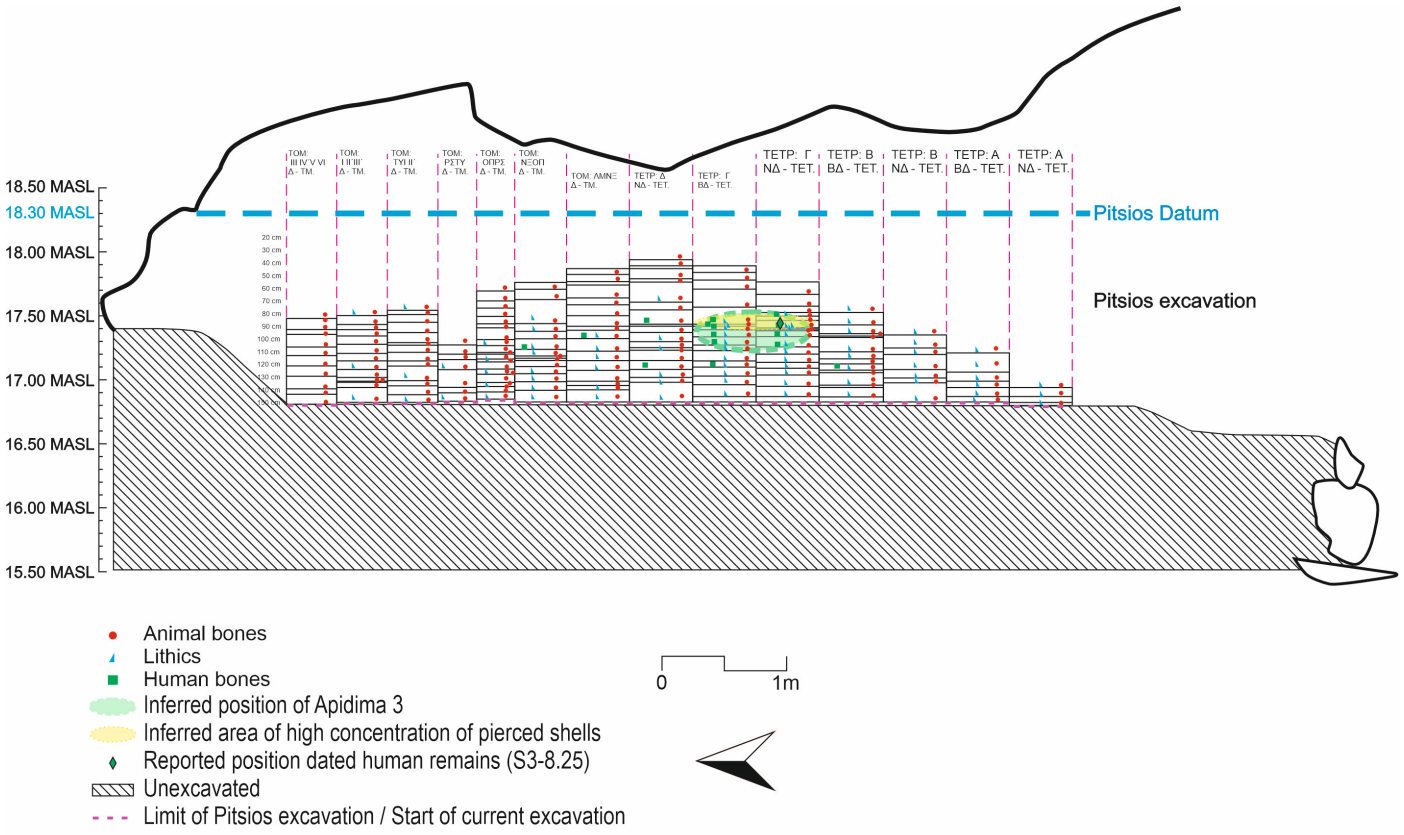

Figure 1. Cross-section (North-South) of Apidima Cave C showing the approximate position of the burial of Apidima 3 and surrounding finds as reported by Mompherratou and Pitsios (1995) and Liebhaber and Pitsios (1995). Plot redrawn and adapted from Pitsios and Liebhaber (1995: 175: Figure 3). The position of the Apidima 3 sternum, which was directly dated by Harvati et al. (2021) with U-series dating is also indicated, based on its position as reported by Mompherratou and Pitsios (1995).

eton with the lithic assemblage they had assigned to the Aurignacian, as well as from two absolute dates obtained from cave deposits by Liritzis and Maniatis (1995) (see Pitsios 1999: 7). However, as stated above, the association of the lithics with the skeleton is uncertain. Furthermore, the Liritzis and Maniatis dates were not based on materials from Cave C, but instead are U-series dates (25–45 ka and 20–30 ka) obtained from travertine samples from the openings of Cave B and D, respectively (Liritzis and Maniatis 1995; see also Harvati et al. 2009; 2021). As such, they have no bearing on the human remains from Cave C, as stated also in the original report (Liritzis and Maniatis 1995). A direct U-series date obtained from human samples (taken from the sternum S3 8.25; see also Figure 1) from Cave C (poor collagen preservation excluded radiocarbon dating) produced a minimum age of the terminal Pleistocene for all the samples. The two samples from the Apidima 3 skeleton yielded minimum ages of 9.9±1.0 ka and 15.4±1.8 ka, which as such do not exclude an earlier Upper Paleolithic cultural affiliation (Harvati et al. 2021). Although the dating confirmed that the human remains are not from the Holocene, it could not answer whether they are associated with the cultural material from the layer in which they were found or if they belong to a younger burial that was intrusive to the sedimentary deposit containing the Protoaurignacian assemblage (Harvati et al. 2021; see also Karakostis et al. 2026 [this issue]; Lombardo et al. 2026b [this issue]).

To better understand the constraints on the chronological position of Apidima 3, our team conducted U-series and radiocarbon dating on samples from Apidima Caves C (Harvati et al. 2026b [this issue]). U-series dating was applied to sample APU5 from a travertine crust preserved on the cave wall and interpreted as likely capping the original sedimentary sequence excavated by the Pitsios' team (Harvati et al. 2026b [this issue]). This sample produced a range of 34.5±4.8 ka and thus indicates a minimum age of 29 ka for the sediments excavated by Pitsios (Harvati et al. 2026b [this issue]), consistent with our attribution of the legacy lithic collection from Apidima Cave C as Protoaurignacian (Lombardo et al. 2026b [this issue]). Additionally, radiocarbon dating was conducted on three pierced shells reported to have potentially been associated with the burial of Apidima 3 (Mompherratou and Pitsios 1995), although a clear spatial relationship is indicated only for sample E288.2/VIE-1952 based on information from its museum tag (see also highlighted position in Figure 1; Harvati et al. 2026b [this issue]). The radiocarbon dating of this sample produced a range of 25.8–25.0 ka cal BP. Considering also the dating results for the pierced shells E560/VIE-1953 and E507.2/VIE-1954, which might have been associated with

Apidima 3, we have a possible range of 24.5–31.8 ka cal BP. As this temporal range postdates the known chronological record of Protoaurignacian and Aurignacian sites in Greece (see Harvati et al. 2026b [this issue]) it appears likely that the shell beads may not be related to the legacy Protoaurignacian lithic assemblage. Therefore, if (some of) the pierced shells were associated with Apidima 3, as reported by Mompherratou and Pitsios (1995), the burial may represent an intrusive, potentially Gravettian, rather than Aurignacian, context. Additional direct dating of the skeleton is necessary to resolve these questions (Harvati et al. 2026b [this issue]).

The first publication describing the discovery of the human remains of Apidima 3 as a Paleolithic ritual burial followed soon after its excavation (Pitsios 1985). The first anatomical study and inventory list, short morphological descriptions, and some limited information about relative spatial relationships (unit, square, depth) of Apidima 3's remains (Mompherratou and Pitsios 1995), as well as an odontological study of the individual's dental remains (Ligoni and Papagrigorakis 1995), were published in a collected edited volume in 1995 (Pitsios 1995). Mompherratou and Pitsios (1995), however, did not provide quantitative descriptions of bone morphology, and the presented information on the biology of the human remains was incomplete. Consequently, Apidima 3 has rarely been recognized by the scientific community and has not been the subject of independent investigations until recently, even though its potential Aurignacian chronology would make it one of the few near-complete skeletons known from this period across Europe.

Here, we conducted a comprehensive reinvestigation of the Cave C human remains, starting with a detailed qualitative and quantitative morphological description, an updated inventory comprising previously unreported specimens, and a new accession system for the remains. We re-assessed the age and sex of Apidima 3, estimated stature and body mass, investigated the level of asymmetry in limb proportions, and placed these estimates in the comparative context of other European Upper Paleolithic individuals. We also carefully examined the bones for indications of pathology and habitual activity/stress. We furthermore provide osteometric data as a source for future comparative research. This article thus provides the first comprehensive morphological description and updated biological profile of Apidima 3, a rare representative of the hunter-gatherer populations that inhabited what is now modern Greece in the Late Pleistocene.

MATERIALS AND METHODS

INVENTORY AND ACCESSION SYSTEM

The human skeletal remains of Apidima 3 are housed in the collection of the National Archaeological Museum of Athens, Greece. All human remains associated with the Upper Paleolithic context of Cave C were found packed in various plastic bags and stored in cardboard boxes in the museum collection. All available boxes containing skeletal remains were carefully examined, leading to the identification of a few additional previously unreported specimens. All human skeletal elements recognized by the excavators are listed serially and ordered by the date of their discovery in the catalogue of human remains from Cave C provided by Mompherratou and Pitsios (1995). The serial numbers available in this catalogue do not correspond to the IDs written on the bones themselves. Instead, the IDs found on the bones are repetitive and associated with the spatial finding position (unit, depth). Thus, each originally assigned accession ID summarizes all human skeletal remains found at the same elevation within a one-square-meter sub-square.

To address the lack of organization in the inventory and the unclear naming of the finds, we created a new series of sub-IDs, which were added to the existing original accession IDs. Each skeletal element described here now has a unique ID that can be used to clearly refer to the specimen of interest. A few cases of very fragmentary and unidentifiable bones also exist. Since no detailed individual information will be provided for these cases, we have summarized them under a single shared sub-ID, including a general description of the characteristics of the related bone fragments. To identify and verify the human skeletal remains from Apidima Cave C, we used the information on the excavation labels, which contained the most essential details (Cave C, find ID, excavation year, and unit), and compared them with the catalogue of Mompherratou and Pitsios (1995). Our updated catalogue of human remains now contains all bones attributed to Apidima 3, as well as the human skeletal remains that are not associated with this individual, and those that were not included in the original inventory. The isolated skeletal elements and teeth that were not attributed to Apidima 3 were each assigned a Σ ID by Pitsios, numbering up to Σ 26, further complicating the picture of individual accession numbers, as the original descriptions also do not provide any explanation for their decisions. Additional Σ IDs among the skeletal remains of Apidima 3 were also investigated here, and if reasonable similarities in the preservation, morphology, and osteometry were found in comparison to Apidima 3's remains, they were added to its inventory. Considering the lack of spatial and stratigraphic descriptions, all other skeletal remains were assigned to a second adult individual, Apidima 4, if they could not be matched with Apidima 3. An overview of the inventory of human remains from Apidima Cave C is provided in Table 1. All elements in this inventory are associated with Apidima 3, except for those indicated by an asterisk, which were assigned to Apidima 4. Furthermore, the skeleton sketches in Figures 2 and 3 show the preserved and missing bones of Apidima 3 and the bones attributed to Apidima 4, respectively.

COMPARATIVE SAMPLES

Several published measurements of Upper Paleolithic individuals were included for osteometric comparisons of Apidima 3's limb proportions (humeri, radius, ulna, femora, tibia, fibulae) and for comparisons with other stature and body mass estimates. We did not distinguish between

TABLE 1. INVENTORY OF HUMAN REMAINS FROM APIDIMA CAVE C, RETRIEVED DURING THE EXCAVATIONS IN JULY 1984.

ID	Sub-ID	Associated bone ID	Bone Category	Element	Side
S3 (6)	6	-	Carpalia	Capitate	L
S3 (8)	24	-	Carpalia	Hamate	L
S3 (8)	2	-	Claviculae	Clavicula	R
S3 (10)	3	-	Costae	Costae	R
S3 (10)	1	-	Costae	Costae	R
S3 (10)	2	-	Costae	Costae	R?
S3 (11)	4	-	Costae	Costae	-
S3 (12)	3	-	Costae	Costae	-
S3 (13)	3	-	Costae	Costae	-
S3 (14)	2	-	Costae	Costae	-
S3 (15)	1	-	Costae	Costae	L
S3 (15)	2	-	Costae	Costae	L
S3 (15)	3	-	Costae	Costae	L
S3 (16)	2	-	Costae	Costae	-
S3 (17)	4	-	Costae	Costae	-
S3 (21)	1	-	Costae	Costae	R
S3 (5)	1	-	Costae	Costae	L
S3 (6)	7	-	Costae	Costae	-
S3 (7)	1	-	Costae	Costae	-
S3 (8)	11	-	Costae	Costae	-
S3 (8)	20	-	Costae	Costae	-
S3 (8)	18	-	Costae	Costae	R
S3 (8)	17	-	Costae	Costae	L
S3 (17)	8	-	Costae	Costae	L
S3 (17)	7	-	Costae	Costae	-
S3 (17)	6	-	Costae	Costae	L
S3 (8)	19	-	Costae	Costae	L
S15	1	-	Cranium	Maxilla	L

TABLE 1. INVENTORY OF HUMAN REMAINS FROM APIDIMA CAVE C, RETRIEVED DURING THE EXCAVATIONS IN JULY 1984 (continued).

ID	Sub-ID	Associated bone ID	Bone Category	Element	Side
S3 (10)	5	-	Dentes	Dens	-
S3 (18)	4	-	Dentes	Dens	L
S3 (18)	3	-	Dentes	Dens	L
S3 (21)	4	-	Dentes	Dens premolaris	L?
S3 (21)	3	-	Dentes	Dens molaris	R?
S3 (7)	2	-	Dentes	Dens	-
S3 (18)	2	-	Dentes	Dens	R
S7	1		Dentes	Dens	-
O107a	1		Dentes	Dens	-
S5	1		Dentes	Dens molaris	-
S6	1		Dentes	Dens premolaris	-
S4	1		Dentes	Dens premolaris	R
S11a	1		Dentes	Dens premolaris	L?
S3 (12)	16	-	Femora	Femur	L
S3 (12)	15	-	Femora	Femur	R
S3 (12)	18	S3 9.2	Fibulae	Fibula	L
S3 (12)	12	S3 8.27	Fibulae	Fibula	R
S3 (8)	27	S3 12.12	Fibulae	Fibula	R
S3 (9)	2	S3 12.18	Fibulae	Fibula	L
S3 (13)	1	-	Humeri	Humerus	L
S3 (8)	1	-	Humeri	Humerus	R
S3 (16)	1	S3 18.1	Mandibula	Mandibula	-
S3 (18)	1	S3 16.1	Mandibula	Mandibula	-
S3 (25)	1	-	Metacarpalia	1st Metacarpus	L
S3 (20)	3	-	Metacarpalia	2nd Metacarpus	R
S3 (8)	13	-	Metacarpalia	2nd Metacarpus	L
S3 (6)	1	-	Metacarpalia	3rd Metacarpus	L
S3 (8)	14	-	Metacarpalia	4th Metacarpus	L
S3 (11)	6	-	Metatarsalia	1st Metatarsus	L
S3 (11)	2	S3 9.4	Metatarsalia	2nd Metatarsus	R

TABLE 1. INVENTORY OF HUMAN REMAINS FROM APIDIMA CAVE C, RETRIEVED DURING THE EXCAVATIONS IN JULY 1984 (continued).

ID	Sub-ID	Associated bone ID	Bone Category	Element	Side
S3 (6)	2	-	Metatarsalia	2nd Metatarsus	L
S3 (9)	4	S3 11.2	Metatarsalia	2nd Metatarsus	R
S3 (9)	3	-	Metatarsalia	3rd Metatarsus	L
S3 (20)	2	-	Metatarsalia	4th Metatarsus	L
S3 (12)	17	-	Patellae	Patella	L
S3 (12)	9	-	Patellae	Patella	R
S3 (12)	8	S3 8.21	Pelvis	Coxae	L
S3 (17)	5		Pelvis	Coxae	R
S3 (8)	21	S3 12.8	Pelvis	Coxae	L
S3 (14)	1	-	Phalanges manus	Phalanx distalis	-
S16	1	-	Phalanges manus	Phalanx distalis	R?
S10a	1	-	Phalanges manus	Phalanx distalis	L?
S3 (12)	7	-	Phalanges manus	Phalanx distalis	R
S3 (12)	6	-	Phalanges manus	Phalanx media	L
S3 (12)	5	-	Phalanges manus	Phalanx media	L
S13	1	-	Phalanges manus	Phalanx media	L
S12	1		Phalanges manus	Phalanx proximalis	-
S3 (19)	4	-	Phalanges manus	Phalanx proximalis	-
S3 (6)	3	-	Phalanges manus	Phalanx proximalis	L
S3 (11)	3	-	Phalanges manus	Phalanx proximalis	-
S3 (1)	1	-	Phalanges manus	Phalanx proximalis	R
S12	1	-	Phalanges manus	Phalanx proximalis	-
S10	1	-	Phalanges manus	Phalanx proximalis	R
O302	1	-	Phalanges manus	Phalanx proximalis	R
S3 (15)	4	-	Phalanges pedis	Phalanx media	R
S3 (23)	1	-	Phalanges pedis	Phalanx proximalis	R
S3 (12)	4	-	Phalanges pedis	Phalanx proximalis	R
S3 (24)	1	-	Phalanges pedis	Phalanx proximalis	R
S3 (8)	4	-	Phalanges pedis	Phalanx proximalis	R
S3 (22)	1	-	Phalanges pedis	Phalanx distalis	R

TABLE 1. INVENTORY OF HUMAN REMAINS FROM APIDIMA CAVE C, RETRIEVED DURING THE EXCAVATIONS IN JULY 1984 (continued).

ID	Sub-ID	Associated bone ID	Bone Category	Element	Side
S3 (17)	2	-	Radii	Radius	L
S3 (11)	5	-	Scapulae	Scapula	-
S3 (13)	2	-	Scapulae	Scapula	L
S3 (8)	10	-	Scapulae	Scapula	R
S3 (6)	8	-	Sesamoidea	Sesamoideum	-
O551	1		Sesamoidea	Sesamoideum	-
S3 (8)	25	-	Sternum	Corpus sterni	-
S3 (8)	22	-	Sternum	Manubrium	-
S3 (12)	14	-	Tarsalia	Calcaneus	L
S3 (17)	3	-	Tarsalia	Calcaneus	R
S3 (10)	4	-	Tarsalia	Cuboideum	R
S3 (18)	6	-	Tarsalia	Cuboideum	L
*S3 (6)	5	-	Tarsalia	Cuneiforme laterale	R
S3 (19)	3	-	Tarsalia	Cuneiforme laterale	R
S3 (8)	12	-	Tarsalia	Cuneiforme intermedium	L
S3 (19)	1	-	Tarsalia	Cuneiforme mediale	R
S3 (19)	2	-	Tarsalia	Cuneiforme mediale	L
S3 (6)	4	-	Tarsalia	Naviculare	L
S3 (9)	1	-	Tarsalia	Naviculare	R
S3 (23)	2	-	Tarsalia	Talus	L
S3 (8)	5	-	Tarsalia	Talus	R
*S26	1		Tarsalia	Talus	R
S3 (11)	1	S3 12.13	Tibiae	Tibia	R
S3 (12)	13	S3 11.1	Tibiae	Tibia	R
*S9	1	-	Tibiae	Tibia	L
S3 (17)	1	-	Ulnae	Ulna	L
S3 (8)	15	-	Vertebrae	V. cervicalis	-
S3 (8)	3	-	Vertebrae	V. cervicalis	-
S3 (7)	3	-	Vertebrae	V. cervicalis	-
S3 (18)	5	-	Vertebrae	V. cervicalis	-

TABLE 1. INVENTORY OF HUMAN REMAINS FROM APIDIMA CAVE C, RETRIEVED DURING THE EXCAVATIONS IN JULY 1984 (continued).

ID	Sub-ID	Associated bone ID	Bone Category	Element	Side
S3 (3)	1	-	Vertebrae	V. cervicalis	-
S3 (8)	6	-	Vertebrae	V. thoracica	-
S3 (8)	16	-	Vertebrae	V. thoracica	-
S3 (8)	9	-	Vertebrae	V. thoracica	-
S3 (8)	7	-	Vertebrae	V. thoracica	-
S3 (8)	8	-	Vertebrae	V. thoracica	-
S3 (12)	1	-	Vertebrae	V. lumbale	-
S3 (12)	2	-	Vertebrae	V. lumbale	

*Apidima 4

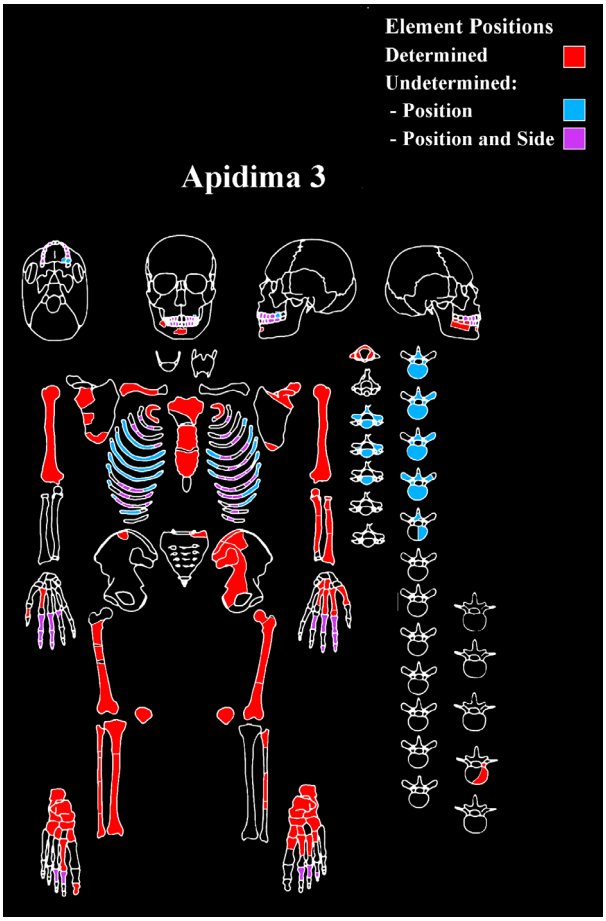

Figure 2. Overview of preserved skeletal elements associated with Apidima 3. The skeleton sketch was modified based on the file made available by the Staatssammlung für Anthropologie München (SNSB): https://sam.snsb.de/wp-content/uploads/sites/9/2023/09/db0f3e83-1.pdf, 01.07.2025.

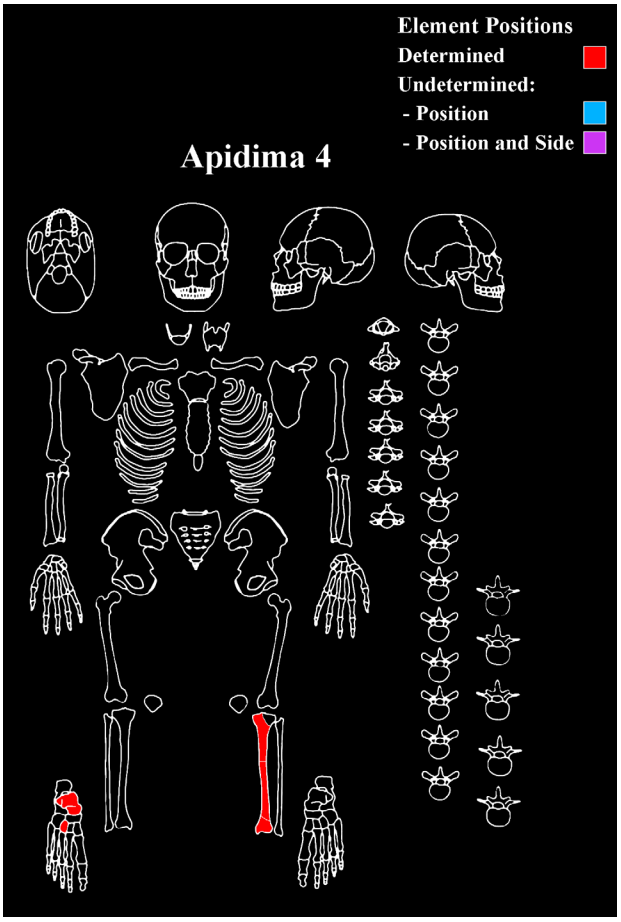

Figure 3. Overview of preserved skeletal elements associated with Apidima 4. The skeleton sketch was modified based on the file made available by the Staatssammlung für Anthropologie München (SNSB): https://sam.snsb.de/wp-content/uploads/sites/9/2023/09/db0f3e83-1.pdf, 01.07.2025.

chronological groups within the Upper Paleolithic, nor did we separate geographic groups. Since our own measurements on Apidima 3 were based on the definitions by Bräuer (1988), we included only samples from studies with the same measurements, measured directly on the bone (estimates of measurements were not included).
For the descriptive group statistics, we included only female individuals, as we agree with the sex determination published by Mompherratou and Pitsios (1995), which was based on the morphology of Apidima 3's pelvic remains (see below, Results, Age and Sex Determination).

Supplementary Information (SI)-Table 1 provides a list of all comparative samples included for the osteometric comparisons of the Apidima 3 limb bones. SI-Table 2 and SI-Table 3 provide an overview of comparative samples used in stature and body mass estimates. When measurements were reported bilaterally, we calculated the mean of the right and left sides and included the resulting value for comparison with Apidima 3 measurements. In all other cases, we included the available measurement if only the right or only the left side was sufficiently preserved.

METHODS

Measurement Acquisition

All linear measurements were collected with digital calipers, and a simple measurement tape was used for circumference measurements. All measurements followed the definitions of Bräuer (1988). We estimated biological parameters, such as age at death, biological sex, stature, and body mass. Additionally, we searched for signs of pathological conditions and examined the effects of taphonomy on the preservation of the skeletal material.

To assess Apidima 3's body proportions relative to other Upper Paleolithic individuals, we calculated mean and standard deviations (SD) for females, who are chronologically placed in the Upper Paleolithic and for whom directly comparable measurements were published.

Additionally, we produced violin and box plots, including comparative data for Upper Paleolithic males and females, to provide a general overview of Upper Paleolithic variability for different measurements, independent of biological sex. This was conducted in the software R version

4.4.2 by use of the packages ggplot2 (Wickham 2016), ggpubr (Kassambara 2023), and dplyr (Wickham et al. 2023) for measurements for which at least four comparative specimens (mixed sex) were available. Colors were used to visually distinguish between the respective group associations for males and females.

Sex and Age Assessment

The assessment of Apidima 3's biological sex was conducted mainly based on the identification and evaluation of sexually dimorphic morphological traits. Due to limited preservation of skeletal remains and high fragmentation, we could investigate only the morphology of preserved traits in the left os coxae with respect to their sexually dimorphic characters. We used definitions provided by Buikstra and Ubelkar (1994), Novak et al. (2012), and Karsten (2017) to determine whether a trait should be considered morphologically female or male and to assign scores based on these assessments. We furthermore considered the results of our osteometric comparisons with other Upper Paleolithic sites as indicators for Apidima 3's biological sex. The final assessment was conducted after considering all results.

Age determination was based on changes in the auricular morphology of the left os coxae. We carefully studied the preserved surface and assigned it to the best-matching age category based on the definitions and examples provided by Lovejoy et al. (1985). Additionally, we assigned age scores using the method of Buckberry and Chamberlain (2002). The scores were assigned twice, with a two-week break in between, and the final composite average was used to assign the score to one of Buckberry and Chamberlain's (2002) age categories. Our evaluation of Apidima 3's age at death also included degenerative changes, although these markers were only considered for discussion, along with considerations of the potential multifactorial origin of their appearance. These features included dental wear, oral health, and degenerative changes in postcranial articular morphology. The presence of such morphological changes and their complexity and severity were factors we considered, along with the results of our assessment of changes in pelvic auricular morphology, to determine a final age-at-death.

Stature Estimation

Stature was calculated using multiple well-established anthropometric equations to provide a range of possible estimates, based on those published by Pearson (1899), Trotter and Gleser (1952), Sjøvold (1990), and Formicola and Franceschi (1996). We decided to apply these equations to provide a more reliable range of body-size estimates, as they were developed from diverse geographic and population samples. We estimated Apidima 3's stature based on the lateral condyle-malleolar length (M1) and the maximum length (M1a) of the right tibia, but we also estimated the maximum length of Apidima 3's fragmented left femur and calculated a range of stature estimates with the maximum length (F1) and the bicondylar length (F2). We decided to use Apidima 3's tibia for comparisons of our stature estimates due to its weight-bearing function, similar to the femur, which makes it the next preferable proxy for the stature estimation if the femur length is not preserved well. Unfortunately, it was not possible to directly measure the maximum femoral length since the Apidima 3 femur's distal articular surface is covered by sediment concretions, which also hold the right patella attached to the surface, thus preventing direct measurement. We nevertheless estimated their maximum length and bicondylar length by articulating the fragments as accurately as their condition allowed, and measured the distances according to the definitions of Bräuer (1988). As it was possible to directly measure the tibia and the estimation results from both did not diverge significantly, we decided to use the more reliable tibia measurement for the comparative examination.

The equations developed by Sjøvold (1990) are based on published mean values of regressions of bone length on stature from globally mixed modern populations of males and females. These equations incorporate measurements derived from skeletal dimensions and from length-corrected cadaver measurements, depending on the study's source. The samples used for the diverse-population equations from Sjøvold (1990) are listed in Rösing (1988). Since the diverse samples originated from different populations with varying sample sizes, the mean values of each population were weighted by their sample sizes, with larger weights assigned to larger samples (Sjøvold 1990). The weighted line of organic correlation equations by Sjøvold (1990) has the broadest applicability, and it is therefore assumed to provide the most representative formulae for fossil bone stature estimations compared to population-specific equations (Carretero et al. 2012). The remaining referenced equations used in our study are based on population-specific samples for females. The samples used in the Trotter and Gleser (1952) equations were also included by Sjøvold (1990). Formicola and Franceschi (1996) developed their equations using European Neolithic samples.

Body Mass Estimation

Lower limb joints are considered the most precise skeletal features for estimating body mass due to their crucial role in supporting body weight (Ruff and Wood 2023). We chose the well-established equations for body mass estimations based on the superoinferior femoral head breadth (FHSI) by Ruff et al. (2012; 2018). These equations were established based on geographically diverse populations, including separate equations for males and females, as well as combined equations. We consider the greater variability encountered in globally mixed population samples to be more robust for estimating body mass in Apidima 3 than equations that rely on geographically more limited reference populations. Therefore, we used body mass equation results from worldwide, combined-sex reference samples to compare our body mass estimate for Apidima 3 with those of other Upper Paleolithic specimens reported in the literature.

Additional Examinations

Part of our study of Apidima 3's life history was also the identification and examination of paleopathological conditions, non-metric traits, and skeletal modifications. We examined the health status of all preserved joints and musculotendinous attachment sites in the postcranial remains to assess the extent of degenerative changes and investigate the aetiology of morphologically distinctive features. We furthermore examined the oral health based on the few preserved jaw fragments and several isolated teeth.

Finally, we carefully examined the preserved context of the skeletal remains. Even though the presence of the solidified sediment crust limited our examinations by covering important morphological features, it fortunately preserved the context of several skeletal elements, allowing us to study burial taphonomy in a way that is usually not possible after the excavation of archaeological remains. Many skeletal elements were found attached to one another, and the solidified sediment crust served as the glue that preserved their context. Thanks to this condition, we were able to study the spatial relationship between attached skeletal elements and their degrees of displacement. This information helped us draw conclusions about the original context of Apidima 3 and the initial burial, as well as the taphonomic processes that affected the human remains until their discovery and excavation.

RESULTS

MORPHOLOGICAL DESCRIPTION OF APIDIMA 3 AND APIDIMA 4

Detailed descriptions of morphological characteristics and the state of preservation of skeletal elements attributed to Apidima 3 and Apidima 4 are provided in the supplementary information, including photographic material shown in SI-Figures 1–18.

AGE- AND SEX DETERMINATION

Assessment of the Sexual Dimorphism in Apidima 3's Skeletal Remains

The sex determination of Apidima 3 was limited by the incomplete preservation and the high degree of fragmentation of the skeletal remains. No sexually dimorphic cranial traits are preserved. Only a few meaningful morphological features are available on the partially preserved posterior aspect of the left os coxae that could be considered for sex determination. The most indicative preserved pelvic trait in Apidima 3 is the greater sciatic notch. Its morphology can be described as very wide and U-shaped, which matches, e.g., scoring category 1 in Novak et al. (2012) and the scoring category -2 "hyperfeminin" in Buikstra and Ubelaker (1994), both of which are typically found in females. The auricular surface of Apidima 3 is elevated, and the auricular morphology of the left os coxae shows a very well pronounced preauricular sulcus that deeply incises the auricular surface and undercuts it in the posterior aspect. The groove is present along the entire inferior aspect of the auricular surface, and its width is greater than 0.5cm along most of its length. The morphology of Apidima 3's preauricular sulcus corresponds well to the definition for score 1 in Karsten (2017) and score 1 in Novak et al. (2012), which, in both studies, was found to be strongly associated with their female samples. Figure 4 illustrates the sexually dimorphic morphology of Apidima 3's left os coxae (S3 8.21) with a focus on the auricular morphology. We also compared the osteometry of Apidima 3, as well as its stature and body mass estimates, with published data from Upper Paleolithic males and females (see "Osteometry of Apidima 3 in a Comparative Context with other European Upper Paleolithic Specimens"). The results of our metric comparisons place Apidima 3's body proportions, stature, and body mass within the wider range of variation for Upper Paleolithic female individuals, with clear distinctions from Upper Paleolithic males evident in most measurements included in our comparisons.

Age-at-Death Determination of Apidima 3

The skeletal remains of Apidima 3 provide several indications that could be considered for the age assessment of this individual. Apidima 3 had certainly reached adulthood, as evidenced by skeletal remains that show the completion of several developmental markers (Schaefer et al. 2009). This includes the complete fusion of all preserved epiphyses and apophyses. Unfortunately, late developmental ossification centers, such as the spheno-occipital synchondrosis or the medial clavicular epiphysis, are not preserved. However, full epiphyseal fusion is present in all preserved parts of the iliac crest, and the limb remains. The right mandibular fragment (S3 16.1) contains three fully erupted molars (tooth positions: 46–48) aligned in the occlusal plane, which is another supporting indication to classify Apidima 3's minimum biological age as adult (Smith 1991; Timme et al. 2024). Alveolar bone in this mandibular fragment seems to be partially resorbed to the level of root exposure. Unfortunately, the alveolar process has also been fractured by agents of taphonomy, and it is therefore macroscopically not possible to evaluate the degree of age-related degeneration. The degree of dental wear is very high in all teeth that were found in one context associated with Apidima 3, i.e., none of the teeth exhibit a preserved tooth crown morphology, and all teeth of Apidima 3 show a degree of abrasion that caused the exposure of dentine in most of the occlusal view, including several teeth that are worn down to the pulp. The mandibular molars show the strongest occlusal wear on the buccal surface, while the preserved maxillary second molar (tooth position: 27) shows the highest degree of occlusal wear among all molars of Apidima 3, with the strongest abrasion located on the lingual surface, where the dental abrasion reached the upper part of the root and exposed the lingual pulp. See "Paleopathology, Non-Metric Traits, and Skeletal Modifications" for more

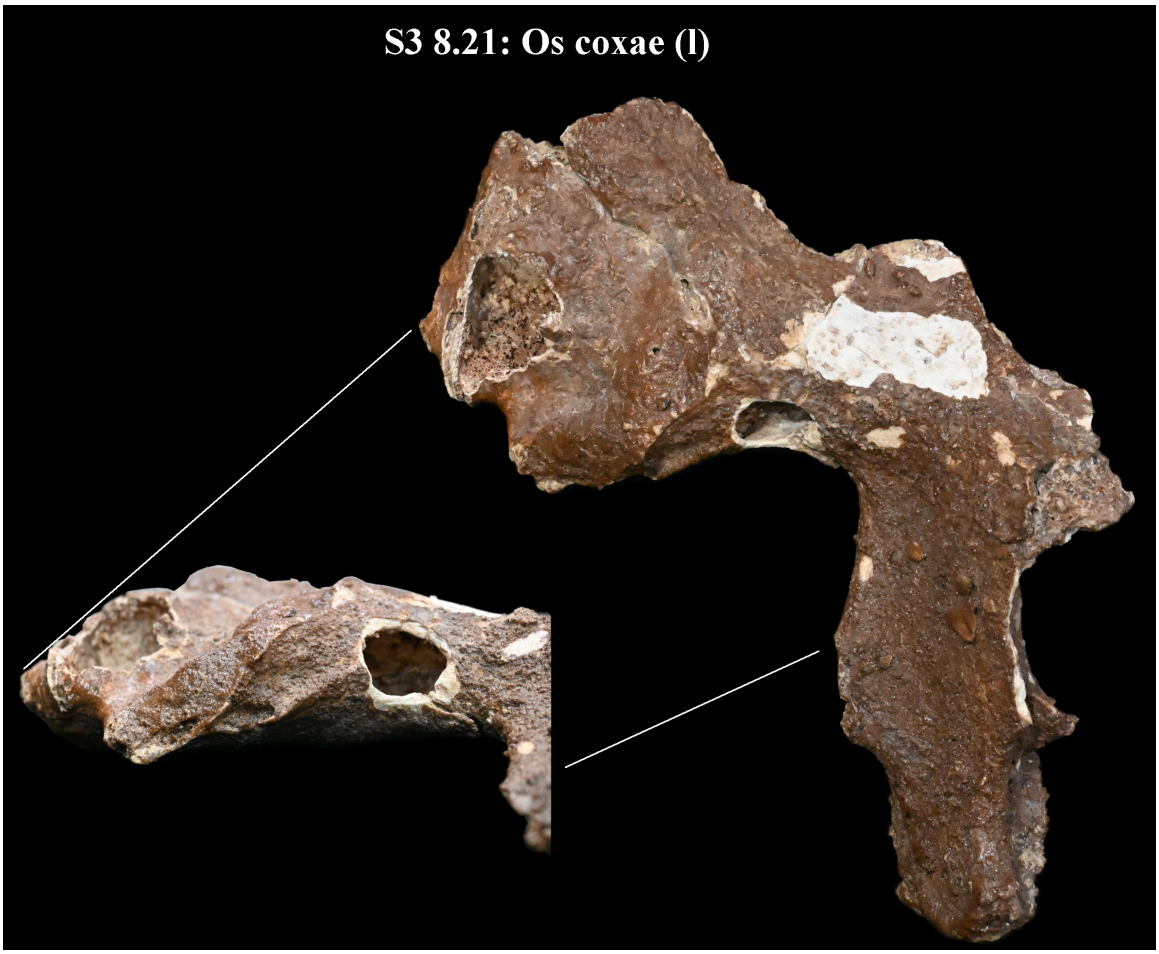

Figure 4. The left os coxae (S3 8.21) of Apidima 3. The bone is shown from its ventral aspect. In focus below, the inferior aspect of the auricular morphology.

information about potential age-related implications and considerations of other factors that could have had an impact on dental wear.

For the age determination of Apidima 3, we also considered age-related degenerative changes of the postcranial remains. The left os coxae shows signs of an age-progression beyond early adulthood, but only the auricular surface was sufficiently preserved for an assessment of age-related alterations. It should be noted beforehand that the elevated auricular surface and the lipping of its inferior joint margin are related to the wide and long preauricular sulcus; thus, these traits cannot be considered as being primarily influenced by age. Lipping of the auricular margin, however, also extends to the posterior joint margin of the inferior demiface, and anteriorly it extends to the apex. The shape of the joint margin is rather irregular, but it does not exhibit signs of severe degeneration. The inferior demiface retains a slight transverse organization of the surface, but it is only present inferiorly on the posterior area, and the major portion of the inferior demiface is characterized by coarse granularity. Transverse organization of the superior demiface is completely absent, and, instead, the surface is defined by dense compact bone and some coarse granularity. An evaluation of macro- and microporosity was difficult due to the thin sediment crust attached to the bone surface; however, it appears to be absent, as no porosity type was identifiable where the sediment crust is less prevalent. The auricular surface morphology of Apidima 3's left os coxae is thus characterized by increased densification of the auricular surface with some coarse granularity and a lack of transverse organization in most areas of the superior and inferior demifaces, by the presence of light lipping and irregularity of the apex and the posterior joint margin, and by the absence of macro- and microporosities. With this information, we concluded that the left os coxae of Apidima 3 best matches the descriptions of the age group 40–49 provided by Lovejoy et al. (1985). We also assigned scores to these traits using the age-determination method developed by Buckberry and Chamberlain (2002). We re-scored the morphological traits after two weeks and calculated the average composite score to assign an age category. The repeated scoring of the auricular surface yielded an average composite score of 12, corresponding to stage IV, and a mean age of 51.41±14.47 years (Buckberry and Chamberlain, 2002). Our scoring results for the Buckberry and Chamberlain (2002) method are summarized in Table 2.

TABLE 2. AGE DETERMINATION OF APIDIMA 3 BASED ON THE AURICULAR SURFACE MORPHOLOGY OF THE LEFT OS COXAE AND THE SCORING SYSTEM BY BUCKBERRY AND CHAMBERLAIN (2002).

Buckberry and Chamberlain (2002)	Apidima 3 1st round	Apidima 3 2nd round
Transverse organization	4	4
Surface texture (granularity)	4	4
Microporosity	1	1
Macroporosity	1	1
Apical changes	2	2
Composite score	**12**	**12**
Average composite score	**12**	

QUANTITATIVE DESCRIPTION OF THE POSTCRANIAL MORPHOLOGY

Postcranial Osteometry of Apidima 3

A detailed quantitative description of the postcranial remains of Apidima 3 and the additional human skeletal elements is provided in the supplementary information (SI-Tables 4–23). All measurements are based on the definitions provided by Bräuer (1988) and are summarized by skeletal element category.

Asymmetry in Apidima 3's Postcranial Osteometry

Absolute differences (mm) and relative differences (%) were calculated for bilaterally preserved skeletal elements for which we could also obtain comparable measurements. It was possible to compute these measures for the scapulae (SI-Table 4), the humeri (SI-Table 5), the femora (SI-Table 10), the patellae (SI-Table 13), the calcanei (SI-Table 14), the tali (SI-Table 15), the naviculares (SI-Table 16), the cuboidea (SI-Table 17), and for the medial cuneiformia (SI-Table 18). Absolute differences were calculated by subtracting the measured value for the left side from the right side, and the obtained result implies the directionality of the asymmetry as left-dominant (positive value) or right-dominant (negative value). We consistently found small differences among the sufficiently preserved and comparable skeletal elements, with only a few exceptions, in which measurements showed low to modest asymmetry. For the scapulae (see SI-Table 4), only the glenoid height could be compared, resulting in a difference of 0.01mm (0.03% difference). The humeri (see SI-Table 5) measurements range from -3.72mm to 1.26mm (0–6.7% difference). Differences between the femora (see SI-Table 10) range from -3.98mm to 2.78mm (0.01–11.95% difference). The relative difference of 11.95% was found in the posterior breadth of the medial condyle (M21c) of the femora and is, in general, the largest degree of asymmetry we found among Apidima 3's skeletal elements. The patellae (see SI-Table 13) show a low range of differences with only 0.1mm to 1.16mm (0.27–2.73%). Very low differences were furthermore observed among the tarsal bones. Apidima 3's calcanei (see SI-Table 14) resulted in a range of -1.46mm to 0.94mm (0.09–5.34%), and the differences found among the tali (see SI-Table 15) ranged from -0.34mm to 1.53mm (0.02–3.97%). The largest level of asymmetry among Apidima 3's tarsal bones was found in the minimum thickness (M7) of her navicular bones, with a difference of -0.66mm (10.23%). The range of differences among the naviculares (see SI-Table 16) is -0.93mm to 0.72mm (0.04–10.23%). For the cuboidea and the medial cuneiformia, again, very low asymmetry was observed. The results for the cuboidea (see SI-Table 17) range from -0.02mm to -0.79mm (0.09–5.59%). Finally, for the medial cuneiformia (see SI-Table 18), the differences ranged from -0.51mm to 0.16mm (0.16–2.46%).

Osteometry of Apidima 3 in a Comparative Context With Other European Upper Paleolithic Specimens

The results of our osteometric comparison of Apidima 3's postcranial skeletal elements (humerus, radius, ulna, femur, tibia, fibula) with those of the Upper Paleolithic females group means are presented in Tables 3–8 (below). In addition, SI-Figures 19–28 illustrate the positions of measurements from Apidima 3 relative to published data on Upper Paleolithic female and male individuals. The increase in comparative samples resulting from the inclusion of male individuals enabled further visual comparisons, including violin and box plots, as well as measurements of Apidima 3 that are not provided in the only female-based osteometric comparisons shown in Tables 3–8 (below).

Table 3 presents the results of the comparison between

TABLE 3. COMPARISON OF MEASUREMENTS OBTAINED FROM THE RIGHT AND LEFT HUMERI OF APIDIMA 3 WITH MEAN AND STANDARD DEVIATION (SD) VALUES FROM HUMERI OF UPPER PALEOLITHIC COMPARAIVE SAMPLES (female sex).*

Measurement definitions by Bräuer (1988)	UP female comparative samples (N=8)			Apidima 3 (r+l)
	mean	*SD*	*n*	
maximum length (M1)	298.86	23.88	7	300.61
total length (M2)	305.00	20.51	2	299.32
proximal epiphyseal breadth (M3)	46.13	2.38	6	46.5
epicondylar breadth (M4)	56.50	4.04	8	54.05
anteroposterior humeral head diameter (M9)	40.01	2.11	6	38.7

*All measurement values are given in (mm). SI-Table 1 lists the female specimens used to calculate the group values provided in this table, as well as females and specimens of undetermined sex included as comparative samples in the violin and box plots of humerus measurements (SI-Figure 19 and SI-Figure 20).

humerus measurements (right and left combined) of Apidima 3 and Upper Paleolithic female individuals. It was possible to compare the dimensions of the maximum length (M1), total length (M2), proximal epiphyseal breadth (M3), epicondylar breadth (M4), and the anteroposterior humeral head diameter (M9). All comparable humerus dimensions measured for Apidima 3 fall within the range of the standard deviations for the Upper Paleolithic female samples, and the position of Apidima 3 was consistently close to the group mean values. Additionally, violin and box plots also include measurements for the dimensions of mediolateral breadth of trochlea (M11), mediolateral breadth of capitulum (M12), width of distal articular surface (M12a), trochlear depth (M13), width of olecranon fossa (M14), and depth of olecranon fossa (M15). We produced separate violin and box plots (see SI-Figures 19–20) to show the distributions of humerus measurements for the maximum length (M1), the total length (M2), and other humerus dimensions. Only one female sample, Cro-Magnon Beta, provided comparative data for measurements of distal articular morphology (M11–M14), whereas most comparative data for these measurements originated from Upper Paleolithic skeletal remains of male individuals. Apidima 3's relative position to Cro-Magnon Beta and the remaining male individuals appears to have similar indications as our measurements with bigger Upper Paleolithic female comparative data. Apidima 3 falls consistently below the median and below or within the lower range of variation of Upper Paleolithic males. Apidima 3 is also smaller in all measurements compared to Cro-Magnon Beta, and for the width of the distal articular surface (M12a), Apidima 3 even appears as an outlier, although this observation is most likely related to the lack of variation in the female comparative data.

The results of the comparison for the left radius of Apidima 3 are shown in Table 4. We could compare Apidima 3's maximum length (M1), minimal circumference of the distal diaphyseal half (M3), maximum transverse shaft diameter (M4), and the minimum sagittal shaft diameter (M5). All radius measurements of Apidima 3 are within the range of the standard deviations and, like in the comparison of the humeri, close to the group mean values for Upper Paleolithic female samples. It should also be noted that Apidima 3's measurements are tendentially slightly above the group mean and fall thus into the upper range of variation of Upper Paleolithic females, while the visual inspection of violin and box plots reveals a position that is better described as the range of overlap between Upper Paleolithic males and females. The radius maximum length (M1) is shown in SI-Figure 21, in which Apidima 3 lies well placed within the general variation of the female comparative group, but close to the combined median of males and females.

The remaining dimensions that could be included in the osteometric comparison shown in Table 3 are presented together with the head-neck length (M1a), transverse neck diameter (4(2)), sagittal neck diameter (5(2)), neck circumference (5(4)), and the mid-shaft circumference (5(5)) in the violin and box plots in SI-Figure 22. Measurements of Apidima 3 are consistently within the lower interquartile range and mostly close to or within the lower range of variation of the Upper Paleolithic male individuals. Only for the transverse neck diameter (4(2)), Apidima 3 appears well separated from the males. Overall, the radius measurements of Apidima 3 tend to fall within the overlap range between our male and female comparative groups.

For the left ulna of Apidima 3, it was possible to directly compare the minimal circumference of the distal di-

TABLE 4. COMPARISON OF MEASUREMENTS OBTAINED FROM THE LEFT RADIUS OF APIDIMA 3 WITH MEAN AND STANDARD DEVIATION (SD) VALUES FROM RADII OF UPPER PALEOLITHIC COMPARATIVE SAMPLES (female sex).*

Measurement definitions by Bräuer (1988)	UP female comparative samples (N=9)			Apidima 3 (l)
	mean	*SD*	*n*	
maximum length (M1)	232.30	11.97	5	232
smallest circumference of distal diaphyseal half (M3)	35.86	3.94	9	39
maximum mediolateral shaft diameter (M4)	14.40	1.86	9	15.19
minimum anteroposterior shaft diameter (M5)	10.56	1.04	9	10.5

*All measurement values are given in (mm). SI-Table 1 lists the female specimens used to calculate the group values provided in this table, as well as females and specimens of undetermined sex included as comparative samples in the violin and box plots of radius measurements (SI-Figure 21 and SI-Figure 22).

aphyseal portion (M3), olecranon breadth (M6), olecranon height (M8), dorsoventral shaft diameter (M11), transverse shaft diameter (M12), superior transverse diameter (M13), and superior dorsoventral diameter (M14).

All results of the osteometric comparison with Upper Paleolithic female individuals are summarized in Table 5. Measurements of Apidima 3's left ulna are again close to the comparative group measurements and do not exceed the range of the standard deviation, except for the measurements of the minimal circumference of the distal diaphyseal portion (M3) with 3.79mm above the comparative group mean (0.79mm above the upper limit of standard deviation) and the transverse shaft diameter (M12) for which Apidima 3 resulted in a position that lies 2.41mm below the mean and 0.38mm below the lower range of the standard deviation of the female comparative group. All other comparable measurements were found to be within the range of variation of the female comparative samples. The violin and box plots for the ulnar dimensions are presented in SI-Figure 23 and include, furthermore, the distribution of published measurements for the depth of olecranon (M7) and trochlear-notch height (M7(1)). Apidima 3's position in both measurements is also consistent with our observations from the osteometric comparison. Albeit there is an absence of female comparative samples in M7 and M7(1), Apidima 3 falls in both measurements below the variation of the male comparative group, though for M7, Apidima 3's relative position has no clear distinction and should thus be considered as being within the range of overlap between Upper Paleolithic males and females.

For the femora, comparisons with the female Upper Paleolithic group were made for the anteroposterior mid-shaft diameter (M6), mediolateral mid-shaft diameter (M7), circumference of mid-shaft (M8), mediolateral diameter of proximal diaphysis (M9), anteroposterior diameter of proximal diaphysis (M10), mediolateral head diameter (M18), and for the transverse head diameter (M19). The results of the femoral comparison are summarized in Table 6. Apidima 3's anteroposterior mid-shaft diameter (M6) was found to be 3.19mm above the mean and 0.28mm above the upper range of standard deviations of the female comparative group. The relatively big mid-shaft dimensions of Apidima 3 are also reflected in the mid-shaft circumference (M8), in which our measurement for Apidima 3 is 10.92mm bigger than the mean and 3.6mm above the upper limit of the standard deviation of the female comparative group, but the small sample size (n=3) might have affected Apidima 3's relative position. Even though the mediolateral mid-shaft diameter (M7) of Apidima 3 lies within the variation of the female comparative group, it is worth pointing out that our measurement for Apidima 3 is 3.33mm smaller than the comparative group mean. Considering that the mid-shaft circumference (M8) and especially the mid-shaft anteroposterior diameter (M6) have relatively big values, while the mediolateral diameter (M7) appears rather small, it might be indicative that the femora of Apidma 3 show adaptations to stronger resistance of anteroposterior bending forces. Except for this observation, measurements for the femora of Apidima 3 are all within the range of variation of the female comparative group. A relatively low value compared to the Upper Paleolithic females was furthermore found in the transverse head diameter (M19), in which Apidima 3 falls 3.41mm below the group mean and 0.72mm below the lower range of the standard deviation, though also in this measurement it seems very likely that the small sample size (n=2) might have affected the relative position of Apidima 3. A visual representation of the results from our osteometric comparison is provided in the violin and

TABLE 5. COMPARISON OF MEASUREMENTS OBTAINED FROM THE LEFT ULNA OF APIDIMA 3 WITH MEAN AND STANDARD DEVIATION (SD) VALUES FROM ULNAE OF UPPER PALEOLITHIC COMPARATIVE SAMPLES (female sex).*

Measurement definitions by Bräuer (1988)	UP female comparative samples (N=10)			Apidima 3 (l)
	mean	*SD*	*n*	
smallest circumference of the distal diaphyseal portion (M3)	31.21	3.00	7	35
olecranon breadth (M6)	22.25	3.07	4	23
olecranon height (M8)	20.70	3.82	2	17
dorsoventral shaft diameter (M11)	13.88	1.86	6	14.57
mediolateral shaft diameter (M12)	14.65	2.23	6	12.04
superior transverse diameter (M13)	17.43	1.72	7	18.04
superior dorsoventral diameter (M14)	21.64	2.27	7	20.75

*All measurement values are given in (mm). SI-Table 1 lists the female specimens used to calculate the group values provided in this table, as well as females and specimens of undetermined sex included as comparative samples in the violin and box plots of ulna measurements (SI-Figure 23).

TABLE 6. COMPARISON OF MEASUREMENTS OBTAINED FROM THE RIGHT AND LEFT FEMUR OF APIDIMA 3 WITH MEAN AND STANDARD DEVIATION (SD) VALUES FROM FEMORA OF UPPER PALEOLITHIC COMPARATIVE SAMPLES (female sex).*

Measurement definitions by Bräuer (1988)	UP female comparative samples (N=12)			Apidima 3 (r+l)
	mean	*SD*	*n*	
anteroposterior mid-shaft diameter (M6)	27.19	2.91	10	30.38
mediolateral mid-shaft diameter (M7)	29.67	6.22	10	26.34
mid-shaft circumference (M8)	80.58	7.32	3	91.5
mediolateral diameter of proximal shaft (M9)	30.39	3.75	11	33.98
anteroposterior diameter of proximal shaft (M10)	24.87	3.48	11	23.49
superoinferior head diameter (M18)	42.59	2.98	3	42.87
anteroposterior head diameter (M19)	44.10	2.69	2	40.69

*All measurement values are given in (mm). SI-Table 1 lists the female specimens used to calculate the group values provided in this table, as well as females and specimens of undetermined sex included as comparative samples in the violin and box plots of femur measurements (SI-Figure 24).

TABLE 7. COMPARISON OF MEASUREMENTS OBTAINED FROM THE RIGHT TIBIA OF APIDIMA 3 WITH MEAN AND STANDARD DEVIATION (SD) VALUES FROM TIBIAE OF UPPER PALEOLITHIC COMPARATIVE SAMPLES (female sex).*

Measurement definitions by Bräuer (1988)	UP female comparative samples (N=9)			Apidima 3 (r)
	mean	*SD*	*n*	
lateral condyle-malleolar length (M1)	366.61	19.46	7	347.95
bicondylar breadth (M3)	75.13	1.30	6	68.55
mediolateral diameter of distal epiphysis (M6)	46.63	1.75	4	47.73
anteroposterior mid-shaft diameter (M8)	31.87	5.58	6	31.3
mediolateral mid-shaft diameter (M9)	21.88	3.55	6	18.75

*All measurement values are given in (mm). SI-Table 1 lists the female specimens used to calculate the group values provided in this table, as well as females and specimens of undetermined sex included as comparative samples in the violin and box plots of tibia measurements (SI-Figure 25 and SI-Figure 26).

box plots shown in SI-Figure 24, which include the measurement dimensions of vertical neck diameter (M15), anteroposterior neck diameter (M16), and neck circumference (M17). SI-Figure 24 shows nicely how Apidima 3's mid-shaft circumference (M8) and mid-shaft anteroposterior diameter (M6) fall close to the median of the mixed males and females' comparative groups, reflecting the increased anteroposterior strength in the mid-shaft of Apidima 3. It is also interesting that the proximal femoral diaphysis shows increased strength in the opposite direction, i.e., the mediolateral diameter of the proximal diaphysis (M9) shows greater values compared to the Upper Paleolithic females and lies close to the median of males and females, while the anteroposterior diameter of the proximal diaphysis (M10) is below the group mean of Upper Paleolithic females shown in Table 6 and clearly below the peak of density in comparative measurements (males and females) as indicated by the violin plot in SI-Figure 24. The neck measurements M15–M17 could only be compared to measurements of Upper Paleolithic males and Apidima 3 falls consistently below the variation of the comparative group. Additionally, the femoral head morphology described by M18 and M19 is more closely associated with the variation in the female comparative group and is clearly distinct from the measurements provided for Upper Paleolithic males.

Our comparison of measurements of the right tibia of Apidima 3 with the Upper Paleolithic female comparative group is summarized in Table 7. Comparisons could be made for the lateral condyle-malleolar length (M1), bicondylar breadth (M3), transverse diameter of the distal epiphysis (M6), anteroposterior mid-shaft diameter (M8), and transverse mid-shaft diameter (M9). The results of the comparison of tibial measurements are again very similar to our previous observations, which placed Apidima 3's limb properties well within the variation of Upper Paleolithic females; however, the bicondylar breadth (M3) resulted in a more contrasting position, with a difference of 6.58mm lower to the comparative group mean and with 5.28mm below the lower boundary of the standard deviation. SI-Figure 25 shows the violin and box plots for the lateral condyle-malleolar length (M1) and the maximum length (M1a), while the violin and box plots for the remaining measurements that are also presented in the osteometric comparison in Table 7 are shown in SI-Figure 26. The lateral condyle-malleolar length (M1) is, even though still within the variation of the female Upper Paleolithic group, among the smallest values we have observed among all of our comparative samples. Only the female individuals from Cap Blanc and Grotte des Enfants 5 have similar values, as do the male Grotte des Enfants 6 and the male Romito 6, which is known for its small body size. In the tibial maximum length (M1a), Apidima 3 marks the lowest position among all comparative samples, but the comparative data for this dimension were very limited. The distribution of comparative measurements from Upper Paleolithic males and females, shown in SI-Figure 26, mostly indicates Apidima 3's relative position in the range of overlap of both comparative groups for the diaphyseal dimensions—mediolateral diameter of distal epiphysis (M6), anteroposterior mid-shaft diameter (M8), and mediolateral mid-shaft diameter (M9). Only the bicondylar breadth (M3) takes on a rather unique position among all comparative samples, as it has been observed in the direct osteometric comparison with the female group. The bicondylar breadth of Apidima 3 is even smaller than that of the male Romito 6, whose skeletal dimensions are often at the lower range or even be-

TABLE 8. COMPARISON OF MEASUREMENTS OBTAINED FROM THE RIGHT FIBULA OF APIDIMA 3 WITH MEAN AND STANDARD DEVIATION (SD) VALUES FROM FIBULAE OF UPPER PALEOLITHIC COMPARATIVE SAMPLES (female sex).*

Measurement definitions by Bräuer (1988)	UP female comparative samples (N=7)			Apidima 3 (r)
	mean	*SD*	*n*	
maximum length (M1)	366.00	22.63	2	341.32
maximum mid-shaft diameter (M2)	16.50	2.35	7	16.5
minimum mid-shaft diameter (M3)	12.36	1.88	7	10.6

*All measurement values are given in (mm). SI-Table 1 lists the female specimens used to calculate the group values provided in this table, as well as females and specimens of undetermined sex included as comparative samples in the violin and box plots of fibula measurements (SI-Figure 27 and SI-Figure 28).

low the variation of Upper Paleolithic female individuals.

For the right fibula of Apidima 3, the osteometric comparison with Upper Paleolithic female individuals was limited to the maximum length (M1), maximum mid-shaft diameter (M2), and the minimum mid-shaft diameter (M3). The results are summarized in Table 8. All three measurements of Apidima 3 fall well within the variability of the comparative samples. The maximum length (M1) of Apidima 3 falls closer to the lower limit of the variation of the female comparative group, though this observation might be affected by small sample sizes (n=2). The maximum mid-shaft diameter (M2) of Apidima 3 resulted in the same value that was calculated for the comparative group mean, and the minimum mid-shaft diameter (M3) is close to the lower boundary of the standard deviation. SI-Figure 27 shows Apidima 3's fibular maximum length (M1) relative position to Upper Paleolithic males and females, which marks the lowest value among all comparative samples and is clearly distinct from the male individuals. The violin and box plots for the maximum mid-shaft diameter (M2) and the minimum mid-shaft diameter (M3) are presented in SI-Figure 28. The comparative samples in both measurements are well distributed, and Apidima 3 plots consistently well within the variation of the female comparative samples and below the median of males and females. Nonetheless, none of these measurements appear to be reliable indicators for distinguishing Upper Paleolithic males and females, as both groups exhibit high variability, and the overlap in the range of both measurement dimensions encompasses the spread of data points in both groups.

STATURE AND BODY MASS

Stature Estimation and Comparison of Apidima 3 With the Upper Paleolithic Record

All stature estimates of Apidima 3 are summarized in Table 9 (for estimates based on tibia measurements) and in Table 10 (for estimates based on femur measurements). The tibia stature estimates were performed based on the lateral condyle-malleolar length (M1), the maximum length (M1a), and the medial condyle-malleolar length (M1b). The maximum length (F1) and bicondylar length (F2) were used for the femur-based stature estimation.

The tibia produced a body height of 160.5cm using the European Neolithic female-based equation by Formicola/Franceschi (1996) for the lateral condyle-malleolar length (M1), whereas the Sjøvold (1990) equation, based on modern, globally mixed-sex samples, resulted in a stature estimate of 164.04cm. The maximum length (M1a) was applied to the equations of Trotter and Gleser (1952), which were established for American Black and American White females. This resulted in stature estimates of 161.78cm for the equation of American Black females and 166.57cm for American White females. Finally, the medial condyle-malleolar length (M1b) was applied to the equations for females by Pearson (1899), yielding a stature estimate of 161.35cm. Taken together, our stature estimates based on different length measurements from the right tibia of Apidima 3 ranged from 160.5cm to 164.04cm, with an average stature inferred from these estimates of 162.85cm. This is very close to the range of stature estimation results obtained from femoral length

TABLE 9. STATURE ESTIMATIONS OF APIDIMA 3 AND THE CORRESPONDING REFERENCES FOR THE EQUATIONS USED TO CALCULATE THE BODY HEIGHT VALUES.*

Equations for tibia-based stature estimation	Stature estimate (cm)
Sjøvold 1990 (M1, modern globally mixed-sex sample)	164.04
Formicola/Franceschi 1996 (M1, European Neolithic female sample)	160.50
Tr./Gl. 1952 (M1a, Terry collection - American White, female)	166.57
Tr./Gl. 1952 (M1a, Tibia max., Terry collection - American Black, female)	161.78
Pearson 1899 (M1b, modern European female sample)	161.35

*The equations were developed based on tibia measurement definitions from Bräuer (1988) and include the lateral condyle-malleolar length (M1), the maximum length (M1a), and the medial condyle-malleolar length (M1b).

TABLE 10. STATURE ESTIMATIONS BASED ON THE LEFT FEMUR OF APIDIMA 3.*

Equations for femur-based stature estimation	Stature estimate (cm)
Sjøvold 1990 (F1, modern globally mixed-sex sample)	163.47
Sjøvold 1990 (F2, modern globally mixed-sex sample)	162.55
Formicola/Franceschi 1996 (F1, European Neolithic female sample)	159.32
Tr./Gl. 1952 (F1, Terry collection - American White, female)	163.80
Tr./Gl. 1952 (F1, Terry collection - American Black, female)	161.21
Pearson 1899 (F1, modern European female sample)	157.26

*Corresponding references for the equations used to calculate the body height values are provided next to the results obtained. The equations were developed based on femur length measurement definitions from Bräuer (1988) and include the maximum length (F1) and the bicondylar length (F2).

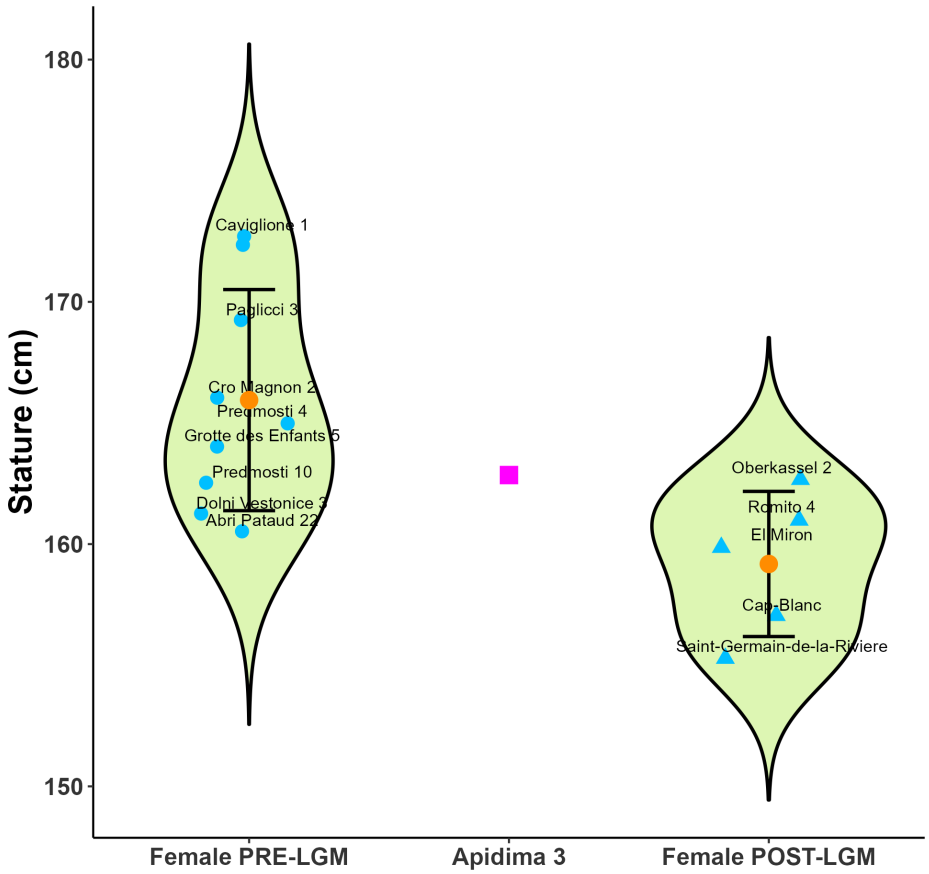

Figure 5. Violin- and box plot showing the average stature estimation result of Apidima 3 in comparison to Upper Paleolithic females (blue). The comparative data used here are summarized in SI-Table 2. Circles indicate whether individuals lived before the Last Glacial Maximum, and triangles indicate individuals from the period after the Last Glacial Maximum. The orange circle indicates the position of the group mean, and the whiskers show the range of the standard deviation.

measurements, indicating consistency in the proportions of the tibia and femur. The stature estimates from the femur were nevertheless slightly smaller, ranging from 157.26cm to 163.80cm and averaging 161.27cm.

Figure 5 shows Apidima 3's average stature (tibia-based estimations) compared to Upper Paleolithic female samples in a violin plot, including indications about the mean (orange dot) and the spread of data (black whiskers) for each group. We used an average stature of 162.85cm for comparison, and we categorized the Upper Paleolithic female comparative samples as either "PRE-LGM" or "POST-LGM" based on their chronological association before/within the last glacial maximum (PRE-LGM) or after it (POST-LGM). The female comparative samples exhibit a clear distinction in stature variation based on their chronological association, as previously reported in studies on Late Pleistocene body proportions (Formicola and Giannecchini 1999; Holt and Formicola 2008). The mean in our PRE-LGM group is 165.94cm (n=9), and the mean of the POST-LGM group is 159.18cm (n=5). Apidima 3's tibia-based stature estimates thus have an intermediate position between the mean values of both comparative groups, though the average stature estimate of 162.85cm falls slightly closer to the mean of the PRE-LGM females. Furthermore, the relative position of Apidima 3's average stature estimates, as well as its range of stature estimates, all plot well within the density peak for the number of individuals from the PRE-LGM group. Our stature estimates of Apidima 3 thus suggest a closer affinity with females from the period before the last glacial maximum (PRE-LGM) than with females from the Upper Paleolithic after the last glacial maximum (POST-LGM).

Body Mass Estimation and Comparison of Apidima 3

The body mass estimates for Apidima 3's left femur range from 56.69kg to 58.27kg, with an average of 57.54kg. These estimates were calculated based on the equations from Ruff et al. (2012; 2018) for the superoinferior breadth of the femoral head, which was measured on the left femur with a result of 42.87mm. The body mass estimation results obtained from the humerus-based equations were 55.02kg (left humerus) and 55.13kg (right humerus). For the estimation of body mass based on the humerus, we used Apidima 3's distal articular mediolateral breadth measurements of 38.95mm (right) and 38.9mm (left) and applied them to the

TABLE 11. BODY MASS ESTIMATIONS OF APIDIMA 3 AND THE CORRESPONDING EQUATIONS USED TO CALCULATE THE WEIGHT (kg).*

Ruff and Wood (2023) body mass equations	Body mass (kg)	
	R	L
FHSI (European, Females)	-	57.66
FHSI (European and combined sexes)	-	56.69
FHSI (worldwide and combined sexes)	-	58.27
HDML (worldwide and combined sexes)	55.13	55.02

FHSI = femoral head superoinferior diameter
HDML = humeral distal articular mediolateral breadth
*The equations were developed based on the superoinferior diameter of the femoral head and the distal articular mediolateral breadth of the humerus.

body mass equation provided in Ruff et al. (2020) for mixed sex and globally mixed samples. All body mass estimation results for Apidima 3 are summarized in Table 11.

Figure 6 shows violin and box plots of the body mass estimate of Apidima 3 relative to other Upper Paleolithic male and female individuals. Additionally, the comparative samples were categorized into chronological groups, as was done for the plot of the stature estimates. For this comparison, we used the estimated 58.27kg, calculated using the equation based on the geographically most diverse reference samples (Ruff et al. 2018). Male comparative specimens were more numerous than female ones. The violin plot in Figure 6 shows that the highest density of data points lies above the mixed-group median in most male samples. In contrast, the lower 50% of data points include males and females with a larger and more irregular spread of body mass estimates. All body mass estimates for the less well-represented female individuals fall below the interquartile range; the only exceptions are the female specimen Veneri 2, whose body mass estimate lies above the mixed-sex group median, and which is known to be one of the most robust Upper Paleolithic females, and Romito 4, who falls into the range of overlap between males and females. The estimated body mass position of Apidima 3, shown in the box plot, is below the median and interquartile range of Upper Paleolithic samples, including males and females. Even though the number of available body mass estimates for Upper Paleolithic females is small compared to the Upper Paleolithic males, there is a tendency for most females to plot in closer association to each other below the first quartile and to form a first concentration of data points, irrespective of the lower density relative to the upper density peak created by male individuals. Apidima 3's position falls well within this concentration of Upper Paleolithic females. The classification of PRE- and POST-LGM groups, however, did not provide any further indications about the distribution of the Upper Paleolithic body mass estimates used in this comparison.

Paleopathology, Non-Metric Traits, and Skeletal Modifications

Throughout Apidima 3's postcranium, several skeletal elements with osteoarthritis or signs of joint degeneration were found. Osteoarthritis was diagnosed based on the presence of at least two morphological changes in a joint, as proposed by Waldron (2019). The sacroiliac joint in S3 8.21 shows marginal lipping and inferior osteophytic enlargement of the auricular surface, including the presence of deeply incising grooves on the auricular and preauricular area, as can be seen in Figure 4. Marginal lipping was found around the condyles of both femora S3 12.15 and S3 12.16. The lateral margins of the capitulum and the lateral epicondyle of the right humerus S3 8.1 also show progressive bone proliferation. Osteophytes are present on the quadriceps tendon attachment of both patellae, S3 12.9 and S3 12.17, and on the calcaneal tendon attachment in the calcanei, S3 12.14 and S3 17.3.

Different types of bone lesions were found among the skeletal remains. The proximal interphalangeal joint of the proximal hand phalanx S3 11.3 is likely affected by osteoarthritis as it presents a mix of several smaller and larger lesions on its articular surface (Figure 7), and it seems that also marginal lipping of the joint contour occurred. Unfortunately, the postmortal damage present in the outline of the phalangeal base also affected most of the contour, which limits this assessment. In the better-preserved distal end of the bone, however, an early-stage proliferation of the dorsal articular outline could be observed with confidence. The left ulna S3 17.1 has an ovoid lesion that enters the bone in the lateral aspect of the olecranon (Figure 8), and the right fibula S3 8.27 has a lesion on the interosseous crest located in the proximal half of the diaphysis.

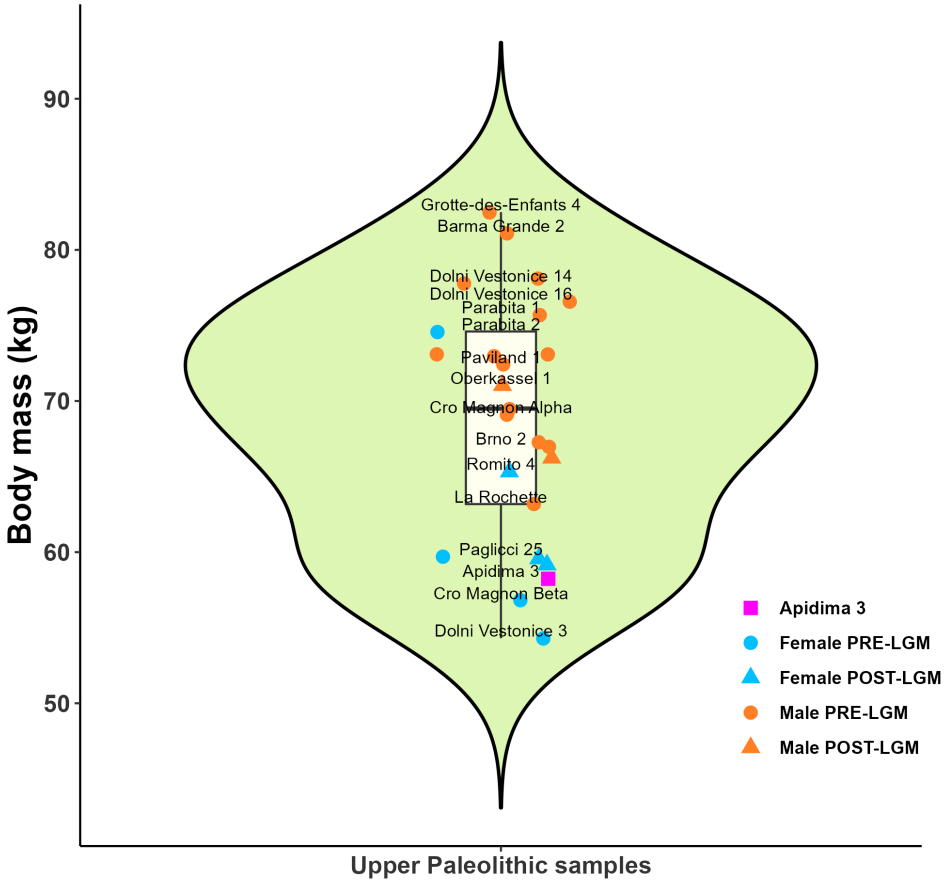

Figure 6. Violin and box plot showing the average body mass estimation result of Apidima 3 in comparison to Upper Paleolithic females (blue) and males (orange). The comparative data used here are summarized in SI-Table 3. Circles indicate whether individuals lived before the peak of the Last Glacial Maximum, and triangles indicate individuals from the period after the peak of the last ice age.

Also, in both tali, S3 8.5 and S3 23.2 (see Figure 8), a bone lesion was found located anteriorly in the center of the inferior margin of the trochlea, though the nature of formation was likely mechanical since well-outlined squatting facets exist right next to these lesions in both tali. S3 23.2 shows a well-pronounced medial trochlear extension, and in S3 8.5, two facets formed bilaterally as lateral and medial trochlear extensions. The stress-induced formation of lesions due to habitual pedal hyperdorsiflexion and the coincident formation of the squatting facets are the most likely explanations for these observations. Pedal hyperdorsiflexion occurs physiologically during squatting, and the observed lesions and squatting facets have been frequently reported in populations that habitually perform many tasks in a squatting body posture (Baykara et al. 2010; Boulle 2001; Satinoff 1972). As these facets typically form on both surfaces of the involved joints (Boulle 2001), we expected to find them also in the preserved distal tibial remains, and indeed, the right tibia S3 12.13 exhibits one large squatting facet (see Figure 8). Interestingly, however, we could not find even the initial state of formation of a squatting facet in the left tibia S9.1. This is an important observation considering the presence of the strong medial trochlear extension found in the left talus S3 23.2, and might be indicative of S9.1 to be, in fact, the tibia of a different individual. This aligns with the morphological differences observed in diaphyseal shape. It is very unfortunate that this assessment must rely on subjective visual inspection of bone morphology due to the extensive fragmentation resulting from the compression and reworking of S9.1 before its discovery.

A severe case of arthritic bone destruction was found in the proximal interphalangeal joint of the first distal pedal phalanx S3 22.1 (see Figure 7); here, an inflammatory process took place over a longer time, which resulted in the advanced erosion and reactive bone proliferation of the phalangeal base. The inflammation further spread to the surrounding bone, where it led to the development of highly vascularized reactive bone material on the plantar surface up to the distal phalanx, as well as increased vascularization of the dorsal bone surface.

Several vertebrae showed strong osteophyte formation. The superior vertebral body of the fourth lumbar vertebra shows anterior bone proliferation (SI-Figure 11), and the inferior surface of the vertebral body shows slight depression and porosity. Osteophytic growth was furthermore observed in the lateral aspects of the superior vertebral

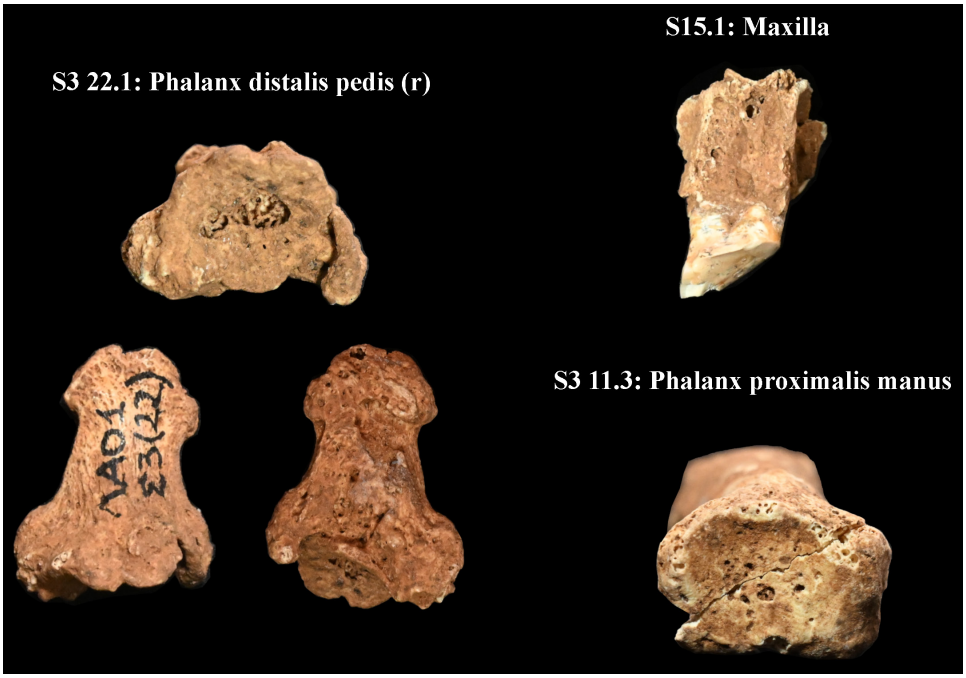

Figure 7. Examples of skeletal remains of Apidima 3 exhibiting signs of osteoarthritis and periodontitis. S3 22.1: proximal view of the phalanges base (top), dorsal (bottom left), and inferior (bottom right) views of the distal phalanx. Destructive inflammatory condition and reactive bone formation are visible in all aspects; S15.1: view on the mesial surface of the alveolus of a missing molar. Small lesions and increased porosity are evident in the bone surface; S3 11.3: proximal view on the phalangeal base. Several lesions are present on the articular surface.

body of the cervical vertebra S3 8.3 and around the posterior margin of the superior vertebral body of the thoracic vertebra S3 8.6 (see Figure 8). In the case of the thoracic vertebra S3 8.6, the left superior costal articular facet is highly degraded, and the remaining surface is very porous.

The mix of osteoarthritic changes distributed irregularly throughout the postcranium of Apidima 3, including inflammatory and mechanically induced joint alterations, indicates that this individual lived into advanced adulthood. This observation aligns with our age-determination results, which concluded that Apidima 3's biological age at death was between 40 and 60 years.

During our careful examination of the degenerative and pathological changes in the skeletal remains of Apidima 3, we also observed unusual bone morphologies and artificially produced modifications. The second metacarpus (S3 20.3) appears to have experienced developmental problems during the fusion of the proximal epiphysis, resulting in malalignment of the epiphyseal plate relative to the metacarpal base (Figure 9). There is no evidence for physical trauma to have caused the malalignment, but we cannot exclude this possibility. Such trauma or a congenital origin of this unusual metacarpal base morphology are possible explanations for this observation.

Another congenital anomaly was identified in the fifth lumbar vertebra, S3 12.2 (SI-Figure 12). Initially thought to be the fragment of the first sacral vertebra (S1), this specimen exhibits morphological characteristics that match those of a lumbosacral transitional vertebra. The fragment is relatively small, limiting the ability to describe this condition in detail; however, important morphological features are preserved, indicating the (almost) complete sacralization of L5, corresponding to a Type III lumbosacral transitional vertebra (Castellvi et al. 1984). The presence of a developed sacral ala with a superior auricular surface indicates that the fusion with S1 was likely complete or near complete. These features alone do not appear unusual, and there are no signs of pathological conditions affecting the bone morphology. There is, however, a relatively large tubercle located on the dorsal surface between the superior articular facet, the auricular surface, and the sacral promontory/superior body of L5. The likeliest explanation for the presence of this tubercle is that of an abnormally retained transverse process of L5 due to the fusion process in the sacralization of L5 and S1. Similar changes in spinal morphology resulting from the sacralization of L5 have been reported in clinical radiographic studies on morphological changes associated with processes of lumbarization and sacralization (Nakajima et al. 2014). For the Upper Paleolithic record, lumbosacral transitional vertebrae have rarely been reported, which is certainly partially due to the lack of preservation of the fragile sacra; however, cases of this congenital condition have been described in detail, for example, for the Gravettian individuals Parabita 1 and 2 (Mal-

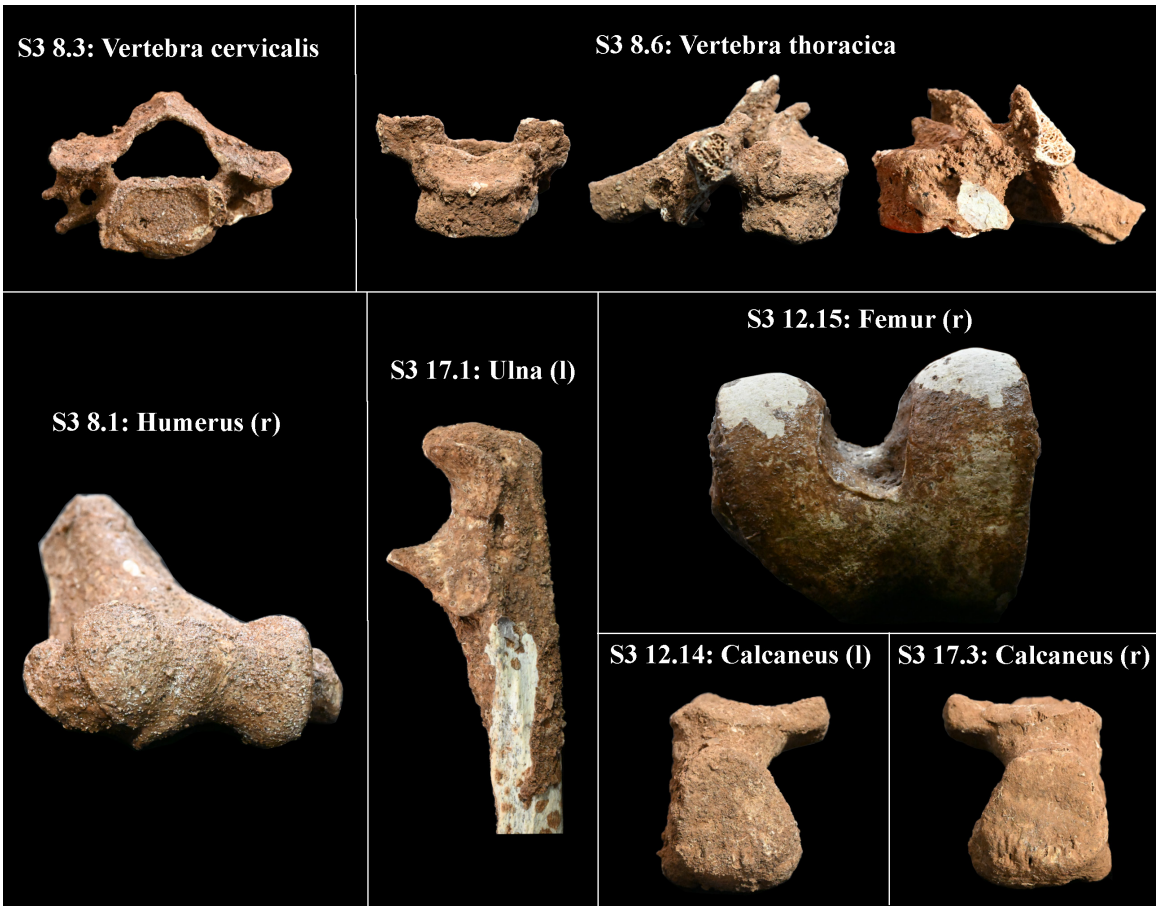

Figure 8. Degenerative changes and signs of osteoarthritis in the bones of Apidima 3. S3 8.3: superior view, osteophytic outgrowth is visible anterior and lateral to the vertebral base; S3 8.6: the vertebra is shown (from left to right) in anterior and lateral views. Osteophytic outgrowth is visible on the superior vertebral body around the posterior half. The lateral views show the unilateral destroyed superior articular demifacet on the left side, while the right side's demifacets remained intact; S3 8.1: inferior view on the lateral and anterior aspect. The right humerus exhibits bony outgrowths around the lateral rim of the capitulum and the lateral epicondyle; S3 17.1: lateral view. The left ulna has a lesion lateral to the trochlear notch where the joint capsule aligns; S3 12.15: inferior view, posterior shows up. The right femur exhibits osteophytic outgrowth around the joint margins surrounding the intercondylar notch; S3 12.14 and S3 17.3: posterior view, heel spurs are present on the calcaneal tuberosity in both calcanei.

legni et al. 2000). Apidima 3 thus adds another important record of this hereditary congenital condition for the Late Pleistocene fossil record.

Finally, our examination concentrated also on the dentition of Apidima 3, which revealed additional important information about its life history and oral health. Two small jaw fragments were found preserved, and fortunately, with some teeth still in place within their alveoli. The maxilla fragment S15.1 shows a portion of the palate and the alveolar process, including the first left molar. Distally, a remnant of the neighbouring alveolus is preserved and exhibits several smaller lesions that might be indicative of periodontitis (see Figure 7). Unfortunately, there is very little additional bone surface available for further investigation of this condition. On the distal surface of the molar S15.1, we found an artificially produced and deeply incising groove oriented parallel to the occlusal surface right at the contact between the tooth crown and the root. This artificial dental modification was observed in several teeth of Apidima 3. An example of a nicely pronounced groove is shown in the third molar (S3 21.3) presented in Figure 9, but it is not present in all interdental contact surfaces. The grooves are always oriented parallel to the occlusal line, and their position is always on the mesial/distal surface. There, the grooves incise the root right underneath the tooth crown and often extend into the enamel.

The mandibula fragment S3 16.1 is the only other jaw fragment with dentition. The fragment represents the right posterior mandibular corpus with all three molars fully developed. Interestingly, the artificial groove is present only at the contact between the first and the second molar, but it is absent at the contact with the third. This mandibula fragment shows a mix of taphonomy-related bone fragmentation and an age- and/or oral health-related retention of the alveolar process down to the exposure of the roots. The state of preservation, however, limits the potential to

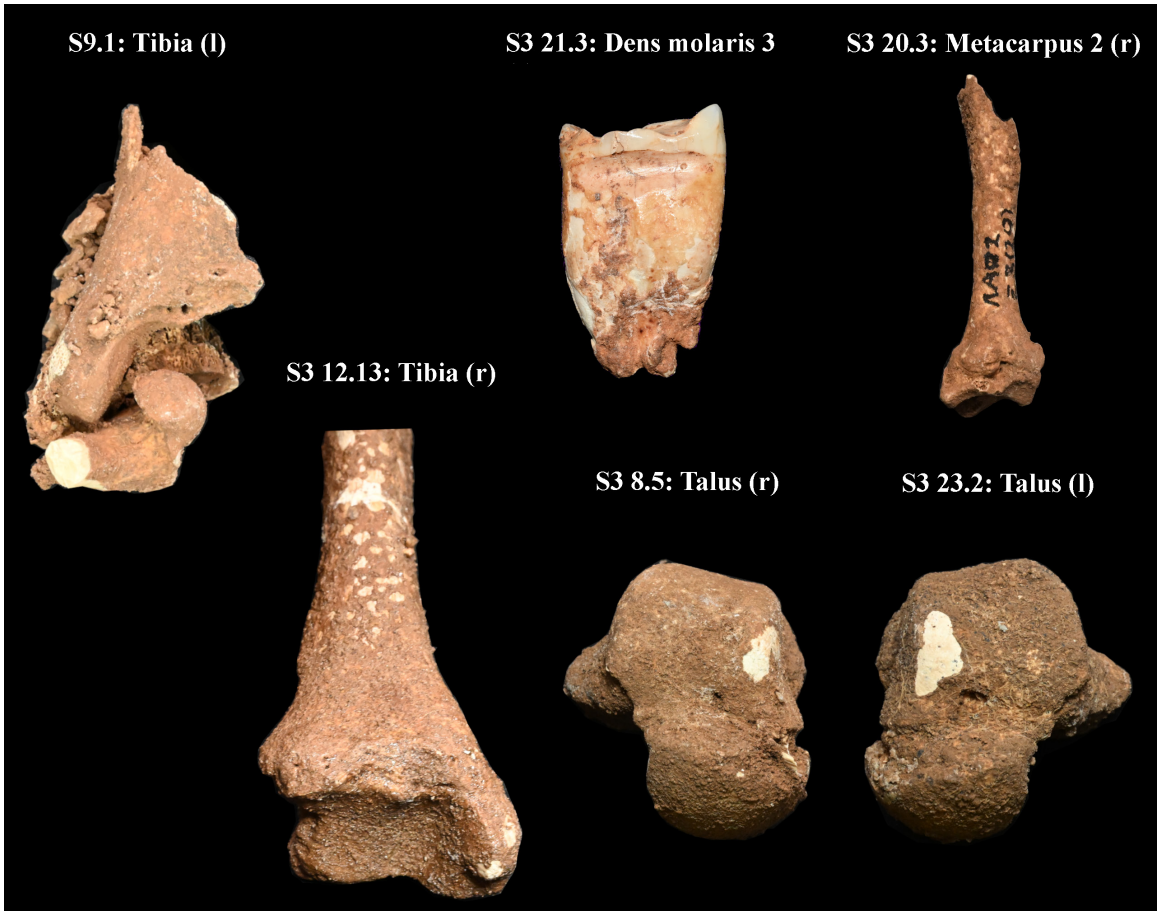

Figure 9. Non-metric anatomical variants, developmental anomalies, and artificial modifications in the remains of Apidima 3. S9.1: anterior view. The picture shows the absence of a squatting facet; S3 12.13: inferior view of anterior aspect. The right tibia exhibits a well-pronounced squatting facet; S3 8.5 and S3 23.2: superior view of anterior aspect. Both tali have trochlear extensions; S3 21.3: example of an interproximal groove as it is present in several of her dental remains; S3 20.3: dorsal and lateral view of the second metacarpal showing the developmental misalignment in the epiphyseal plate and the metacarpal base.

determine the exact extent of bone resorption, and differentiation of this process based on tooth position was not possible.

Burial Taphonomy

S3 12.1: 4th lumbar vertebra (L4) and S3 12.2: lumbosacral transitional vertebra: The left inferior articular facets of L4 and the superior articular facet of the sacralized L5 were found preserved in articulation. A fresh breakage at the transition of L4's vertebral body to its inferior articular facet separated the bone into two refitting pieces. The articulated position of the vertebrae proves that they remained in close anatomical order until the surrounding and connecting sediment solidified. The bones experienced only minor displacements by a slight posteroinferior rotation of L4 that did not cause the disarticulation of the vertebrae, and as such, they remained undisturbed until the solidification of the surrounding sediment was completed. S3 12.1 also contains old fractures that occurred before its excavation, as evidenced by sediment embedded within the trabecular architecture of the vertebral body. Also, in fragment S3 12.2, old fractures were identified based on the distinctive darker coloration of the fracture edges and by the presence of sediment infill in areas where the internal bone structures must have been exposed before the excavation. The shape of these older fracture edges is usually irregular and sharp. Since the anatomical order of these skeletal elements was maintained in the presence of strong bone fragmentation, it is likely that local compression of the sediment caused the postmortal fracturing observed in these bones.

S3 12.15: Femur (R): Despite the very good preservation of many bones, which show little to no surface damage, several bones experienced strong postmortem fragmentation prior to excavation. The right femur S3 12.15 shows how both post-excavational damage and taphonomy affected bone preservation. The proximal epiphyses and apophyses are not preserved, while the exposed internal bone structure appears filled with solidified sediment that reaches through the medullary cavity down to the distal end. The three preserved femoral fragments were therefore most likely found as a single fragile piece that split into the fragments after removal, as preserved today. This is also in-

dicated by the distinctive appearance of the fractured edges compared to the surrounding external surfaces. There appear to be two centers of energy impact associated with femoral fracture. The first fracture is oriented obliquely and located between the proximal and the intermediate diaphyseal portion. The second breakage occurred between the intermediate diaphyseal portion and the distal end. Here, the fragmentation is more irregular, with vertical, horizontal, and oblique fracture lines that separate the bone into several diaphyseal pieces, which were glued after excavation. A mix of old and fresh surface damage was also found in the lateral and medial condyles. On both sides, small bone fragments are missing, but the internal trabecular architecture appears free of sediment. While the medial condyle has clear, irregular, and sharp edges, with barely any sediment visible in its internal structures, the lateral condyle shows low amounts of sediment that could fill the internal space and might thus also be older. Most of the fractured edges are rounded and darker, while a smaller area anteriorly appears rather fresh, with a brighter appearance and irregular edge destruction.

S3 11.1/S3 12.13: Tibia (R), S3 12.12: Fibula proximal (R), and S3 12.18: Fibula diaphysis (L): Fragments of the right tibia and the right and left fibulae are attached to a rock and connected by solidified sediment as well as by some type of adhesive that was applied by previous examiners for the conservation of the block. The consistent sediment coverage and identical fracture morphology observed on these bones are strong indications that the solidified sediment block containing the bones represents the original finding context. All three bones are superimposed and attached to a relatively flat rock surface. The fragment of the right proximal fibula is obliquely aligned to the lateral surface of the right tibia. Its proximal diaphyseal portion is pointing towards the posterior surface of the tibia, and its malleolar articular facet is facing laterally away from its anatomical position. This indicates that the proximal ends of the right tibia and right fibula experienced only slight displacements of their original articulation.

The right tibia and right fibula superimpose the left fibula. The shaft of the left fibula forms a 35-degree angle with the diaphysis of the right tibia. The medial surface of the left fibula is in contact with the lateral surface of the right fibula. The distal end of the diaphysis fragment of the left fibula is located under the right tibia and fibula, and its proximal end is oriented cranially.

The preserved contextualization of these skeletal elements suggests that the left fibula was also not displaced far from its original burial position. This matches the depiction of the burial arrangement described in Mompherratou and Pitsios (1995) where they assessed, based on the spatial distribution of the disturbed lower leg remains, that the legs were crossed and in hyperflexion, i.e., the lower right limb was crossing the left leg and then placed underneath the left lower limb, while the body was placed laying on the left side (Mompherratou and Pitsios 1995). It also makes sense that the fibulae were found in direct contact with each other. It is likely that the rock found agglomerated with the bones moved to its present solidified position during an erosive phase of the depositional environment, which could have forcefully pushed away the left tibia from its anatomical alignment, while the left fibula experienced rotation primarily around its long axis. Another indication of this scenario is the fracturing patterns observed in the right tibia and fibula. All three bones are compressed against each other, and right at their contact points, there is a fracture line going through all bones up to the point where the left fibula is compressed against an angular point on the rock surface. Figure 10 shows this fracture pattern very nicely. That the right tibia and the fibulae remained in such a proximity to each other is very interesting, considering the strong evidence for an erosive event in the depositional environment that led to the destruction, removal, or displacement of the left tibia from its original anatomical alignment. The severely fractured left tibia S9.1 might be associated with the other lower limb remains of Apidima 3, but such a relationship could only be established based on the minimum number of skeletal elements. Nevertheless, it cannot be excluded that it belongs to a second individual, and considering the definite presence of at least two adult individuals, considering it was not found together with the other skeletal remains, and considering the previously described morphological differences, including the absence of the squatting facet, it seems more likely that the left tibia S9.1 belongs to a different individual.

S3 12.16: Femur (L), S3 12.17: Patella (L), and S3 8.21: Os coxae (L): Important information about Apidima 3's burial body posture and the burial taphonomy is preserved in the left femur S3 12.16 and the left patella S3 12.17, as well as in the left os coxae S3 8.21. The patella and distal femoral articular surface were found in anatomical articulation. The connection was preserved by a solidified sediment crust. The position of the patella is on the inferior aspect of the distal femoral joint. This indicates that the left leg was in a state of hyperflexion at the time of sediment solidification. The sediment crust was strong enough to keep the patella in place during an erosive event of the depositional environment that caused the subsequent compression, fragmentation, and displacement of the femur. The sedimentary erosion and displacement of the femur, however, did not occur in a high velocity movement of sediment mass, but rather as a slow and energetically impactful process that caused the fracturing of the acetabular rim of the left os coxae and the posterior displacement of the femur, where both bones were forcefully compressed against each other again. This is indicated by a thin layer of compact bone that replaced the destroyed lesser trochanter of the left femur and that refits to a negative in the compact bone of the left os coxae. The negative is located on the posterior surface of the ilium superior of the acetabular rim. It is likely that an event of sedimentary erosion led to the forceful dislocation of the left femur in a superior-posterior direction and to lateral rotation of the femoral head. Eventually, this erosional event also led to the destruction of the acetabular rim and the trochanteric morphology. However, the displacement of the femur ultimately stopped after approximately

Figure 10. Posterior view of the right tibia (S3 11.1). The right and left fibulae of Apidima 3 are attached to the lateral surface of the right tibia. All three bones are together compressed against the surface of a rock. Visible is a crack going through all three bones and originating at the contact point of the rock surface.

5–10cm, and the posterior surface of the femoral proximal end became compressed against the posterior surface of the left coxae.

S3 13.1: Humerus (L), S3 13.2: Scapula (L): The left humerus and the left scapula are preserved in similar agglomerations as the previously described cases. Based on our visual examination, we can conclude that the components of the left glenohumeral joint were found connected in anatomical order and preserved as such by a solidified sediment crust. The elements were affected only by a low degree of disarticulation due to compression within their depositional environment. The compression led to extensive destruction of the scapular blade, but areas in direct contact with the humerus remained attached to it as the surrounding sediment solidified over time. This includes the anterior margin of the glenoid fossa that was compressed into the posterior surface of the humeral head and the inferior angle that was found attached to the anterior surface of the humeral diaphysis. The compression of the left humerus against the scapula also led to the fracturing of the humerus diaphysis. The agglomeration of the left humerus and left scapula near their original articulation indicates that the skeletal remains remained undisturbed until the connecting sediment solidified. This is furthermore indicated by preserved rib shaft fragments that are also attached to the humeral diaphysis.

S3 8.10: Scapula (R): The left scapula is also heavily fragmented. Unlike the right scapula, it did not solidify in agglomeration near a corresponding joint, but its lateral border fragment agglomerated with several costal head fragments on it. Most likely due to an erosive event or due to the compression of the decomposed body, the ribs turned upside down before they were compressed against the right scapula.

DISCUSSION AND CONCLUSION

The Upper Paleolithic of Greece is known from only a few sites, where human remains are either absent, highly fragmented, or recovered from insecure contexts (e.g., Harvati 2016; Harvati et al. 2009; Tourloukis and Harvati 2018). Additionally, human skeletal remains of Early Upper Paleolithic affiliation are rare across Europe and typically consist of isolated specimens rather than burials (d'Errico and Vanhaeren 2015; Riel-Salvatore and Gravel-Miguel 2013). New dating results for three pierced shells that may have been associated with the burial of Apidima 3 indicate the possibility of an intrusive Gravettian burial context within the sedimentary environment that contained the Protoaurignacian lithic assemblage excavated during Pitsios' excavations (Harvati et al. 2026b [this issue]; Lombardo et al. 2026b [this

issue]). Further refinement of the chronocultural affiliation and biology of Apidima 3 is therefore of great interest, not only for the fossil record of Greece but also for Europe in general, as it can provide crucial biological information on these elusive populations.

Our comprehensive investigation of Apidima 3 supports the original assessment of female biological sex based on pelvic morphology (Mompherratou and Pitsios 1995; Pitsios 1999). This is also consistent with our osteometric comparisons of long bone measurements and body mass estimates of 56.69kg to 58.27kg, in which Apidima 3 falls within the range of Upper Paleolithic females. In contrast, our age-at-death determination differs from the originally assigned age range of 20 to 25 years. Based on our careful examination of the auricular morphology, combined with severe tooth abrasion and signs of advanced joint degeneration, including inflammatory processes of osteoarthritis in several joints, we concluded that Apidima 3 lived into advanced adulthood, with a likely age at death between 40 and 60 years. However, the presence of a (possibly partially) fused lumbosacral transitional vertebra and associated sacral dysmorphism altered the position and morphology of the auricular surface (Mahato 2020; Matson et al. 2020), and might have contributed to the development of osteoarthritis (Illez et al. 2018), thereby influencing our assessment of Apidima 3's age-at-death based on the auricular surface of the left os coxae (S3 8.21). Calce et al. (2018) tested the effects of osteoarthritis on the accuracy of age determination using the Buchberry and Chamberlain (2002) method (among others), which we also included in our assessment. They found a significant error in the age determination of younger individuals; however, they concluded that the presence of osteoarthritis in hip joints (including the sacroiliac joint) is frequently found in older individuals and thus a good indication of advanced age as long as it developed due to biomechanical stress (not trauma) and as long as it is considered together with other age indicators and skeletal elements since the etiology of osteoarthritis can be multifactorial (Calce et al. 2018). Apidima 3 shows signs of joint degeneration with varying degrees of bone proliferation and inflammatory destruction in several skeletal elements. Moreover, the severe occlusal wear on her teeth also indicates intensive use going beyond food mastication over a long period of time, again suggesting that the individual died in her mature years.

The presence of deeply incising, artificially produced grooves on the interproximal surfaces of several of her teeth, furthermore, indicates the use of teeth for non-masticatory activities. Similar observations have been made in the dentition of individuals from other European Upper Paleolithic sites, such as Neuessing, Grotte des Enfants, or Barma Grande (Formicola 1988), and have also been reported from Middle Paleolithic contexts, including the nearby Kalamakia Neanderthal site in Mani (Harvati et al. 2013), and in early *Homo* specimens from Olduvai Gorge (Estalrrich et al. 2020; Ungar et al. 2001). Possible activities that could have produced interproximal grooves include, for example, the use of toothpicks for dental healthcare (Estalrrich et al. 2020; Estalrrich and Marín-Arroyo 2021; Frayer 1991; Ungar et al. 2001) and the processing of sinew and fibers (Brown and Molnar 1990), but the exact etiology of these grooves may be diverse (Ungar et al. 2001). A natural cause for the formation of such grooves, e.g., due to accumulated fibrous plant material, seems to be unlikely as the grooves appear only in the posterior dentition with almost identical elongated shape and orientation (Ungar et al. 2001). The presence of microstriations in the interproximal grooves of Apidima 3 should be confirmed microscopically to underline the use of toothpicks as the likely cause of their formation.

Apidima 3's discovery and excavation were, unfortunately, poorly documented. The descriptions of the burial and information provided by Mompherratou and Pitsios (1995), Pitsios and Leibhaber (1995), and Pitsios (1999) offer insight into the discovery of the human remains and the excavators' interpretation of the burial arrangement; however, little underlying data are provided to illustrate the spatial relationships between the skeletal remains and the material culture or depositional environment. Therefore, we carefully investigated bone preservation and the arrangement of skeletal elements to better understand the burial taphonomy, as several bones were preserved in connection by a solidified sediment crust. Several anatomical regions were thus preserved in a conglomerate of bones, where the skeletal elements were situated near their actual anatomical positions or in articulation. This indicates that Apidima 3 was covered by sediment soon after death, confirming that her lower limbs were flexed to her body, as described by Mompherratou and Pitsios (1995) and Pitsios (1999). We could not find any evidence that her arms were also flexed and close to the thorax; however, elements of the glenohumeral joints and bone fragments of ribs and vertebrae were found attached to the humeri, suggesting preservation in anatomical order. The fact that the sediment crust is present on the surface of all bones and connects several skeletal elements of different body parts in their approximate anatomical position suggests that the solidification of the sediment occurred soon after the body's decomposition. This furthermore implies that the body was covered by sediment soon after the individual's death, potentially as part of an intentional inhumation or due to massive sediment deposition related to an erosional event.

The excavators described that the upper part of the skeleton was found intact, while the lower limbs were affected by disturbances of the depositional context (Mompherratou and Pitsios 1995; Pitsios 1999). The thorax was found facing down, and the body was lying on its left side, perpendicular to the long axis of the cave, with the head facing the cave entrance—although the cranium itself was not recovered (Pitsios 1999). The exact discovery situation and skeletal arrangement cannot be examined anymore, and, unfortunately, no image data were published showing the context of any of Apidima 3's disturbed or undisturbed remains. The only excavation image is a photo of low quality showing the finding situation of the left tibia (S9.1) in a non-localizable position in the cave, stuck be-

tween several larger rocks (Pitsios 1999: Figure 4). Only an idealized artistic sketch showing the reconstructed burial arrangement has been published (Mompherratou and Pitsios 1995; Pitsios 1999). It does not appear unlikely that Apidima 3 was buried in a side position, given our observations of preservation in the lower limbs and assuming the excavators' description of the undisturbed upper body is accurate. Similar burials that match the descriptions and observations of Apidima 3's skeletal arrangement were observed, e.g., for the Gravettian burials Dolní Věstonice 3 (Trinkaus and Jelínek 1997) and Caviglione (Formicola and Holt 2015), but also individuals associated with the Magdalenian culture, like El Mirón (Carrero et al. 2015), were found lying on the side with flexed limbs.

The largely intact anatomical order of the skeletal elements, the level of skeletal completeness, and the absence of gnawing or bite marks strongly suggest that there was no carnivore activity around the skeleton. Most of the missing bones are elements of the hands and feet, which are the smallest components of the skeleton and can also be easily overlooked during excavation or displaced by erosion of the depositional environment (Mompherratou and Pitsios 1995; Pitsios 1999). The state of bone preservation also suggests that pressure and compression were likely the primary causes of the displacement and fragmentation of most bones, while erosion of the depositional environment might have disturbed the lower limbs, as described by the excavators (Mompherratou and Pitsios 1995; Pitsios 1999). The few fragments that were found from Apidima 3's cranium imply that the head must have been preserved until some event caused the severe fragmentation and, apparently, also the loss of most of the cranial bones. The excavators describe a stone slab located at the anatomical position of Apidima 3's cranium and interpreted it as part of the ritual burial to support the head (Mompherratou and Pitsios 1995; Pitsios 1999). However, it is also possible that this stone slab was part of a depositional erosion event that could have caused the skull's fragmentation. As several teeth of Apidima 3 were found in different square units at varying depths, according to the original description in Mompherratou and Pitsios (1995), it seems likely that the upper body and/or the cranial region were also affected by reworking of the depositional context.

The description of the Apidima 3 burial, as published in Mompherratou and Pitsios (1995) and Pitsios (1999), should thus not be considered as an accurate depiction of the original inhumation. Apidima 3 has been presented as a ritual burial context that included grave goods such as lithics, 43 pierced seashells of the species *Nassa neritea*, a small piece of quartzite, a special stone disc, and a tibia of a cervid, which were all arranged around the bones as part of the ritual according to the excavators (Mompherratou and Pitsios 1995; Pitsios 1999). While we do not question that these finds were retrieved from the same depositional environment, one should be cautious about considering them associated with the burial itself, since no clear spatial information or other data are provided alongside the excavators' descriptions and interpretations. It is also possible that Apidima 3 is intrusive into the surrounding depositional context, and that its true affiliation is to a younger phase of the Upper Paleolithic rather than the Aurignacian, as suggested by the latest dating results on samples from Cave C that placed pierced shells reported to be found with Apidima 3 in a range of 24.5 and 31.8 ka cal BP, pointing to a potential Gravettian attribution. It is worth noting that a late Gravettian / early Epigravettian assemblage has been identified in Cave D (Lombardo et al. 2026a [this issue]; Harvati et al. 2026b [this issue]), showing human presence in the Apidima cave complex also during this period. However, the question of the chronocultural attribution of Apidima 3 can only be resolved with additional direct dating of the skeleton, and efforts to that effect are currently ongoing.

Some weak support for an early Upper Paleolithic attribution comes from our comparative analysis of the Apidima 3 stature estimates. The mean stature estimate of 162.85cm is closer to the PRE-LGM female group mean of 165.94cm (n=9)—although some of the individual estimates are placed closer to the mean of the POST-LGM female group of 159.1 cm (n=5). It should also be noted that the variation in Apidima 3's femur-based stature estimates is greater compared to the tibia and produces values that fall closer to the group mean of the PRE-LGM group as well. Even though Figure 5 shows a clear difference in the distribution of stature estimates between individuals of the PRE- and POST-LGM groups, as it has been described previously (Formicola and Giannecchini 1999; Holt and Formicola 2008), our results should be considered with caution, as the sample sizes of the comparative groups are small and cover a wide geographic range. Apidima 3's stature estimates fall within the overlap range between both groups. A slight tendency towards the lower end of the variation range, typical of the PRE-LGM group, is also apparent. If Apidima 3's actual chronological position is POST-LGM, it would be one of the tallest (body size) female representatives known for this chronological group.

Our study also provided an inventory update of human remains from Cave C, reinvestigated the biology and health status of Apidima 3, and detailed morphological descriptions, along with osteometric data, of this individual's skeletal elements. The inventory reassessment was an important task, as several additional individuals were originally reported to have been found in Apidima Cave C (Mompherratou and Pitsios 1995; Pitsios 1985, 1999). However, it was unclear which finds might be associated with these additional individuals and what the minimum number of individuals found in Cave C was. During our reassessment of the inventory of human remains from Cave C, we identified 17 IDs that had received an individual ID but had not been assigned to Apidima 3. Among these 17 IDs, we identified one tooth (S11.1) as belonging to an animal. ID S26.1 was identified as definitely belonging to a second adult individual, since it represents a second right talus that can be distinguished from Apidima 3's right talus (S3 8.5) based on differences in preservation and based on the presence of trochlear extensions (squatting facets) in both

of Apidima 3's tali. Also, the left tibia (S9.1) was identified as belonging to a second adult individual despite the lack of left tibia fragments among Apidima 3's skeletal elements. The squatting facets on Apidima 3's tali are also evident in her right tibia (S3 12.13); however, the left tibia (S9.1) does not exhibit any similar characteristics. S9.1 also appears morphologically very distinctive in diaphyseal shape; however, the severe fragmentary condition makes reliable morphological assessments and quantitative comparisons with the right tibia impossible. The remaining bone IDs of human remains that were originally not assigned to Apidima 3 are all hand phalanges and isolated teeth. Among these remains are three IDs (O551.1: sesamoid; O302.1: proximal hand phalanx; O107a.1: incisor) that were originally assigned to the fauna of Cave C but are now identified as human bones, likely also from Apidima 3. Even though several of these elements exhibit similar characteristics of Apidima 3's remains, such as the degree of dental occlusal wear combined with the presence of interproximal grooves, uncertainty persists regarding their association with either Apidima 3, Apidima 4, or a potentially unrecognized additional individual due to the lack of spatial information and archaeological contextualization.

The osseous finds from Cave C typically exhibit similar preservation characteristics, namely, generally good bone preservation with partial to severe fragmentation and a solid sediment crust covering most or all of the bone surface. Therefore, bones could only be distinguished from Apidima 3's remains based on differences in their morphological characteristics. In the case of the dental remains, all teeth were found with severe occlusal abrasion, and several teeth were found with interproximal grooves similar to those found in the maxilla (S15.1) and mandibula (S3 16.1) fragments of Apidima 3. The severe degeneration and fragmented state of preservation of the dental remains from Cave C do not provide any other morphological characteristics to distinguish whether they belong to more than one individual. The last bone identified as belonging to a second adult individual was found among the bones originally assigned to Apidima 3. There, we found a second right lateral cuneiform (S3 19.3) and identified it as not part of Apidima 3 based on its distinctive morphological appearance compared to the other tarsal remains. In summary, only the left tibia (S9.1), the right talus (S26.1), and the right lateral cuneiform (S3 19.3) could be identified as secured human remains of a second adult individual. Since several uncertainties exist about the depositional context and the excavated stratigraphy from the first excavation in 1984 (Pitsios 1985, 1999), including the spatial relationships of the human remains, we can at this point only be confident about the presence of at least two adult individuals retrieved from the Upper Paleolithic context of Apidima Cave C. Most bones listed in the inventory of human remains in Table 1 are associated with Apidima 3, which is confirmed based on their preservation and our morphological assessments, however, the presence of a second adult individual—Apidima 4—is also secured and its remains are marked with an asterisk in Table 1. Nevertheless, several uncertainties exist about the discovery and excavation of the human remains from Apidima Cave C, and it cannot be excluded that isolated human remains might actually belong to additional, unrecognized individuals.

It will also depend on future discoveries of new human remains to enhance our understanding of Upper Paleolithic human skeletal biology, cultural behavior, and mortuary practices in Greece. Information about Apidima 3's skeletal morphology, biology, behavior, and health status is, therefore, so far, the most representative source about the Upper Paleolithic hunter-gatherer populations that inhabited this region. Our study thus provides important and unique data for an area that currently lacks comparable records, highlighting the need for a detailed examination of the human remains from Apidima Cave C and their international recognition as a significant case for future comparative research on Upper Paleolithic human remains. This is further underscored by the geographic position of Greece and the Balkan peninsula, which served as an important route for the migration of human populations from lower to higher latitudes during the Middle and Late Pleistocene (Dennell et al. 2011; Harvati and Roskandic 2016; Harvati et al. 2009; 2019), as well as a climatic refugium during glacial times (e.g., Karaiskou et al. 2014; Kyrikou et al. 2025; Roditi et al. 2024; Tourloukis and Harvati 2018).

ACKNOWLEDGEMENTS

This research was supported by the European Research Council (ERC-AdG-101019659, "FIRSTSTEPS"). K.H. is also supported by the DFG (FOR 2237; HA 5258/19 Leibniz award 2021) and by the Carl Friedrich von Siemens Foundation. This study was conducted under permit from the Hellenic Ministry of Culture (ΑΔΑ: 6Σ0Σ46ΝΚΟΤ-44Ζ; ΥΠΠΟ/Φ77/333615π.ε.) under the auspices of the Norwegian Institute at Athens. We are grateful to Professor M. Kouloukoussa for her support during the initial phases of this study, and to Nicholas C. Thompson, Arazik Baboomian, and Saman Hamzavi-Zarghani for their support with photography and image processing. We thank the anonymous reviewers for their helpful comments and suggestions which greatly improved this work.

DATA AVAILABILITY STATEMENT

The authors confirm that the data generated by this study or data used to produce the findings are available within the article and the supplementary material.

CONFLICT OF INTEREST

The authors declare no conflicts of interest.

AUTHOR CONTRIBUTIONS

DN: Conceptualization, Data curation, Formal analysis, Investigation, Methodology, Project administration, Visualization, Writing – original draft, Writing – review & editing; **KH**: Conceptualization, Funding acquisition, Methodology, Project administration, Supervision, Writing – original draft, Writing – review & editing; **VG**: Resources; **KE**: Resources.

REFERENCES

Baykara, I., Yilmaz, H., Gültekin, T., Güleç, E., 2010. Squatting facet: a case study Dilkayaand Van-Kalesi populations in wastern Turkey. Coll. Antropol. 34, 1257–1262.

Bollow, M., Braun, J., Eitel, B.M., Fischbach, R., Gieseke, J., Grampp, S., Heuck, A., Lang, P., Layer, G., Lutterbey, G., Schnarkowski, P., Stäbler, A., Träber, F., Winter, P., 2000. Sacroiliac joints. In: Vahlensieck, M., Genant, H.K., Reiser, M., Johnston, J.O., Steinborn, M. (Eds.), MRI of the Musculoskeletal System. Georg Thieme Verlag KG, Stuttgart. https://doi.org/10.1055/b-0034-51209

Boulle, E.-L., 2001. Evolution of two human skeletal markers of the squatting position: a diachronic study from antiquity to the modern age. Am. J. Phys. Anthropol. 115, 50–56.

Brown, T., Molnar, S., 1990. Interproximal grooving and task activity in Australia. Am. J. Phys. Anthropol. 81, 545–554.

Bräuer, G., 1988. Osteometrie. In: Knußmann, R. (Ed.), Wesen und Methoden der Anthropologie. 1. Teil Wissenschaftstheorie, Geschichte, morphologische Methoden. Gustav Fischer Verlag, Stuttgart, New York, pp. 160–231.

Buckberry, J.L., Chamberlain, A.T., 2002. Age estimation from the auricular surface of the ilium: a revised method. Am. J. Phys. Anthropol. 119, 231–239.

Buikstra, J.E., Ubelaker, D., 1994. Standards for Data Collection From Human Skeletal Remains. Arkansas Archeological Survey Research Series no. 44, Fayetteville, AR.

Calce, S.E., Kurki, H.K., Weston, D.A., Gould, L., 2018. Effects of osteoarthritis on age-at-death estimates from the human pelvis. Am. J. Phys. Anthropol. 167, 3–19.

Carretero, J.M., Rodríguez, L., García-Gonzalez, R., Arsuaga, J.L., Gomez-Olivencia, A., Lorenzo, C., Bonmatí, A., Gracia, A., Martínez, I., Quam, R., 2012. Stature estimation from complete long bones in the Middle Pleistocene humans from the Sima de los Huesos, Sierra de Atapuerca (Spain). J. Hum. Evol. 62, 242–255.

Carrero, J.M., Quam, R.M., Gomez-Olivencia, A., Castilla, M., Rodríguez, L., García-González, R., 2015. The Magdalenian human remains from El Miron Cave, Cantabria (Spain). J. Archaeol. Sci. 60, 10–27.

Castellvi, A.E., Goldstein, L.A., Chan, D.P., 1984. Lumbosacral transitional vertebrae and their relationship with lumbar extradural defects. Spine 9(5), 493–495. https://doi.org/10.1097/00007632-198407000-00014

Darlas, A., 1995. L'industrie lithique trouvée avec le squelette de femme LAO 1/S 3 de la Grotte d'Apidima (Mani – Grèce). Acta Anthropol. 1, 59–64.

Dennell, R.W., Martinón-Torres, M., Bermúdez de Castro, J.M., 2011. Hominin variability, climatic instability and population demography in Middle Pleistocene Europe. Quatern. Sci. Rev. 30, 1511–1524.

d'Errico, F., Vanhaeren, M., 2015. Upper Palaeolithic mortuary practices: reflection of ethnic affiliation, social complexity, and cultural turnover. In: Renfrew, C., Boyd, M., Morley, I. (Eds.), Death Rituals, Social Order and the Archaeology of Immortality in the Ancient World: 'Death Shall Have No Dominion.' Cambridge University Press, Cambridge, UK, pp. 45–62.

Estalrrich, A., Alarcón, J.A., Rosas, A., 2020. Toothpicking in early *Homo* OH 62 from Olduvai Gorge (Tanzania): an indirect evidence of intensive meat consumption? J. Hum. Evol. 143, 102769.

Estalrrich, A., Marín-Arroyo, A.B., 2021. Evidence of habitual behavior from non-alimentary dental wear on deciduous teeth from the Middle and Upper Paleolithic Cantabrian region, Northern Spain. J. Hum. Evol. 158, 103047.

Facorellis, Y., Kyparissi-Apostolika, N., Maniatis, Y., 2001. The Cave of Theopetra, Kalambaka: radiocarbon evidence for 50,000 years of human presence. Radiocarbon 43, 1029–1048

Formicola, V., 1988. Interproximal grooving of teeth: additional evidence and interpretation. Curr. Anthropol. 29, 663–671.

Formicola, V, Franceschi, M., 1996. Regression equations for estimating stature from long bones of early Holocene European samples. Am. J. Phys. Anthropol. 100, 83–88.

Formicola, V., Giannecchini, M., 1999. Evolutionary trends of stature in Upper Paleolithic and Mesolithic Europe. J. Hum. Evol. 36, 319–333.

Formicola, V., Holt, B.M., 2015. Tall guys and fat ladies: Grimaldi's Upper Paleolithic burials and figurines in an historical perspective. J. Anthropol. Sci. 93, 71–88. https://doi.org/10.4436/jass.93007

Frayer, D.W., 1991. On the etiology of interproximal grooves. Am. J. Phys. Anthropol. 85, 299–304.

Harvati, K., Panagopoulou, E., Runnels, C., 2009. The paleoanthropology of Greece. Evol. Anthropol. 18, 131–143.

Harvati, K., Darlas, A., Bailey, S.E., Rein, T.R., El Zaatari, S., Fiorenza, L., Kullmer, O., Psathi, E., 2013. New Neanderthal remains from Mani peninsula, S. Greece: the Kalamakia Middle Palaeolithic cave site. J. Hum. Evol. 64, 486–499.

Harvati, K., Douka, K., Shao, Q., Grün, R., Thompson, N., Gorgoulis, V., Evangelou, K., Tourloukis, V., Panagiotis, K., 2026b. New radiometric dates for the Apidima Caves C and D (Greece) Upper Paleolithic Legacy Collections. Special issue: The Apidima legacy collections: new analyses and interpretations. PaleoAnthropology 2026:2.

Harvati, K., Grün, R., Duval, M., Zhao, J., Karakostis, A., Tourloukis, V., Gorgoulis, V., Kouloukoussa, M., 2021. Direct U-series dating of the Apidima C human remains. In: Reyes-Centeno, H., Harvati, K. (Eds.), Ancient Connections in Eurasia. Kerns Verlag, Tübingen, pp. 37–55.

Harvati, K., Roksandic, M. (Eds.), 2016. Paleoanthropology of the Balkans and Anatolia: Human Evolution and its

Context. Vertebrate Paleobiology and Paleoanthropology Series. Springer, Dordrecht.

Harvati, K., Röding, K., Bosman, A.M., Karakostis, F.A., Grün, R., Stringer, C., Karkanas, P., Thompson, N.C., Koutoulidis, V., Moulopoulos, L.A., Gorgoulis, V.G., Kouloukoussa, M., 2019. Apidima Cave fossils provide earliest evidence of *Homo sapiens* in Eurasia. Nature 571, 500–504.

Harvati, K., Roditi, E., Grün, R., Thompson, N., Röding, C., Gorgoulis, V., Evangelou, K., 2026a. Middle Pleistocene funerary ritual at Apidima? An examination of the evidence. Special issue: The Apidima legacy collections: new analyses and interpretations. PaleoAnthropology 2026:2

Holt, B.M., Formicola, V., 2008. Hunters of the Ice Age: the biology of Upper Paleolithic people. Yrbk. Phys. Anthropol. 51, 70–99.

Illeez, O.G., Atıcı, A., Ulger, E.B., Kulcu, D.G., Ozkan, F.U., Aktas, I., 2018. The transitional vertebra and sacroiliac joint dysfunction association. Eur. Spine J. 27, 187–193.

Karaiskou, N., Tsakogiannis, A., Gkagkavouzis, K., Papika, S., Latsoudis, P., Kavakiotis, I., Pantis, J., Abatzopoulos, T., Triantaphyllidis, C., Triantafyllidis, A., 2014. Greece: a Balkan sub-refuge for a remnant red deer (*Cervus Elaphus*) population. J. Hered. 105, 334–344.

Karakostis, A.F., Hotz, G., Rademaker, K., Gorgoulis, V., Evangelou, K., Harvati, K., 2026. Exploring the habitual manual activities of a possible Upper Paleolithic individual from Greece ("Apidima 3"). Special issue: The Apidima legacy collections: new analyses and interpretations. PaleoAnthropology 2026:2.

Karali-Giannakopoulou, I., 1995. Preliminary report on malacological material found in Apidima Cave in Laconia. Acta Anthropol. 1, 159–163.

Karsten, J.K., 2017. A test of the preauricular sulcus as an indicator of sex. Am J. Phys. Anthropol. 165, 604–608. https://doi.org/10.1002/ajpa.23372

Kassambara, A., 2023. ggpubr: 'ggplot2' based publication ready plots. R package version 0.6.0. https://CRAN.R-project.org/package=ggpubr

Kouloukoussa, M., 2021. Direct U-series dating of the Apidima C human remains. In: Reyes-Centeno, H., Harvati, K. (Eds.), Ancient Connections in Eurasia. Kerns Verlag, Tübingen, pp. 37–55.

Kyrikou, S., Marinova, E., Bludau, I.J.E., Karkanas, P., Panagopoulou, E., Tourloukis, V., Junginger, A., Harvati, K., 2025. The palynological record from Marathousa 1, south Greece, during Marine Isotope Stage (MIS) 12: local environment and fire history. Quatern. Res. 128, 71–90. https://doi.org/10.1017/qua.2024.59

Ligoni, E., Papagrikorakis, M., 1995. Odontological examination of skeleton LAO 1/S 3. Acta Anthropol. 1, 53–58.

Liritzis, Y., Maniatis, Y., 1995. ESR experiments on calcites and bones for dating purposes. Acta Anthropol. 1, 85–92.

Lombardo, S., Thompson, N.C., Gorgoulis, V.G., Evangelou, K., Harvati, K., Tourloukis. V., 2026b. Early Upper Paleolithic technical behavior at Apidima (Peloponnese, Greece): technological analysis of the lithic assemblage from the Cave C legacy collection. Special issue: The Apidima legacy collections: new analyses and interpretations. PaleoAnthropology 2026:2.

Lombardo, S., Thompson, N.C., Roditi, E., Gorgoulis, V.G., Evangelou, K., Harvati, K., Tourloukis. V., 2026a. Apidima Cave at the Last Glacial Maximum: the Lithic Legacy Collection of Cave D (Peloponnese, Greece). Special issue: The Apidima legacy collections: new analyses and interpretations. PaleoAnthropology 2026:2.

Lovejoy, C.O., Meindl, R.S., Pryzbeckm T.R., Mensforth, R.P., 1985. Chronological metamorphosis of the auricular surface of the ilium: a new method for the determination of adult skeletal age at death. Am J. Phys. Anthropol. 68, 15–28.

Mallegni, F., Bertoldi, F., Manolis, S., 2000. Palaeobiology of two Gravettian skeletons from Veneri cave (Parabita, Puglia, Italy). Homo 51(2–3), 235–257.

Manolis, S.K., 1996. The Hellenic Late Pleistocene fossils. Anthropologie 34(1/2), 89–97.

Mompheratou, E., Pitsios. T.K. 1995. Apidima, cave Gamma (Γ): the burial of female skeleton LAO 1 /S3. Acta Anthropol. 1, 27–51.

Nakajima, A., Usui, A., Hosokai, Y., Kawasumi, Y., Abiko, K., Funayama, M., Saito, H., 2014. The prevalence of morphological changes in the thoracolumbar spine on whole-spine computed tomographic images. Insights Imaging 5, 77–83. https://doi.org/10.1007/s13244-013-0286-0

Novak, L., Schultz, J.J., McIntyre, M., 2012. Determining sex of the posterior ilium from the Robert J. Terry and William M. Bass Collections. J. Foren. Sci. 57 (5), 1155–1160. https://doi.org/10.1111/j.1556-4029.2012.02122.x

Ntinou, M., 2021. Vegetation change in southeastern Greece during the Late Pleistocene. The wood charcoal record from Klissoura Cave 1 (Peloponnese, Greece). Quatern. Int. 593–594, 104–117.

Pearson, K., 1899. On the reconstruction of the stature of prehistoric races. Mathematical Contributions to the Theory of Evolution 5, pp. 169–244.

Pitsios, T.K. 1985. Παλαιοανθρωπολογικές έρευνες στη θέση «Απήδημα» της Μέσα Μάνης. Αρχαιολογία 15, 26–33.

Pitsios, T.K. 1995. Paleoanthropological research at the cave site of Apidima, Laconia, Greece. Acta Anthropol. 1, 1–180.

Pitsios, T. 1999. Paleoanthropological research at the cave site of Apidima and the surrounding region (South Peloponnese, Greece). Anthrop. Anz. 57, 1–11.

Pitsios, T., Liebhaber, B. 1995. Research conducted in Apidima and the surrounding region – Taenarius man - . Acta Anthropol. 1, 175–179.

Riel-Salvatore, J., Gravel-Miguel, C., 2013. Upper Palaeolithic mortuary practices in Eurasia: a critical look at the burial record. In: Stutz, L.N., Tarlow, S. (Eds.), The Oxford Handbook of the Archaeology of Death and Burial. Oxford Academic, Oxford, UK, pp. 302–346. https://doi.org/10.1093/oxfordhb/9780199569069.013.0017

Roditi, E., Bocherens, H., Konidaris, G.E., Athanassiou, A., Tourloukis, V., Karkanas, P., Panagopoulou, E., Harvati, K., 2024. Life-history of *Palaeoloxodon antiquus* reveals Middle Pleistocene glacial refugium in the Megalopolis basin, Greece. Sci. Rep. 14, 1390. https://doi.org/10.1038/s41598-024-51592-9

Ruff, C.B., Burgess, M.L., Squyres, N., Junno, J.-A., Trinkaus, E., 2018. Lower limb articular scaling and body mass estimation in Pliocene and Pleistocene hominins. J. Hum. Evol. 115, 85–111.

Ruff, C.B., Holt, B.M., Niskanen, M., Sladék, V., Berner, M., Garofalo, E., Garvin, H.M., Hora, M., Maijanen, H., Niinimäki, S., Salo, K., Schuplerová, E., Tompkins, D., 2012. Stature and body mass estimation from skeletal remains in the European Holocene. Am. J. Phys. Anthropol. 148, 601–617.

Ruff, C.B., Squyres, N., Junno, J.A., 2020. Body mass estimation in hominins from humeral articular dimensions. Am J. Phys. Anthropol. 173, 480–499.

Ruff, C.B., Wood, B.A., 2023. The estimation and evolution of hominin body mass. Evol. Anthropol. 32, 223–237. https://doi.org/10.1002/evan.21988

Rösing, F.W., 1988. Körperhöhenrekonstruktion aus Skelettmaßen. In: Knußmann, R. (Ed.), Anthropologie. Handbuch der vergleichenden Anthropologie des Menschen. Begründet von Rudolf Martin. Fischer, Stuttgart, pp. 586–600.

Satinoff, M.I., Study of the squatting facets of the talus and tibia in ancient Egyptians. J. Hum. Evol. 1, 209–212.

Schaefer, M., Black, S., Scheuer, L., 2009. Juvenile Osteology: A Laboratory and Field Manual. Academic Press (Elsevier), Cambridge, MA.

Sjøvold, T., 1990. Estimation of stature from long bones utilizing the line of organic correlation. Hum. Evol. 5, 431–447.

Smith, B.H., 1991. Standards of human tooth formation and dental age assessment. In: Kelley, M.A., Larsen, C.S. (Eds.), Advances in Dental Anthropology. Wiley-Liss, New York, pp. 143–168.

Stravopodi, E., Manolis, S., Kyparissi-Apostolika, N., 1999. Paleoanthropological findings from Theopetra cave in Thessaly: a preliminary report. In: Bailey, E., Adam, E., Panagopoulou, E., Perlès, C., Zachos, K. (Eds.), The Palaeolithic Archaeology of Greece and Adjacent Areas: Proceedings of the ICOPAG Conference, Ioannina, September 1994. British School at Athens Studies 3, London, pp. 271–281.

Timme, M., Viktorov, J., Steffens, L., Steeter, A., Krach, A., Schmeling, A., 2024. Third molar eruption in dental panoramic radiographs as a feature for forensic age assessment – new reference data from a German population. Head Face Med. 20, 1–9.

Tourloukis, V., Harvati, K., 2018. The Palaeolithic record of Greece: a synthesis of the evidence and a research agenda for the future. Quatern. Int. 466, 48–65.

Trinkaus, E., Jelínek, J., 1997. Human remains from the Moravian Gravettian: the Dolní Věstonice 3 postcrania. J. Hum. Evol. 33 (1), 33–82. https://doi.org/10.1006/jhev.1997.0142

Trotter, M., Gleser, G.C., 1952. Estimation of stature from long bones of American whites and Negroes. Am. J. Phys. Anthropol. 10, 463–514.

Ungar, P.S., Grine, F.E., Teaford, M.F., Pérez-Pérez, A., 2001. A review of interproximal wear grooves on fossil hominin teeth with new evidence from Olduvai Gorge. Arch. Oral Biol. 46, 285–292.

Waldron, T., 2019. Joint Disease. In: Buikstra, J.E. (Ed.), Ortner's Identification of Pathological Conditions in Human Skeletal Remains. Academic Press, London, pp. 719–748.

Wickham, H., 2016. ggplot2: Elegant Graphics for Data Analysis. Springer-Verlag, New York.

Wickham, H., François, R., Henry, L., Müller, K., Vaughan, D., 2023. dplyr: A Grammar of Data Manipulation. R package version 1.1.4. https://CRAN.R-project.org/package=dplyr

Wong, M., Sinkler, M.A., Kiel, J., 2023. Anatomy, Abdomen and Pelvis, Sacroiliac Joint. In: StatPearls [Internet]. StatPearls Publishing, Treasure Island (FL), pp. 1–4.

Special Issue: The Apidima Legacy Collections: New Analyses and Interpretations

Supplement 1 to New Bioanthropological Insights on the Possible Early Upper Paleolithic Cranial and Postcranial Human Remains from Apidima Cave C (Peloponnese)

DAVID NAUMANN
Paleoanthropology, Institute for Archaeological Sciences, Department of Geosciences, Eberhard Karls University of Tübingen, 72070 Tübingen, GERMANY; david.naumann@ifu.uni-tuebingen.de

VASSILIS G. GORGOULIS
Department of Histology and Embryology, Medical School, National and Kapodistrian University of Athens, Athens; Biomedical Research Foundation of the Academy of Athens, Athens, GREECE; Faculty Institute for Cancer Sciences, Manchester Academic Health Sciences Center, University of Manchester, Manchester M20 4GJ; and, Division of Cancer Research, Ninewells Hospital and Medical School, University of Dundee, DD19SY Dundee, UNITED KINGDOM; vgorg@med.uoa.gr

KONSTANTINOS EVANGELOU
Department of Histology and Embryology, and Museum of Anthropology, Medical School, National and Kapodistrian University of Athens, Athens; GREECE; cnevagel@med.uoa.gr

KATERINA HARVATI
Paleoanthropology, Institute for Archaeological Sciences and Senckenberg Center for Human Evolution and Paleoenvironments, Eberhard Karls Universität Tübingen; DFG Center for Advanced Studies 'Words, Bones, Genes, Tools', Eberhard Karls Universität Tübingen; HUMAN ORIGINS – Cluster of Excellence for Integrative Human Origins Studies (EXC 3101), Eberhard Karls University of Tübingen, GERMANY; Centre for Early Sapiens Behaviour (SapienCE), University of Bergen, NORWAY; and, Museum of Anthropology, Medical School, National and Kapodistrian University of Athens, Athens, GREECE; katerina.harvati@ifu.uni-tuebingen.de

SUPPLEMENT 1
This supplement contains: SI-text, SI-Figures 1–28, SI-Tables 1–23, and references.

MORPHOLOGICAL DESCRIPTION OF APIDIMA 3

Cranium

S15.1: Maxilla fragment including M1

A small maxilla fragment is recorded as S15.1 (SI-Figure 1), but it was found among the human remains originally assigned to the ID of an additional individual. The fragment represents a tiny portion of the left palate and a remnant of the left maxillary sinus. The first or second molar is situated in its alveolus, but most of the compact bone surrounding the tooth is damaged, including the enamel portion of the already heavily abraded tooth crown. No information about the cranial or maxillary morphology is preserved. The characteristics of the tooth, however, are very similar to those of other isolated teeth and to those of the mandibular molars preserved in the posterior ramus fragment S3 16.1. These characteristics include the presence of severe occlusal wear, interproximal grooves (located here on the distal surface at the contact between root and crown), a sediment crust covering most of the bone surface, and a high degree of fragmentation. S15.1 should therefore be considered as most likely belonging to Apidima 3, and it is the only preserved bone fragment of Apidima 3's cranium.

Additionally, 13 isolated teeth and their remains were found and are recorded under the IDs S3 7.1, S3 7.2, S3 10.5, S3 18.3, S3 18.4, S3 21.3, S3 21.4, S4.1, S5.1, S6.1, S7.1, S11a.1, O107a.1. All teeth show severe degrees of occlusal abrasion to the exposure of dentine in most of the area, and in several cases, even the pulp(s) are exposed. The strong occlusal abrasion and fragmentary condition of many isolated teeth limited the possibility of detailed assessments, and most of them could not be assigned to a position due to the lack of preservation of diagnostic features. Also, the presence of interproximal grooves in several of the isolated teeth should be noted. Although most isolated teeth exhibit general similarities, such as severe occlusal wear and the presence of interproximal grooves, we consider the possibility that the dental remains of more than one adult individual may have been retrieved from Cave C, but the lack of preservation of morphological characteristics excludes the possibility of confidently differentiating the teeth by individuals and even by intraindividual positions.

Mandibula

S3 16.1: Posterior ramus fragment including M1–M3 and S3 18.1: Anterior alveolar process

Two fragments of Apidima 3's mandible are preserved and shown in SI-Figure 1. S3 16.1 is a ramus fragment representing the posterior aspect of the right mandibular body and alveolar process. The preserved maximum length of the fragment is 44.86 mm. The fragment ends posteriorly 12.5 mm behind the distal aspect of M3. The most anterior portion of the internal oblique ridge is preserved, but the fragment ends at the transition to the ramus. The fracturing line continues vertically down to the inferior border of the mandibular body. The medial surface of the fragment shows the posterior part of the mylohyoid ridge and the submandibular fossa, but compact bone is not preserved anteriorly at the position of M1 and M2. The inferior border of the mandibular body is not preserved. Its fracture line is horizontal on both sides, with sharp, irregular edges. The mandibular fragmentation occurred before its excavation. All exposed internal surfaces are filled with solidified sediment. The posterior dentition is preserved with M1–M3 still sitting inside their alveolar bags. All teeth show a high degree of occlusal wear. Exposed dentin is present in most occlusal areas. The second fragment, S3 18.1, belongs to the anterior mandibular portion and preserves mainly the alveolar process with a maximum length of 29.5 mm. Like S3 16.1, it is broken horizontally on its inferior aspect. The anterior position of the fracture line is superior to the mentum, and posteriorly it is above the mental spines. The lateral fracture lines are vertical and located at the position of the canines. The alveolar bags for the first and second incisors are partially preserved. There is a relatively big gap of about 3.3 mm between the medial margins of the first incisors, which could indicate the presence of mandibular diastema. There are no signs of inflammation or other dental pathologies in the preserved mandibular morphology.

SI-Figure 1. Fragments of the maxilla (S15.1) and the mandible (S3 16.1, S3 18.1) of Apidima 3.

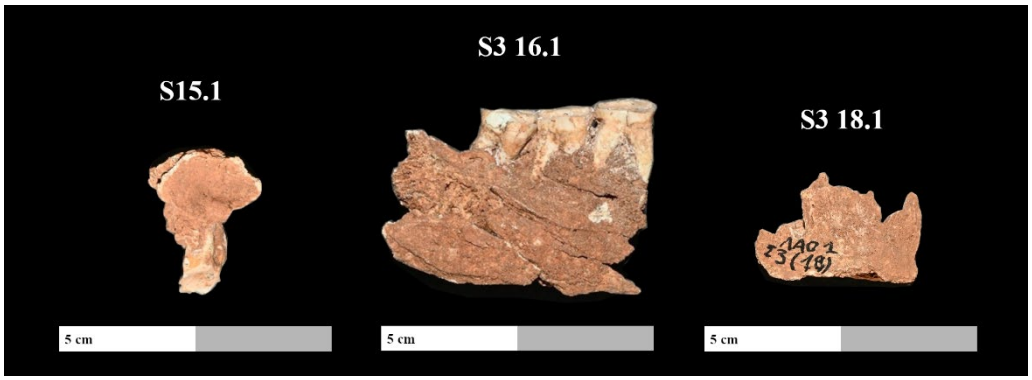

<u>Manubrium and Corpus sterni</u>

S3 8.22: Manubrium

S3 8.22 refers to the superior and left lateral portion of the manubrium. The clavicular articular facets are preserved on both sides, but the bone is broken obliquely from the right first articular facet to the left demifacet for the second rib. The preserved length of the manubrium is 43.52 mm with a width of 50.05 mm.

S3 8.25: Corpus sterni

S3 8.25 is the most distal portion of the sternal body with a preserved length of 40.15 mm. The right side is preserved up to the fifth costal notch. A fracture line extends from this point obliquely down to the sixth costal notch on the left side and demarks the area of preservation. A third fragment exists that represents the cranial portion of the sternal body and is also registered as S3 8.25. It refits with the caudal fragment and is overall well preserved. The first to fourth costal notches are in good condition and its surface is vastly covered with a thin sediment crust. The sediment crust limited visibility of surface details, but a few small lesions are identifiable on the second and fourth costal notches on the left side. The corpus sterni (S3 8.25) and manubrium fragment (S3 8.22) are shown in SI-Figure 2.

SI-Figure 2. Manubrium (S3 8.22; posterior view) and corpus sterni (S3 8.25) of Apidima 3.

Costae

The human skeletal assemblage from Apidima 3 comprises fragments of several ribs, most of which were recovered in a highly fragmented state. SI-Figure 3 provides a complete overview of all costal remains of Apidima 3. A few ribs are exceptionally well preserved, though only one rib (S3 10.3) is actually complete and was found attached to two other mostly complete ribs (posterior ends missing). The first ribs (S3 10.1 and S3 8.19) are both preserved, but the sternal and posterior ends are partially damaged. Overall, 15 rib fragments with preserved posterior ends are available, 11 of which come from left ribs and 4 belong to right ribs (S3 8.19, S3 8.17, S3 8.18, S3 17.6). Thirteen sternal ends are also preserved but mostly as isolated fragments (S3 15.1 - S3 15.3, S3 12.3, S3 10.2, S3 10.3, S3 14.2, S3 6.7, S3 8.20). Furthermore, a total of 43 shaft fragments were found among Apidima 3's costal remains.

The bone surfaces are primarily covered by sediment crust, but the underlying bone structure appears to be well-preserved in all rib fragments.

SI-Figure 3. Costae of Apidima 3.

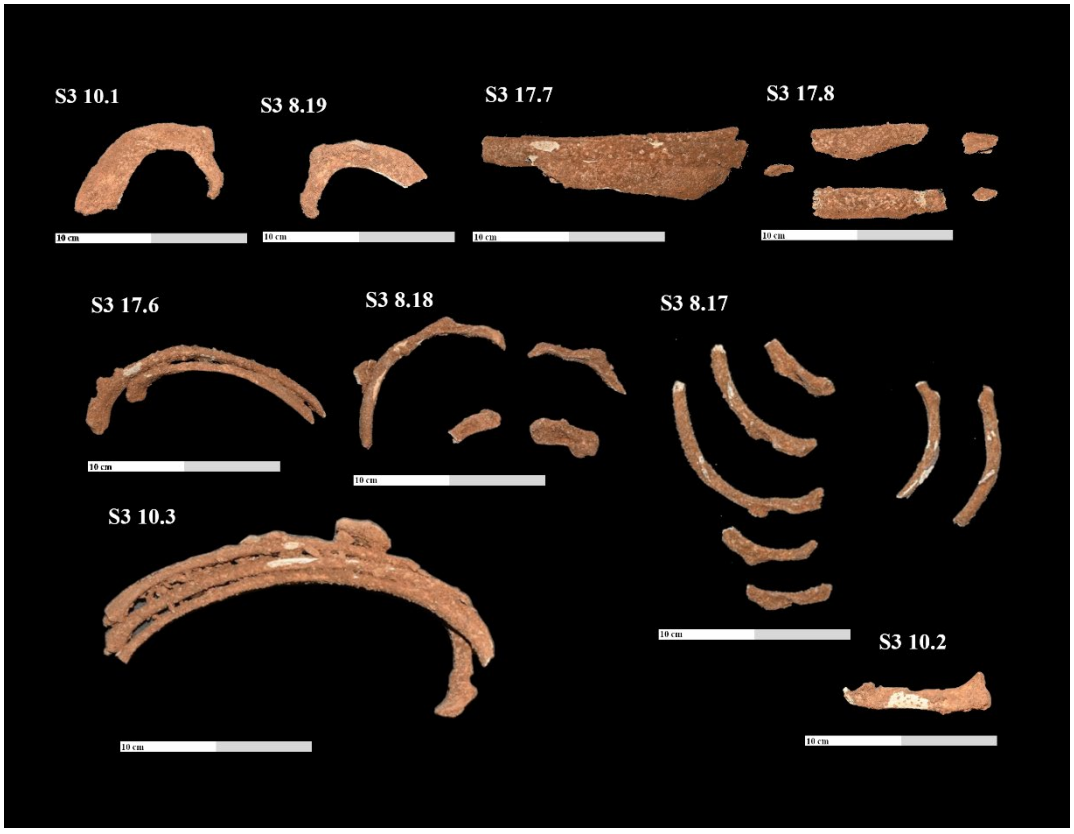

SI-Figure 3(cont.). Costae of Apidima 3.

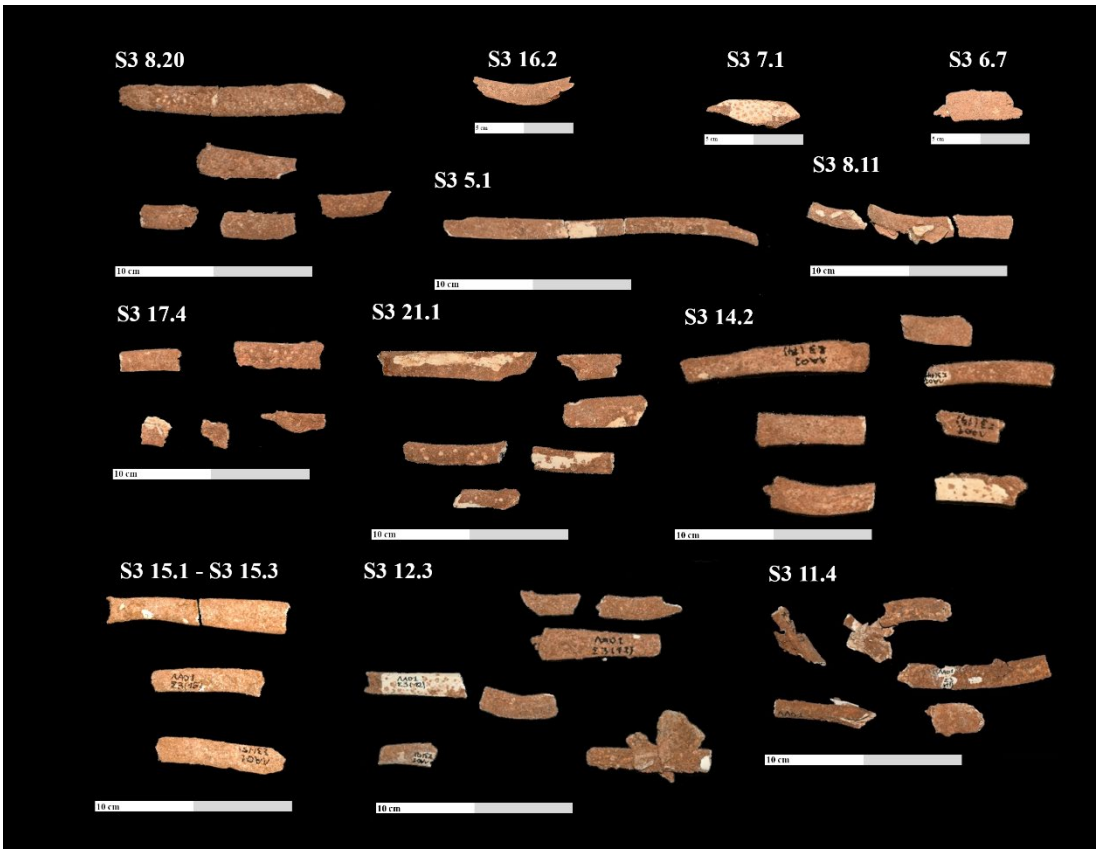

Claviculae

S3 8.2: Clavicula (r)

The right clavicle is preserved in its acromial end and shaft portion. The sternal end is missing. The bone surface is covered by sediment crust, and the bone is agglomerated with the right humerus S3 8.1 and the cervical vertebra S3 8.3, as well as some additional smaller bones (fragments). This is shown in SI-Figure 4 and explained in further detail in the description of the right humerus. The preserved clavicula fragment has a maximum length of 100.8 mm.

There are no unusual characteristics about the clavicular morphology, but its visual inspection is limited due to the sediment coverage. The attachment site for the *m. deltoideus* appears to be slightly pronounced. There are no visible signs of joint degeneration at the acromial end and no signs of pathological alterations.

Scapulae

S3 8.10: Scapula (r)

The right scapula is heavily fragmented, preserved in only four pieces. SI-Figure 4 shows the right scapula of Apidima 3. All fragments are covered by a sediment crust. Its preserved morphology includes the glenoid fossa, the acromion, a fragment of the superior angle with connecting portions of the supraspinous fossa, and the connecting medial portion of the scapular spine, though the continuation of the medial border is interrupted and the border as such is not preserved. The coracoid process is not preserved, even though the fracturing surface at the glenoid fossa fragment appears to be fresh, since there is no sediment fill in the exposed internal bone structure. The last preserved fragment belongs to the lateral border and fits the fracturing line of the lateral border portion inferior to the glenoid fossa. Several rib head fragments are attached to the anterior aspect of the lateral border

fragment, and the strong compression with the scapula seems to have led to the fragmentation of the scapular blade.

The preserved and visible morphology does not indicate any unusual characteristics in the scapular morphology. There are no signs of joint degeneration and no visible indications of pathological conditions.

S3 13.2: Scapula (l)

The left scapula S3 13.2 is preserved in multiple fragments, of which several are glued to reconstruct the superior and lateral morphology. All fragments are covered by a sediment crust. Available features include the glenoid fossa, the acromion, the coracoid process, and the inferior angle of the scapular blade. The scapular spine is preserved, but its continuation to the medial border is interrupted. Similarly, the supraspinous fossa is just partially preserved. The anterior border of the glenoid fossa is compressed against the posterior surface of the left humerus S3 13.1, and as such, is connected by solidified sediment. This is shown in SI-Figure 4. The tip of the coracoid process is compressed against the medial surface of the humeral head, but it does not seem to have caused any damage to the compact bone structure. The inferior angle fragment includes the most inferior portion of the lateral border and is compressed with its posterior surface against the anterior surface of the diaphysis of the left humerus. No identified fragments of the medial border are preserved. Most of the lateral border and the surface area of the scapular blade are also not available.

There are no unusual characteristics, and the state of preservation does not allow a more detailed assessment of the scapular morphology. The preserved and visible surface of the glenoid fossa does not exhibit signs of joint degeneration, nor are there any indications of pathological conditions on the preserved scapular fragments.

<u>Humeri</u>

S3 8.1: Humerus (r)

The complete right humerus is preserved in three fragments, of which the proximal end and the intermediate diaphysis are glued. The right humerus of Apidima 3 is shown in SI-Figure 4. The distal end was also glued, but the adhesive failed to hold the bone structures together. Bone fracturing most likely occurred within the depositional environment, as the exposed medullary cavity in the fractured distal end contains solidified sediment in both directions. The distal end fragment has a maximum length of 73.7 mm, and the proximal portion has a maximum length of 230 mm. The humerus is covered with a sediment crust and has a glossy texture due to treatment with an unknown preservative. Like in the agglomerated block that contains the right tibia S3 11.1 and the fibulae S3 12.12 and S3 12.18, also the right humerus is preserved in an agglomeration of multiple bones that are connected by a solid sediment crust. One of the attached bones is the right clavicle S3 8.2. It is aligned vertically to the humerus shaft axis and located on the medial surface. Two smaller bones lie in direct contact between the humerus and the clavicle. These two bones (fragments) are covered by a thicker sediment crust, so that their anatomical relationship could not be determined visually. One of them could be a distal phalanx, but this remains to be confirmed by further examinations. The second bone is the cervical vertebra S3 8.3, which is aligned with the medial aspect of the humerus and in contact with the clavicle. The inferior surface of the vertebra is pointing to the posterolateral aspect of the humerus, the superior surface is facing in an anteromedial direction, and the transverse axis is rotated in orientation to the humerus shaft axis. The right hemisphere is dipping more to the lateral aspect of the humerus, and the left hemisphere is pointing in the medial direction of the humerus. In attachment with the clavicle and the cervical vertebra, we observed another yet undetermined and heavily encrusted bone (fragment). It appears to have a rounded joint surface that could match the morphology of an intermediate phalanx; however, this assessment requires further validation and may require cleaning parts of the sediment crust.

In general, the morphology of the humerus is very well preserved except for the two fracturing points of the diaphysis. Almost all morphological features are unaffected by surface damage. Only the

medial supracondylar crest is slightly damaged, where a piece of sediment crust chipped off together with some bone material.

The humeral surface is extensively covered by a thick sediment crust, which limits visual examination. What can be inferred from the surface is that the attachments for the *m. pectoralis major* and *m. deltoideus* are well pronounced. Reliefs of other muscle attachment sites are covered by too much sediment to make any assessments. The greater and lesser tubercles appear completely intact, without signs of enthesopathy. Also, the proximal and distal joint morphology appears to be unaltered and thereby not significantly affected by joint degeneration. No pathologies were observed.

S3 13.1: Humerus (l)

All morphological aspects of the left humerus are represented, but partially heavily damaged. The bone is preserved in two portions that represent the fragment of the proximal end with a maximum length of 103.96 mm, and the fragment of the diaphysis with the glued distal end and a total maximum length of 211 mm. The left humerus shows more severe fracturing than the right side. Also, the left humerus is preserved in an agglomeration with other bones that originated from the shoulder and thorax. The left humerus and the attached bones are shown in SI-Figure 4. The posterior aspect of the humeral head is heavily damaged. The surface of the greater tubercle is compressed into the humerus, and the left scapula S3 13.2 is stuck inside the posterior external surface of the humerus. Another possible scapular border fragment is attached to the anterior surface of the humerus, right below the undamaged lesser tubercle. Furthermore, two small rib shaft fragments and the inferior angle of the left scapula are attached to the anterior surface of the humerus diaphysis. Except for the two proximal and distal fracturing lines and a vertical crack on the anterior surface of the distal half, the diaphysis appears to be well preserved. Additionally, the distal end is well preserved, except for the damaged medial epicondyle. Most surface areas are covered with a sediment crust.

The morphology of the left humerus is comparable but slightly more gracile than the right side, except for the deltoid tuberosity, which appears to be as prominent as in the right humerus. The quantitative description also shows that the maximum length of the left humerus is about 3.7 cm shorter than that of the right humerus. A slight tendency for bigger dimensions in the right humerus exists for almost all acquired measurements. The only exception is the width of the olecranon fossa, in which the left humerus is about 1.2 mm wider. The posterior aspect of the trochlea shows osteophytic lipping of up to 1.3 mm with a stronger tendency towards the lateral side. This osteophytic enlargement was not observed in the right humerus and might thus also be related to the wider olecranon fossa of the left side. No further signs of joint degeneration or pathological conditions were observed.

SI-Figure 4. Humeri and scapular fragments of Apidima 3. S3 8.10: Scapula (r); S3 11.5: Fragment of scapular blade; S3 13.1: Humerus (l); S3 13:2: Scapula (l); S3 13.3: Costae (l); S3 8.1: Humerus (r); S3 8.2: Clavicula (r); S3 8.3: Vertebra cervicalis.

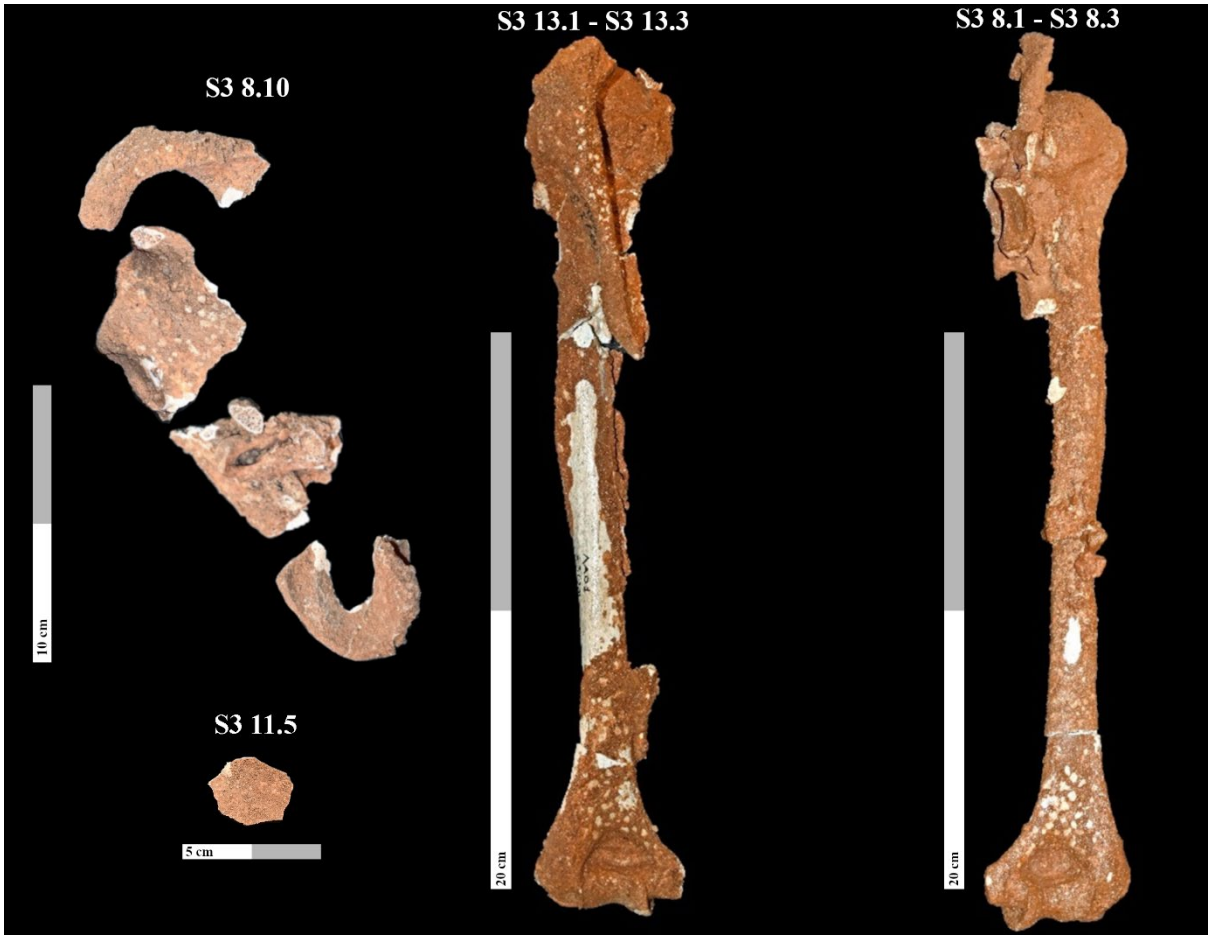

<u>Ulnae</u>

S3 17.1: Ulna (l)

SI-Figure 5 shows the left ulna of Apidima 3 preserved in three fragments that had previously been glued back into one piece. In general, most of the ulnar morphology is represented except for the missing distal end. The fracturing line where the distal end broke off is located right below the attachment site of *m. pronator quadratus*. The diaphyseal and proximal morphology appear well preserved with no signs of damage. The bone is partially covered by a sediment crust.

The preserved morphology shows well-preserved muscle attachment sites. In particular, the pronator and supinator crests are well developed, and the ulnar tuberosity also presents an increase in surface complexity. The attachment site for *m. flexor digitorum profundus* appears as a distinct vertical ridge that runs in parallel to the interosseous crest on the lateral surface of the ulna. There are two lytic deformities located medially and laterally of the trochlear notch at the height of the most concave indentations. The lateral lesion measures 3.7 mm in height and 2.1 mm in width. The medial lesion measures approximately 3.1 mm in length and 0.1 mm in width. The trochlear margins show a slight osteophytic enlargement of up to 0.8 mm with a sharp and protruding appearance. The diaphysis of the ulna has a very slight medial curvature but appears, in general, rather straight.

Radii

S3 17.2: Radius (l)

The left radius is preserved in five fragments, each representing the complete morphology of the bone. It is presented together with the left ulna in SI-Figure 5. The distal end of Apidima 3's radius and the proximal end exist as isolated fragments. The distal end fragment has a maximum length of 64.8 mm, and the proximal end fragment has a maximum length of 49.46 mm. The remaining three fragments are glued and belong to the diaphysis with a cumulative maximum length of 125.64 mm. Except for the fracturing points, which partially contributed to the flaking of small, compact bone pieces, all morphological features are largely intact but exhibit a slight degree of surface damage. The most distal aspect of the interosseous crest is damaged. Surface damage was furthermore observed on the medial aspect of the radial head. A small portion of the posterior surface of the styloid process and the posterior margin of the ulnar notch are also affected by damage to the compact bone, exposing a small area of trabecular bone in both cases.

The dorsal tubercle of the distal radius is well pronounced, and medially next to it runs parallel a prominent ridge. The radial tuberosity is oriented anteromedially. The diaphysis has a very slight lateral curvature. There are no signs of joint degeneration or visible indications of pathological conditions.

SI-Figure 5. The left radius (S3 17.2) and the left ulna (S3 17.1) of Apidima 3.

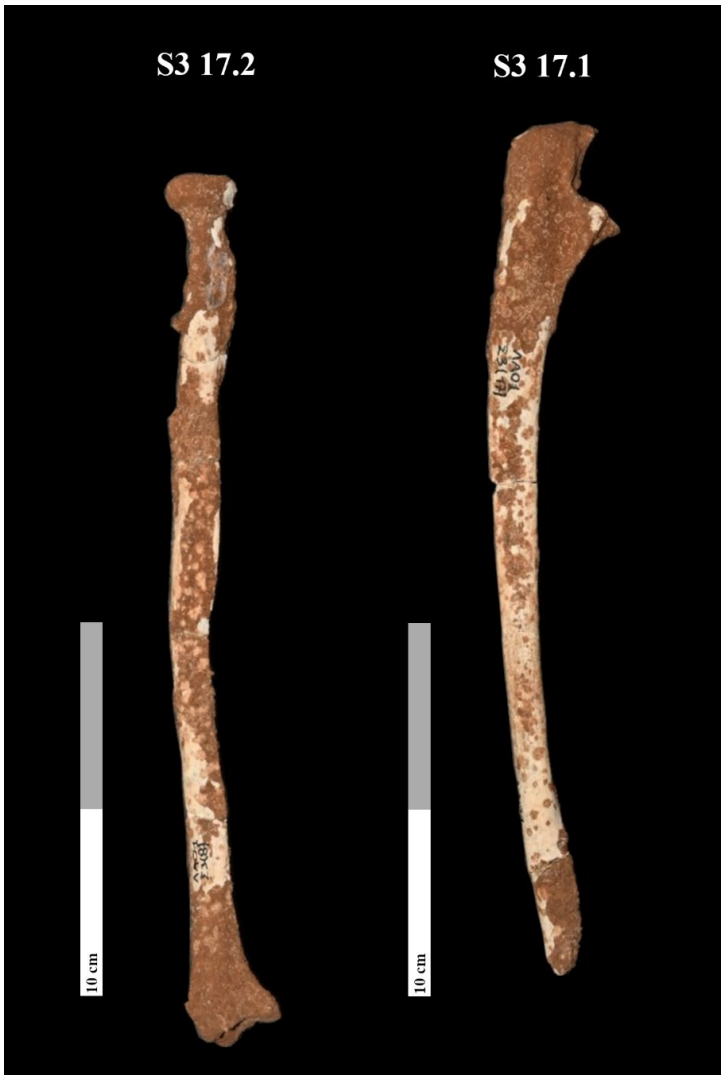

Carpals

S3 6.6: Capitate (l)

SI-Figure 6 shows the left capitate (S3 6.6) and the left hamate (S3 8.24) of Apidima 3. Most of the left capitate is well preserved. Damaged features include the dorsal surface of the capitate's head and the dorsal portion of the trapezoid articular facet. The bone is partially covered by a relatively thick sediment crust.

S3 8.24: Hamate (l)

The left hamate S3 8.24 was found attached to the faunal bone O275. All morphological features are represented, but some have damaged surfaces. Particularly, the ulnar half of the distal articular joint, including the ulnar margin, is damaged. Also, the compact bone surface of the hamate body shows inferiorly larger surface damage in the proximal half. The bone is covered with a thin layer of sediment crust, but the hamulus is covered by thicker concretions.

SI-Figure 6: Carpalia of Apidima 3. S3 8.24: left hamate in view from the capitate (palmar up); S3 6.6: left capitate in view from the hamate (proximal up).

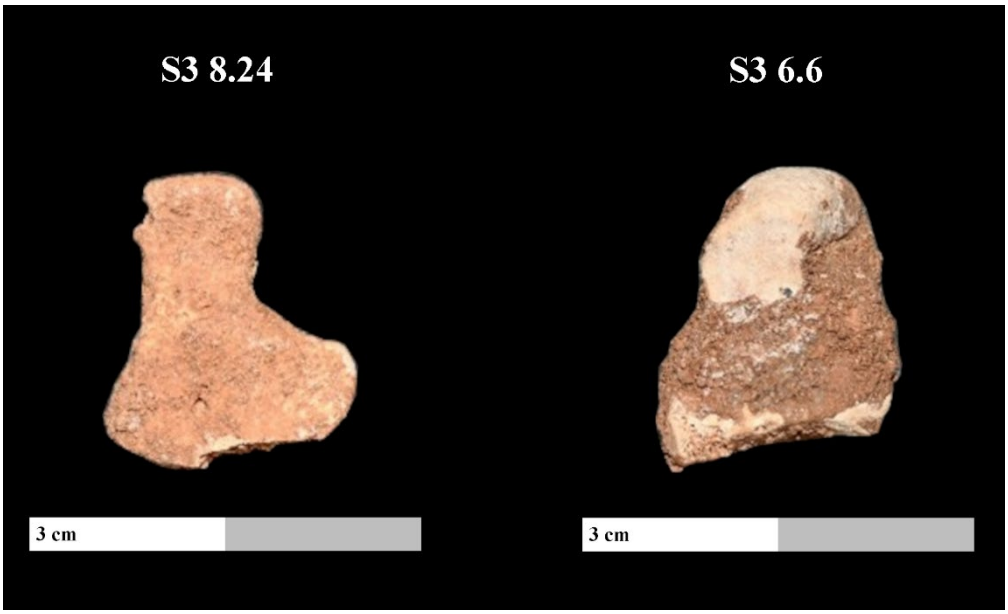

Metacarpals

The metacarpalia of Apidima 3 are shown all together in SI-Figure 7.

S3 6.1: MC 3 (l)

The left third metacarpal is completely preserved. There are no visible signs of damage. The bone surface is covered by a sediment crust.

S3 25.1: MC 1 (l)

The left first metacarpal is complete but preserved in two reglued fragments. A small piece of compact bone is missing on the plantar surface next to the fracturing line. The fracturing of the shaft is oriented obliquely. The bone is partially covered with sediment crust, but most of the surface area is free of sediment.

S3 20.3: MC 2 (r)

The right second metacarpal is represented by its proximal base and most of the shaft portion. The distal end is not preserved. Further signs of damage are located on the ulnar and proximal aspect of the

metacarpal base. The maximum length of the fragment is 56.42 mm. The bone surface is covered by a thin sediment crust.

S3 8.14: MC 4 (l)
The left fourth metacarpal is preserved by its base and shaft morphology. The distal end is separated from the remaining bone by an obliquely oriented fracture in the distal shaft. The preserved length is 45.14 mm. No further signs of damage are visible. The bone surface is covered with sediment crust.

S3 8.13: MC 2 (l)
The left second metacarpal is preserved in two fragments. One fragment represents the metacarpal head with a maximum length of 12.84 mm. The second fragment represents the metacarpal shaft with a maximum length of 54.71 mm. It is broken proximally and distally. The base morphology is not preserved except for a very small area located dorsally at the transition to the shaft. The fracturing of the distal end must have happened more recently since the exposed internal bone structures there are completely free of sediment, while the proximal end contains solidified sediment and discolorations that are not present in the distal fracture. The proximal fracture line is irregular and oriented obliquely between the plantar and the dorsal aspects. Most of the bone surface is covered by sediment crust but partially also the clean bone surface is exposed.

SI-Figure 7. Metacarpalia (MC) of Apidima 3.S3 25.1: MC1 (l); S3 20.3: MC2 (r); S3 8.13: MC2 (l); S3 6.1: MC3 (l); S3 8.14: MC4 (l). The bones are shown in dorsal view, except for S3 8.14, shown in lateral view, and S3 20.3, which also exhibits its medial surface.

<u>Phalanges</u>
S3 1.1, S3 6.3, S3 11.3, S3 19.4, O302.1, S10.1 and S12.1: Proximal phalanges
The proximal hand phalanges of Apidima 3 are shown in SI-Figure 8. Remains of seven distinguishable proximal phalanges were found among the human skeletal remains. S3 1.1, S3 6.3, and S10.1 are complete with no visible signs of damage. S3 1.1 and S10.1 were assigned to the right side, but their exact position remains undetermined. S3 6.3 was assigned to the left hand, also, without a determined position. S3 11.3 is almost complete, but it has been broken into three fragments. A small piece of bone is missing on the inferior aspect. The proximal base fragment of S3 11.3 has a preserved length of 11.25 mm, and including the shaft fragment, the maximum length is 35.88 mm. The third fragment represents a very small compact bone portion of the base fragment only. Another proximal base fragment with a maximum length of 15.06 mm is registered as S3 19.4. It is broken obliquely in the proximal shaft and shows irregular fracture edges. O302.1 and S12.1 represent distal ends with shaft portions that end with an oblique and irregular fracture towards the distal end. The preserved maximum length of O302.1 is

25.09 mm, and it was assigned to the first proximal phalanx of the right hand. For S12.1, the preserved length is 32.74 mm, but its position was not determined. Both S12.1 and O302.1 appear different from the other bones due to the lack of sediment cover that is mostly found attached to the bones of Apidima 3. Possibly, this was the reason they were originally assigned to additional individuals, but there are no morphological reasons for such a separation.

O302.1 and S3 11.3 exhibit signs of osteoarthritic joint degeneration. In the case of O302.1, the phalangeal head exhibits an osteophytic outgrowth of the joint surface measuring approximately 3 mm. This dorsal osteophytic rim is also present in S3 11.3, but its extension there is only about 0.5 mm. Furthermore, the proximal base of S3 11.3 shows several small lesions. The other bones do not exhibit any similar features or signs of joint degeneration or pathological conditions in their visible morphology.

SI-Figure 8. Phalanges proximales of Apidima 3. All phalanges are shown in dorsal view.

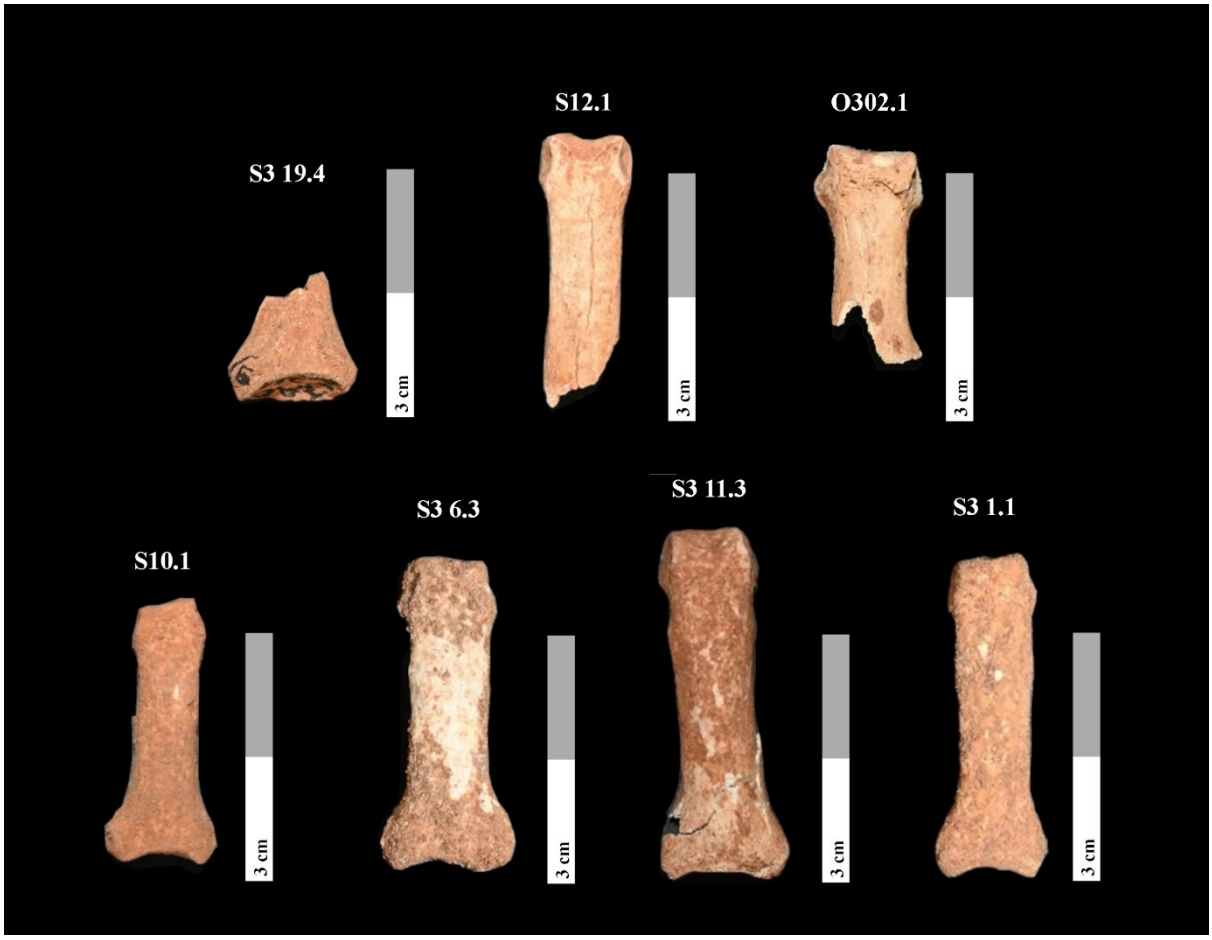

S3 12.5, S3 12.6 and S13.1: Middle phalanges

The three complete left middle phalanges from the skeletal assemblage of Apidima 3 are presented in SI-Figure 9. The bone surfaces are covered by a layer of sediment crust that also contains slightly bigger sediment concretions.

The attachment site for *m. flexor digitorum profundus* is strongly pronounced in S3 12.6 and present only as a slight change in the topography of the bone surface of S13.1 and S12.5. The proximal joint surfaces are well-defined and smooth. No signs of degenerative changes or pathologies were observed. S13.1 matches the overall morphological appearance and preservation of other hand bones of Apidima 3 well. The original assignment to an additional individual is not clear, and it is likely that the bone belongs to the general bone assemblage of Apidima 3.

SI-Figure 9. Phalanges mediae of Apidima 3. All phalanges are shown in dorsal view.

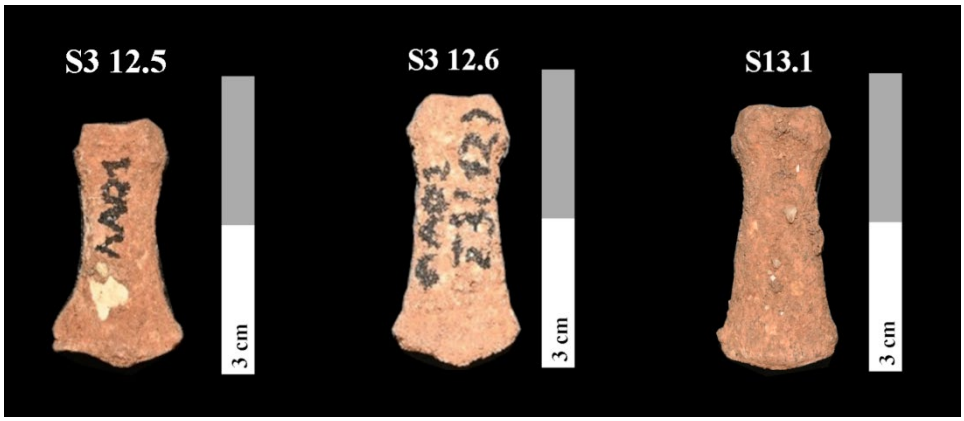

S3 12.7, S3 14.1, S16.1 and S10a.1: Distal phalanges

Four distal carpal phalanges are preserved and depicted in SI-Figure 10. None of them exhibits signs of damage. S3 12.7, S3 14.1, and S10a.1 are covered by thin sediment crust. S16.1 is very clean compared to the general skeletal assemblage, with no attached sediment concretions visible on its surface. Its appearance is thus similar to that of the proximal hand phalanges O302.1 and S12.1, as they both lack a sediment crust on their surface. S10a.1, however, exhibits the same characteristics in morphology and preservation that have been observed in most other hand bones of Apidima 3.

SI-Figure 10. Phalanges distales of Apidima 3. All phalanges are shown in dorsal view.

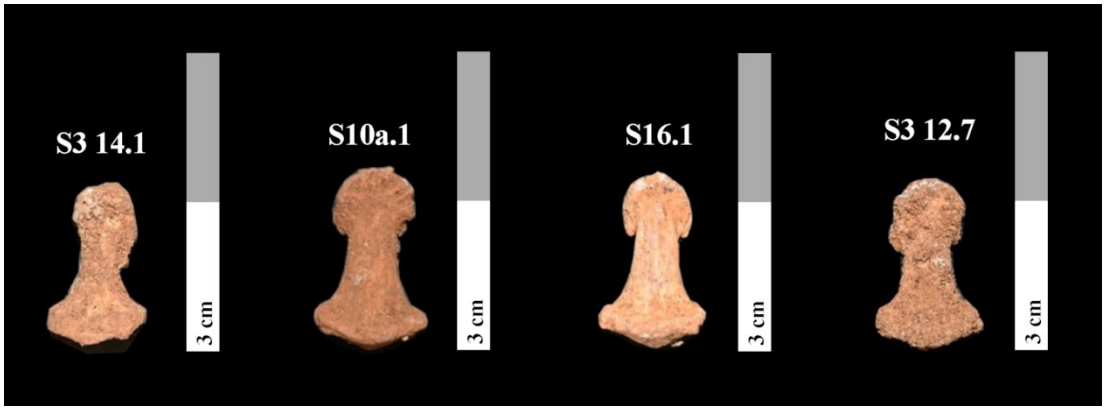

<u>Vertebrae</u>

All vertebrae from the human skeletal assemblage of Apidima 3 are presented in SI-Figure 11.

<u>Cervical vertebrae</u>

S3 3.1: C1 (Atlas)

The first cervical vertebra is largely complete. Only the right transverse process, including the transverse foramen, is not preserved. The superior articular facets show anterior damage at the rim of the articular facets. The left inferior articular facet is also partially damaged. The remaining bone morphology does not present any additional unusual characteristics. The bone is completely covered by sediment crust.

S3 7.3: undetermined position, C3 or C4
The cervical vertebra S3 7.3 is well preserved, but its right lateral transverse process is missing, and the lateral aspect of the right transverse foramen is damaged. Inferiorly, the joint surface of the vertebral body shows anterior damage on its right lateral margin.

S3 18.5: undetermined position, C4 or C5
Most morphological aspects of S3 18.5 are represented but damaged, and most of its surfaces are covered by a thick sediment crust. The left hemisphere and the spinous process of the vertebral arch are not preserved. Only the medial aspect of the left transverse foramen and a tiny area of the superior articular facet are visible. The superior portion of the vertebral body is well-preserved, but the inferior portion is damaged in its left hemisphere, with a few missing pieces of the body morphology. The right hemisphere is less affected and in good condition.

S3 8.3: undetermined position, C5 or C6
The cervical vertebra S3 8.3 is agglomerated with the right humerus S3 8.1 and the right clavicle S3 8.2, as well as some additional smaller bone fragments. This has been described in further detail with the description of the right humerus. The bone surface of the vertebra is covered with a sediment crust. Most morphological features are well preserved but show signs of surface damage. The vertebral body is mostly intact, but an undetermined bone fragment has penetrated the vertebra inferiorly in its left hemisphere. Also, the anterior, inferior, and superior left margins of the vertebral body are damaged. The vertebral arch is intact and connected to the vertebral body; however, the left transverse process and spinous process are not preserved.

S3 8.15: undetermined position, C6 or C7
S3 8.15 represents only the vertebral body. The right hemisphere shows the most medial aspect of the transverse foramen, but nothing else of the vertebral arch morphology is preserved. The vertebral body itself is in good condition and does not exhibit signs of damage.

Morphology of the cervical vertebrae:
No unusual characteristics were observed in the morphology of the cervical vertebrae of Apidima 3. The joint surfaces are in good condition and show neither signs of joint degeneration nor of pathological conditions. The exact position of the cervical vertebrae, except for the first cervical vertebra, could not be determined due to the incompleteness of the cervical spine. What can nevertheless be said is that S3 7.3 must be positioned above S3 18.5, S3 8.3, and S3 8.15 since its vertebral body articulates with the superior joints of S3 18.5 but not vice versa. Furthermore, S3 18.5 must be positioned above S3 8.3 and S3 8.15 since its superior vertebral body is too narrow to articulate with the inferior vertebral body of any of them. The last relative position could be determined for S3 8.3, which has to lie above S3 8.15 for the same reasons that were used to determine the relative positions of the other cervical vertebrae. The lowest position of the cervical vertebrae is thus attributed to S3 8.15, but it remains unclear whether it is position 6 or 7.

<u>Thoracic vertebrae</u>
S3 8.9: undetermined position
Well-preserved and complete thoracic vertebra of undetermined position. The vertebral body is intact and shows no signs of damage. The vertebral arch has a damaged spinous process and a damaged right transverse process. The bone is covered with sediment crust, and a small rock is attached to the right side of the posterior surface. A costal head fragment is attached to the left side and is aligned to the left posterior corner of the superior vertebral body.

S3 8.6: undetermined position
The thoracic vertebra S3 8.6 is partially preserved. The transverse processes are missing, the tip of the spinous process is damaged, and the left lateral margin of the inferior vertebral body is pushed inwards. Despite that, the vertebral body and the vertebral arch are intact. The posterior rim of the superior vertebral body shows superiorly growing osteophytes. The anteroposterior dimension of the vertebral body is relatively short, suggesting a position in the upper thoracic spine.

S3 8.7: undetermined position
The thoracic vertebra S3 8.7 preserved the vertebral body and most aspects of the vertebral arch. In case of the latter, the right transverse process is missing, and the superior surface of the left transverse process, as well as the superior portion of the left superior articular facet, are damaged. The vertebral body is well-preserved and shows no visible signs of damage, nor does it exhibit pathological or degenerative conditions. The bone is completely covered in sediment crust, but the damaged areas and the exposed internal structures are free of sediment infiltration. The vertebra is connected to the superior surface of the thoracic vertebra S3 8.8 and is held together by solidified sediment, though its intervertebral articulation is not in anatomical position. S3 8.7 has been displaced posteriorly and laterally to the right relative to the orientation and position of S3 8.8.

S3 8.8: undetermined position
The preservation of the thoracic vertebra S3 8.8 is very similar to the superiorly attached thoracic vertebra S3 8.7. Most morphological aspects of the vertebra are preserved except for the right transverse process and the tip of the spinous process. The inferior aspect of the vertebral body is damaged posteriorly on the left surface. The bone is completely covered by sediment crust except for the fractured features, where the exposed internal bone structures appear to be free of sediment.

Lumbar vertebrae
S3 12.1: L4
The compact bone surface is covered by a very thin sediment crust. The right hemisphere is not preserved. Only the anterior and left lateral portions of the vertebral body are available and broken into two fragments of the rim region. Visible is also a previous postmortal fracture on the anterior body fragment that had been reconnected with an adhesive. The vertebral arch is barely preserved. Only the transition to the left transverse spinous process and the superior articular facet represent this part of the bone morphology, and both are damaged in their left lateral aspect. The left inferior articular facet is preserved as an isolated fragment attached in articulation to the corresponding articular facet of the sacralized L5 (S3 12.2). Both articular facets are connected through a compact sediment crust. The fresh fracturing surface of the inferior articular surface connects perfectly with the fracturing surface of L4. The bright color of the fracture edges in the vertebral arch and the anterior body suggests that the damage occurred around or shortly after the time of the excavation. The fracturing of the posterior aspect of the vertebral body fragments, on the other hand, must have occurred before excavation, as sediment and a small rock are embedded within the posterior trabecular architecture.

Little can be said about the morphological appearance of L4 due to its high degree of fragmentation. The preserved portion of the superior articular facet and the preserved left lateral aspect of the rim of the inferior vertebral body are well defined and show no degenerative changes, except for a porosity in the inferior surface of the vertebral body. The anterior rim of the superior vertebral body, however, shows strong osteophyte formations, anterior lesions, and the superior vertebral body surface exhibits increased microporosity.

S3 12.2: L5 (Lumbosacral transitional vertebra)
S3 12.2 is a fragment of the left portion of a sacralized fifth lumbar vertebra (L5). The vertebral body is preserved only as a small fragment of the superior aspect that represents the lateral and posterior rim. Preserved is also the superior articular facet that is still in articulation with the inferior articular facet

of L4 (S3 12.1) and connected by a solidified sediment crust. The lateral aspect of the bone fragment presents the superior portion of the auricular surface. The caudal end of the fragment is located at the height of the first sacral foramen. The superior articular facet and the auricular surface are well defined and show no signs of degenerative joint alteration, though it should be noted that the visual inspection is also limited by the sediment crust cover that is present on most surfaces. Located between the superior articular facet and the auricular surface is a well-developed tubercle that formed originally as the transverse process of L5 (see Paleopathology, Non-Metric Traits, and Skeletal Modifications).
The fragmentation of the sacrum and L5 must have taken place before the excavation, since the exposed internal bone structures are filled with sediment. Only the fracture surface of the articulated inferior articular facet of L4 S3 12.1 can clearly be attributed to a fresh breakage by its bright coloration and absence of sediment infill compared to the old, fractured surfaces of the sacral fragment S3 12.2.

SI-Figure 11. Vertebrae of Apidima 3. Vertebrae cervicales: S3 3.1 (Atlas), S3 7.3, S3 18.5, and S3 8.15 in superior view; Vertebrae thoracicae: S3 8.6 and S3 8.16 in superior view, S3 8.9, S3 8.7, and S3 8.8 in inferior view; Vertebrae lumbales: S3 12.1 (L4) in superior view.

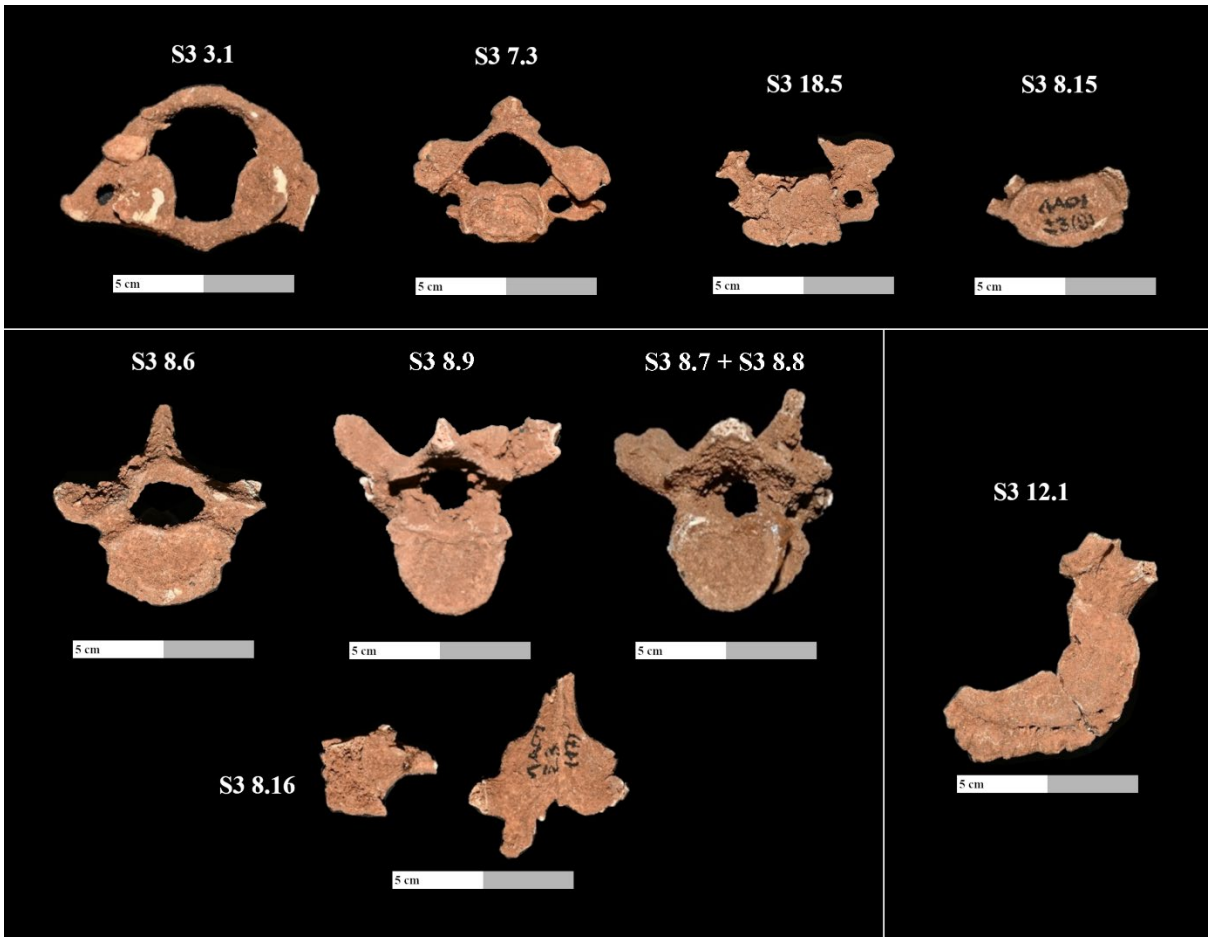

Pelvis
All skeletal remains associated with the pelvis of Apidima 3 are depicted in SI-Figure 12.

S3 17.5: Os coxae (r)
The right os coxae is represented by one small iliac crest fragment that has a maximum length of 57.7 mm. It preserves the posterior aspect of the iliac crest and the anterior portion of the iliac tuberosity, and its position corresponds to the iliac crest fragment S3 12.8 from the left os coxae. The fragmentation occurred before the excavation, as the exposed internal structures are filled with sediment. The bone

fragment is covered by a sediment crust. Two circular depressions are located on the medial surface, but they are likely the result of the erosion and compression of the sedimentary environment. No unusual characteristics exist.

S3 8.21: Os coxae (l) and S3 12.8: Fragment of ilial crest (l)

The main fragment S3 8.21 represents multiple glued fragments of a left os coxae with preserved aspects of ilium and ischium. The pubis is not preserved. Only completely intact but damaged features are the auricular surface, the greater sciatic notch, the lesser sciatic notch, and the ischial tuberosity. The acetabulum is broken in a vertical line at its most lateral aspect from the superior and inferior apex of the lunate surface down to the transition point of the ischial tuberosity to the ischiopubic ramus. Anterior to the ischial tuberosity, only the posterior rim of the obturator foramen is preserved. Assessment of the acetabular morphology is limited since the bone surface around the acetabulum and the acetabular rim are heavily damaged. The posterior superior iliac spine is also preserved but damaged medially and anteriorly, which is connected to a circular fractured surface in the posterior portion of the iliac tuberosity. The isolated iliac crest fragment S3 12.8 has a maximum length of about 76.5 mm, and it refits to the anterior interruption of the posterior iliac crest of S3 8.21. The anterior portion of the iliac tuberosity is preserved in S3 12.8. The bone morphology is not preserved further anteriorly than this fragment.

A general quantitative and qualitative morphological description remained limited to the very few measurements and points presented in this article.

The posterior gluteal line is well pronounced. The anterior and inferior gluteal lines are barely visible, but the major surface areas of their positions are not preserved. The sciatic notch is round and has a wide angle of about 82 degrees, measured based on three points that correspond to the deepest point of the notch and to the superior and inferior posterior end points. It should be noted that the true end point of the inferior rim is expected to be located less than 1 cm further posterior, but this point could not be taken due to damage to the ischial spine. The measured angle of the greater sciatic notch, however, would not be affected significantly since the preserved endpoint lies in very close proximity to the damaged ischial spine, and the state of preservation provides a clear outline of the notch morphology. Important to note is also the presence of a very well-defined, deeply grooved, and wide preauricular sulcus. Interestingly, the wide groove narrows and becomes pointed posteriorly, where a secondary cutting incision/groove appears. The inferior view of the bone in Figure 4 shows this nicely. This groove appears narrower and more elongated, and it is visible at the most posterior point of the preauricular sulcus and in the most inferior part of the auricular surface, where an irregular osteophytic extension of the joint surface is also apparent. The auricular surface shows no perforation, but the close proximity and identical orientation of the two grooves indicate that they have been formed together. The etiology of these grooves is unknown, but possible causing factors might have been the branches of the superior gluteal artery that run together with the superior gluteal nerve above the piriformis muscle through the greater sciatic notch posterior to the sacroiliac joint at the level of S2-S3 (Wong et al. 2023). The artery divides there into the superficial and deep branches, which enter the gluteal muscles and also support the blood supply to the sacroiliac joint (Bollow et al. 2000). Sacral dysmorphism caused by the (partial) fusion of the lumbosacral transitional vertebra and the resulting changes in the morphology of the sacroiliac joint including its biomechanical properties and the hip mobility, could have potentially affected the closely surrounding neurovascular system, e.g., by a lower position of the sacroiliac joint (Ileez et al. 2018; Mahato 2020; Matson et al. 2020). However, the present osteoarthritic condition of the sacroiliac joint exhibits damage to the synovial structures at the location of these grooves, indicating a possible relationship to their formation.

The auricular surface is covered by a sediment crust that makes a detailed assessment of the morphology difficult. Osteophytic joint lipping is clearly visible, with an enlargement of up to 1.4 mm. Also, the morphology of the acetabulum is only partially preserved. The height from the inferior apex of the lunate surface to the most superior point of the lunate surface is about 44 mm. The anterior aspect of the superior lunate surface is not preserved. Also, the acetabular rim is only preserved in the most

inferior portion next to the ischial tuberosity. The border between the lunate surface and the acetabular notch is well defined and elevated.

SI-Figure 12. Remains of Apidima 3's pelvis. S3 8.21: os coxae (l) in posterior view; S3 12.2: lumbosacral transitional vertebra in slight superior view of the anterior aspect; S3 17.5: os coxae (r), ventral aspect of the right ilial crest fragment; S3 12.8: os coxae (l), perspectives of the left ilial crest fragment.

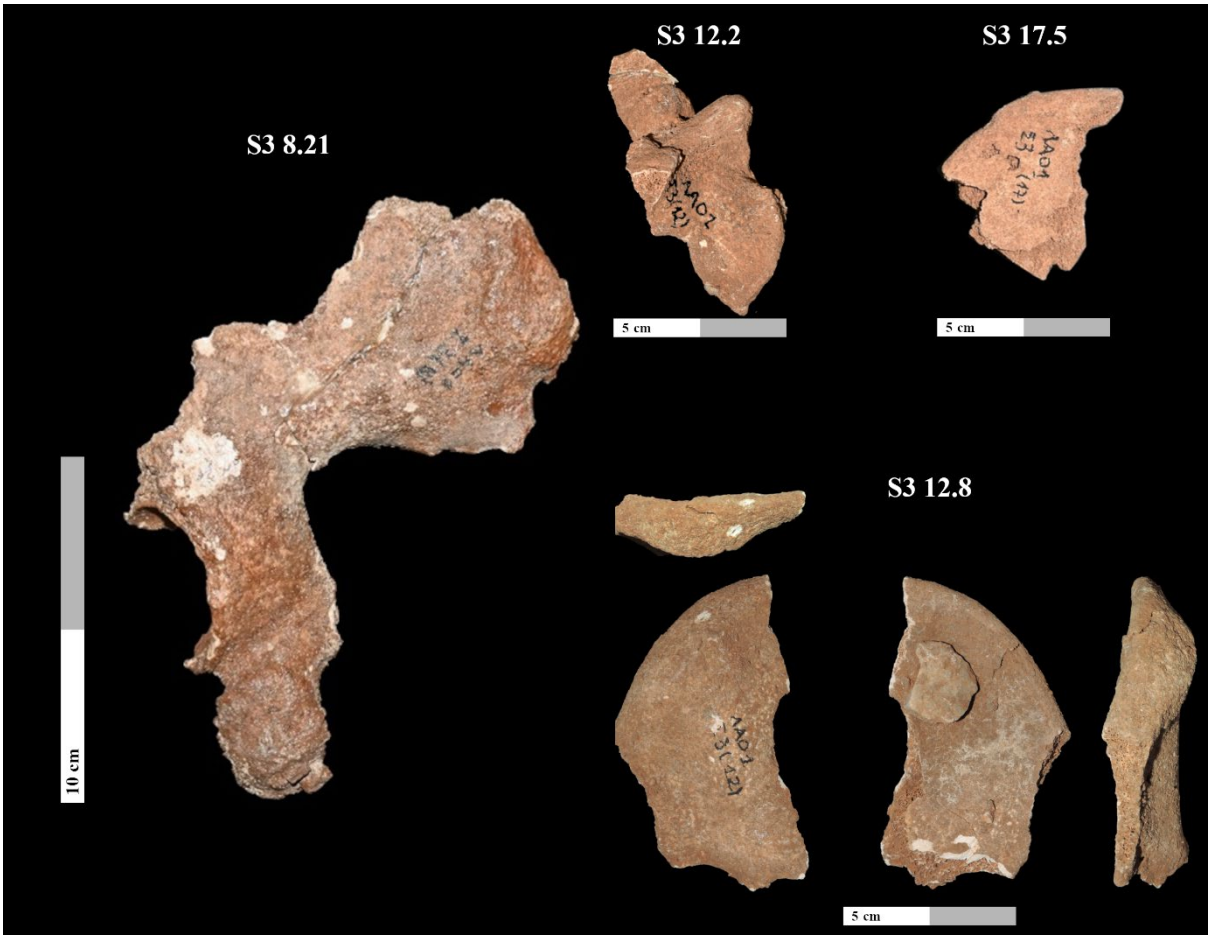

Femora

Apidima 3's femora are shown together with the patella in SI-Figure 13.

S3 12.15: Femur (r)

The right femur S3 12.15 consists of 3 major fragments that represent the distal end, the diaphysis, and the proximal end. All three fragments have refitting ends. The distal end fragment includes approximately the distal third of the diaphysis and has a length of 156.4 mm. The diaphysis fragment has a length of 126.12 mm, and the proximal diaphysis fragment contains the transition to the femoral neck and comes to a total length of 126.76 mm. All fragments are covered by a thin layer of sediment crust and partially by bigger sediment concretions that also include small rock pieces. The distal end is vastly complete, but the surface areas around the medial and lateral epicondyles are damaged. In the case of the lateral epicondyle, at the location of the lateral collateral ligament attachment, there is a small circular piece of bone missing. Both damaged areas appear to have originated after the excavation, as the exposed trabecular architecture resembles that of other post-excavational bone fractures, and the internal space is free of sediment. Posteriorly, the lateral and medial epicondyles are

free of sediment crust and appear bright and white. Similar areas where the original bone surfaces are exposed also exist in other areas of the three bone fragments. It cannot be determined whether this happened unintentionally after the removal of the bones from their depositional environment or if these surfaces were exposed during an attempt to clean the bones from the sediment crust.

Stronger bone fragmentation occurred in the diaphyseal portion, where the medial and lateral supracondylar lines converge and where the linea aspera ends distally. These smaller bone fragments are reattached to the distal femur fragment by an unknown type of adhesive. Remnants of adhesives can also be found on the fracturing surfaces of the three bigger bone fragments. It also appears that the external bone surfaces of all fragments were treated with an unknown type of preservative. This is indicated by the glossy texture of the bone surfaces, regardless of whether the original bone is exposed or covered by sediment crust. The proximal fragment contains the proximal diaphysis, but none of the proximal epiphyseal or apophyseal morphologies are preserved. The fracturing line starts right below the lesser trochanter and follows as an oblique line medially to the beginning of the femoral neck. Laterally, the fracturing line continues below the intertrochanteric line from where it moves almost horizontally to the transition point of the femoral neck and back to the inferior margin of the lesser trochanter so that all essential structures are lost. Since the exposed internal space here is filled with solidified sediment, the fragmentation of the proximal end likely occurred before the excavation. Unfortunately, no femoral remains were found in the collection that could be attributed to these missing pieces.

The distal joint morphology appears in very good condition with no signs of pathological alterations. Joint degeneration is present as a slight osteophytic enlargement anteriorly around the facies patellaris and at the inferiorly located joint margins around the intercondylar notch. There is a tendency towards stronger osteophyte formation in the medial condyle. The popliteal groove is well defined, and the linea aspera appears strongly pronounced. Also, the gluteal tuberosity and a lateral crest along the attachment sites of *m. vastus lateralis* and *m. vastus intermedius* are well pronounced.

S3 12.16: Femur (l)

The left femur S3 12.16 experienced a relatively strong degree of fragmentation in its proximal and distal sections, but previous examiners reconstructed several pieces by application of adhesives. Unfortunately, the morphology of the greater and lesser trochanters is not preserved. The external morphology of the greater trochanter was pushed into the bone, and the lesser trochanter was compressed against the posterior surface of the left os coxae S3 8.21, which led to the destruction of the lesser trochanter, and a thin layer of compact bone covered the fractured surface. This compact bone layer matches a negative in the external compact bone surface superior to the damaged acetabular rim of the left os coxae S3 8.21. The femoral head and neck form a single fragment, and the exposed trabecular architecture reveals remnants of sediment fill. The intermediate diaphysis fragment is the best-preserved piece of the left femur. It does not show any signs of damage other than the fracturing of the posterior and distal ends. The distal end is also vastly intact. Only the lateral condyle and lateral epicondyle are damaged. The patella S3 12.17 is attached to the distal joint surface by solidified sediment and shows that the lower limb was in hyperflexion at the time of the initial burial. The distal end fragment has a maximum length of 125.95 mm. The diaphysis with the glued proximal end has a maximum length of 314.25 mm, and the isolated femoral head fragment has a maximum length of 55.5 mm. All fragments are covered by sediment crust and present a glossy texture that indicates that they were treated with some type of preservative besides the glue that was used to reassemble the single bone fragments.

The morphology of the left femur is similar to the preserved features of the right femur S3 12.15. The popliteal groove is well defined, and the distal joint morphology shows osteophytic enlargement of about 1 mm at the superior and medial margins of the facies patellaris, as well as around the joint margins of the intercondylar notch, though the anterior aspect of the notch cannot be evaluated due to the attached patella S3 12.17. As observed in the right femur and patella, the medial joint surfaces are more strongly affected by joint degeneration than the lateral surfaces. The femoral head does not show

any degenerative alterations of joint morphology. The fovea capitis femoris is located in the posteroinferior quadrant of the femoral head and has a triangular shape in its center that is surrounded by a shallow and smooth oval-shaped groove. The center has a width of 16.7 mm and a height of 13.6 mm. The linea aspera appears very prominent and wide. The gluteal tuberosity is well pronounced with a strong relief, but the pectineal line is barely visible compared to the right femur. Interesting to note is the presence of a trochanter tertius located on the gluteal tuberosity at the height of the lesser trochanter with an oblong, rounded shape. Its presence on the right femur cannot be examined since it would be located above the fracturing line that separates the preserved femur from the missing proximal morphology.

SI-Figure 13. The left (S3 12.16) and right (S3 12.15) femur and the left (S3 12.17) and right (S3 12.9) patella of Apidima 3.

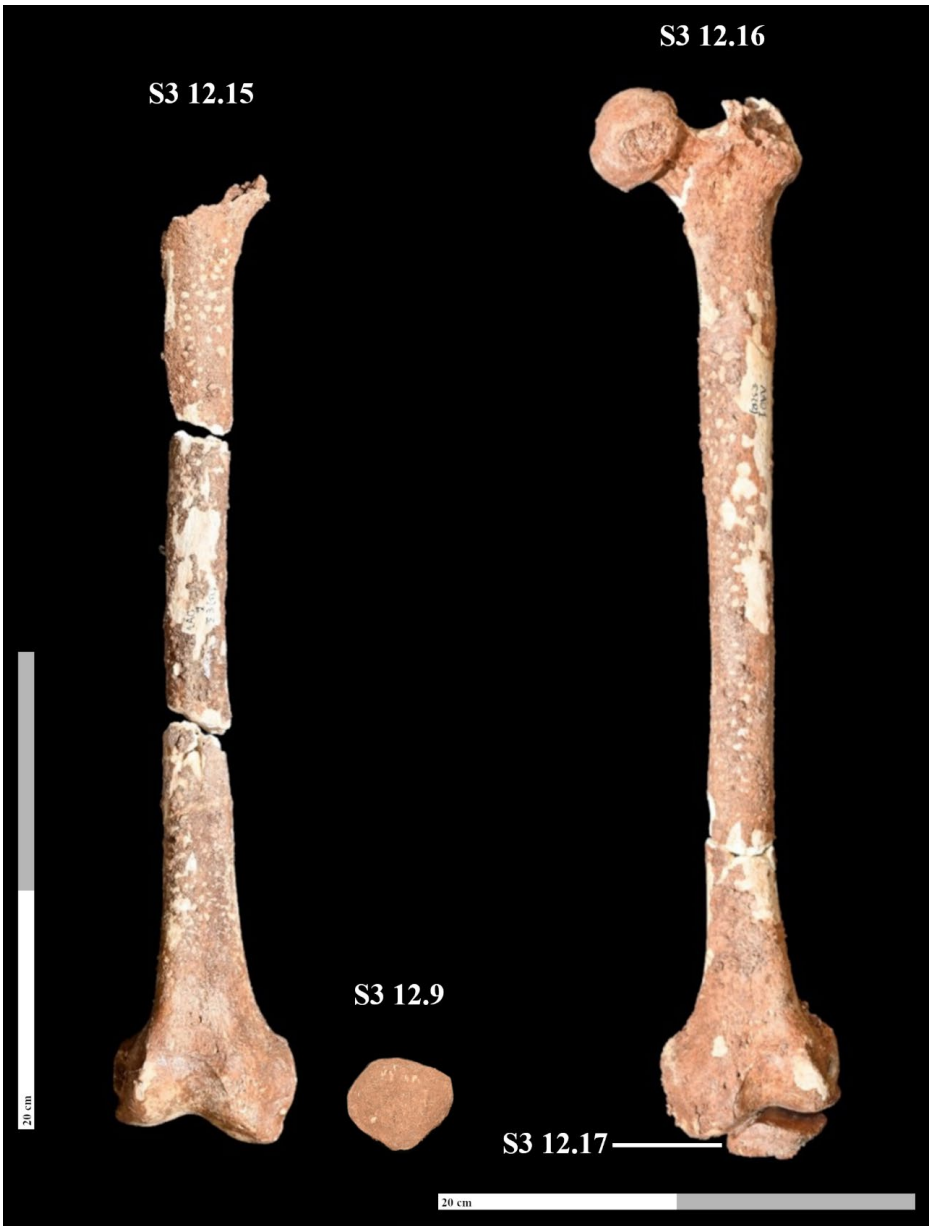

Tibiae

SI-Figure 14 presents the skeletal remains of Apidima 3's right tibia and both fibulae.

S3 12.13 / S3 11.1: Tibia (r)

The right tibia S3 12.13 / S3 11.1 is complete for most of its extent but also is partially fractured and damaged on the surface. It is preserved in two pieces that represent the proximal end with the proximal third of the diaphysis (S3 11.1) and the distal end with the distal two-thirds of the diaphysis (S3 12.13). The proximal fragment has a maximum length of 123.3 mm, and the distal fragment has a maximum length of 230 mm. The tibiae were found independently in the collection of the skeletal remains and could then be refitted during our examinations. Unfortunately, the proximal fragment S3 11.1 is agglomerated with the fragments of the left and right fibulae S3 12.18 and S3 12.12, which limits the macroscopic visual examination of these bones. All three bones are superimposed and sit together on a rock that resembles the original finding situation at the archaeological site (see "Burial Taphonomy"). Like all other bones from the human skeletal assemblage of Apidima Cave C, these bones are also covered by a solidified sediment crust. Like many other bones, the agglomerated block of tibia and fibulae, along with the rock, was treated with an unknown type of preservative that has been applied to all surfaces.

In the case of the proximal tibia fragment S3 11.1, only the medial, anterior, and proximal surfaces are clearly visible. The lateral side points downwards to the rock surface and is covered with sediment, and the obliquely aligned proximal fibula fragments S3 12.12. The diaphyseal connection between the proximal tibia S3 11.1 and the remaining bone S3 12.13 shows a high degree of fragmentation. Two smaller diaphysis fragments are missing at this connection, but the remaining fragments are glued to S3 11.1. The distal portion (S3 12.13) is largely intact but exhibits some vertical cracks in the diaphysis that are filled with sediment, and where the sediment has also entered the medullary cavity. The fibular notch is not preserved, and the fractured surface is entirely covered by sediment. Also, the medial aspect of the talar articular facet is damaged in a vertical line with the damaged fibular notch. Even though many aspects of the right tibia cannot be examined clearly, it is clearly visible that the tibial tuberosity, the morphological features of the proximal epiphysis, and the medial malleolus are intact.

The morphological investigations of the right tibia S3 11.1/S3 12.13 were limited by the agglomeration with other skeletal remains. Nevertheless, a few observations could be made to describe the morphology. The distal end features a well-defined anterior squatting facet with a width of 16.85 mm and a height of 10.4 mm. On the posterior surface, the presence of a nutrient foramen situated on the soleal line is visible. The relief of the soleal line is very well developed. Also, the interosseous crest on the lateral surface of the diaphysis is prominent. There are no signs of pathological conditions. The medial margin of the medial condyle and the posterior-lateral margin of the lateral condyle show osteophytic growth of about 1 mm. Except for that, there are no signs of joint degeneration on the proximal and distal joint surfaces.

Fibulae

SI-Figure 14 presents the skeletal remains of Apidima 3's right tibia and both fibulae.

S3 12.12 and S3 8.27: Fibula (r)

All morphological aspects of the right fibula are preserved, but the bone is broken into several pieces. ID S3 8.27 includes a fragment of the distal end with the distal third of the diaphysis and an additional three glued intermediate diaphysis fragments. The diaphysis fragments have a maximum length of 142.15 mm, and the distal end fragment has a maximum length of 129.13 mm. The proximal third of the diaphysis and the proximal end are saved as ID S3 12.12. The proximal diaphysis fragment has a maximum length of 58.3 mm, and the distal diaphysis fragment has a maximum length of 43.92 mm. These fragments are agglomerated with the right tibia S3 11.1 and the left fibula S3 12.18 on a rock surface. This is explained in greater detail in the description of the right tibia S3 11.1 (also see "Burial

Taphonomy" for additional information). The bone surfaces are covered by a thin layer of sediment crust. The fragmentation of the bone is of an older nature since the exposed internal bone structures at the fracturing locations are filled with sediment. The bone morphology in general is well preserved, and there are barely any visible signs of damage except for the fracturing points.

Due to the sediment crust and the agglomeration of the proximal end of the right fibula, the possibilities for a visual and quantitative description of the bone morphology are not possible, and are, for now, limited to the visible extent of the diaphysis and distal end. The fibular nutrient foramen enters the bone at the interosseous crest in the proximal half of the bone, but close to the mid-shaft location. The attachment site for the *m. fibularis tertius* is strongly pronounced. There are no visible signs of pathology or joint degeneration, though the actual articular surface of the fibular head is not visible due to a relatively high amount of sediment coverage.

S3 12.18 and S3 9.2 Fibula (l)

The left fibula is preserved in 3 fragments. The proximal end is registered as S3 9.2, and two additional diaphysis fragments are registered as S3 12.18. The proximal end fragment S3 9.2 has a maximum length of 71.6 mm. The proximal diaphysis fragment of S3 12.18 has a maximum length of 101.2 mm, and the distal fragment has a maximum length of 58.92 mm. The diaphysis fragments S3 12.18 are agglomerated with the right tibia S3 11.1 and the right fibula S3 12.12 on a rock surface. This is explained in greater detail in the preservation description of the right tibia S3 11.1 and in the section "Burial Taphonomy". The bone surfaces are covered by a thin layer of sediment crust. The morphology of the fibular head is intact. The two diaphysis fragments belong to the mid-shaft and distal third portion of the diaphysis. The distal fragment ends at the transition to the lateral malleolus, and the proximal fracture line is located approximately at the mid-shaft location, about 24 mm proximally to the distal end of the anterior crest. The fracturing line between the two diaphyseal fragments goes from proximal to distal in an oblique direction from the anterior surface through the attachment site for the *m. fibularis tertius*. The lateral surface is not visible since it is aligned with the rock surface. The medial surface with the visible distal portion of the interosseous crest is compressed against the lateral surface of the superimposed proximal end of the right fibula S3 12.12.

The morphological appearance of the left fibula S3 12.18/S3 9.2 is very limited due to the agglomeration with the tibia S3 11.1 and the fibula fragments S3 12.12. The missing distal end, unfortunately, also does not provide information about the morphology of the left lateral malleolus, but the appearance of the *m. fibularis tertius* is similar to that of the right distal fibula fragment S3 8.27. No unusual or remarkable characteristics were observed in the morphology of the fibular head. No signs of pathological or degenerative alterations were observed either. A quantitative description of the left fibula could only be done for the fibular head due to the incompleteness of the bone.

SI-Figure 14. The right tibia (S3 11.1/S3 12.13), as well as the right (S3 12.12/S3 8.27) and left (S3 12.18) fibula of Apidima 3.

Patellae

The patellae of Apidima 3 are shown together with the femora in SI-Figure 13.

S3 12.9: Patella (r)

Complete left patella with a low degree of cortical damage. Only the tip of the apex is broken, and little cortical damage is furthermore located inferiorly along the lateral margin between the lateral articular surface and the apex. Except for the damaged areas, the bone is completely covered by a thin layer of sediment.

The joint surface exhibits osteophytic enlargement of 1–2 mm on its distomedial and lateral margins. On the lateral aspect of the distal surface, the cortical bone shows increased microporosities. Anteriorly, the formation of exostoses at the site of the patellar tendon was observed. Furthermore, a distinctive depression with a dimension of about 8 x 6 mm is located on the lateral articular surface, right next to the crista facies articularis.

S3 12.17: Patella (l)

Complete left patella with no visible damage. The bone is completely covered by a thin sediment crust that connects the patella from the articular facet to the distal joint of the left femur S3 12.16 in position of hyperflexion.

Due to the attachment of the left patella to the joint surface of the left femur, it is not possible to examine the articular morphology visually except for the superior portion of the lateral articular

facet. No clear signs of joint degeneration are visible here. Anteriorly, small exostoses are located at the site of the patellar tendon insertion.

Tarsals

The human skeletal remains from Apidima Cave C contained tarsal bones mainly associated with Apidima 3, but also two tarsals were found that were identified as belonging to a second adult individual – Apidima 4. All tarsals from the human skeletal assemblage of Cave C are shown in SI-Figure 15.

S3 12.14 Calcaneus (l)

Complete left calcaneus. No visible signs of damage, but the bone is completely covered by a thin sediment crust and partially by bigger sediment concretions that contain small rocks.

The left calcaneus does not show any unusual characteristics in its visible morphology, even though the sediment crust limits the macroscopic examination of the bone surface. Formation of exostoses at the location of the calcaneal tendon is present.

S3 17.3: Calcaneus (r)

The right calcaneus is completely preserved with a small degree of surface damage located at the superior margin of the cuboid articular facet, at the posterior margins of the posterior and lateral talar articular facets, as well as on the tip of the lateral process of the calcaneal tuberosity. The bone is covered by a thin layer of sediment.

The general morphology of the right calcaneus is similar to the left side. The calcaneal tuberosity exhibits exostoses at the site of the calcaneal tendon insertion. More clearly visible in the right calcaneus are the joint facets of the anterior and middle talar articular facets. The joint surfaces exhibit a slight osteophytic enlargement, measuring up to 0.7 mm. Despite that, no other signs of joint degeneration or indications of pathological conditions were observed.

S3 8.5: Talus (r), S3: 23.2 Talus (l)

Three tali were found among the human skeletal remains of cave C, and two of them could be associated with Apidima 3. The right talus S3 8.5 and the left talus S3 23.2 are both in very good condition with only a little degree of compact bone damage. The damaged areas in the left talus S3 23.2 are located on the inferior and superior aspects of the talar head and on the medial margin of the posterior subtalar facet, including the inferior border of the groove for the *m. flexor hallucis longus*. On the right talus S3 8.5, surface damage is located on the lateral margin of the talar head as well as on the anterior margin of the posterior subtalar facet. Despite that, all morphological features of S3 8.5 and S3 23.2 are intact, and no further signs of damage are visible. All bones are covered in sediment crust. S3 8.5 has a well-preserved lateral squatting facet that is also reflected in the right tibia S3 12.13. In the left talus S3 23.2, trochlear extensions are present on the medial and the lateral aspects. The general appearance of S3 8.5 and S3 23.2, as well as their state of preservation, is very similar. It seems likely that they belong to the individual Apidima 3 and that the second right talus (ID S26) is more likely the bone of a second individual. Unfortunately, its bad preservation does not allow a morphological and quantitative comparison to the other talus remains. Neither of the preserved and visible joint surfaces of the three tali exhibits signs of pathological conditions.

S3 9.1: Naviculare (r)

The right navicular is complete with no visible signs of damage. Bone covered with a thin sediment crust.

S3 6.4: Naviculare (l)
Preserved maximum length of 35.94 mm. The talar tuberosity is not preserved. The remaining bone morphology is intact with no visible signs of damage. Bone is covered partially by a relatively thick sediment crust.

S3 18.6: Cuboid (l)
The left cuboid is complete but partially damaged. Surface is affected superiorly and laterally at the joint margin of the calcaneal articular facet and the cuboid tuberosity as well as the most lateral margin of the metatarsal articular facet. The articular facet for the lateral cuneiform is slightly abraded posteriorly.

S3 10.4 Cuboid (r)
Complete but partially damaged. The superior joint margin of the calcaneal articular facet is slightly abraded, and a low degree of compact bone damage is located on the medial bone surface between the articular facets of the lateral cuneiform and the calcaneus.

Directly on the superior rim of the metatarsal articular facet is a slight incision in the joint surface. Behind this incision, the compact bone shows a depression that might be related to a lytic process.

S3 19.1: Medial cuneiform (r)
Complete medial cuneiform with a slight degree of surface damage. Only a very small portion of the inferior rim on the proximal and distal articular facets is damaged. No further signs of damage are visible. The bone is covered by a thin layer of sediment crust.

S3 19.2: Medial cuneiform (l)
The inferior lateral surface is damaged in a continuous line from the distal to the proximal articular facets. The medial surface shows a small circular depression that perforated the bone surface at an oblique angle. The medial rim of the proximal articular facet shows a low degree of abrasion. Despite that, all morphological aspects are intact and free of further damage. The bone is covered by a thin layer of sediment crust.

S3 8.12: Intermediate cuneiform (l)
Complete intermediate cuneiform. All morphological aspects are intact and exhibit only a very low degree of surface damage, localized in small areas around the joint margins. Primarily, the inferior and lateral aspect of the metatarsal articular facet is affected, though it didn't damage the joint surface itself. Bone is covered by a thin layer of sediment crust.

S3 19.3: Lateral cuneiform (r)
Two right lateral cuneiforms were found among the human remains from Apidima Cave C. S3 19.3 was identified as the right lateral cuneiform of Apidima 3, based on its good articulation with the right cuboid S3 10.4. The second right lateral cuneiform, S3 6.5, does not align well with the right cuboid and was therefore assigned to Apidima 4 (see "Morphological Description of Apidima 4" for further details). S3 19.3 is completely intact with no visible signs of damage. The bone is covered with sediment crust. No unusual morphological characteristics were identified.

SI-Figure 15: Tarsalia of Apidima 3. S3 9.1 (r) and S3 6.4 (l): navicular bones in proximal view from the talus; S3 18.6 (l) and S3 10.4 (r): cuboids in dorsal view; S3 19.1 (r) and S3 19.2 (l): medial cuneiforms in view from the intermediate cuneiform; S3 8.12 (l): intermediate cuneiform in view from the medial cuneiform; S3 19.3 (r): lateral cuneiform in view from the cuboid; S3 23.2 (l) and S3 8.5 (r): tali in plantar view; S3 12.14 (l) and S3 17.3 (r): Calcanei in dorsal view.

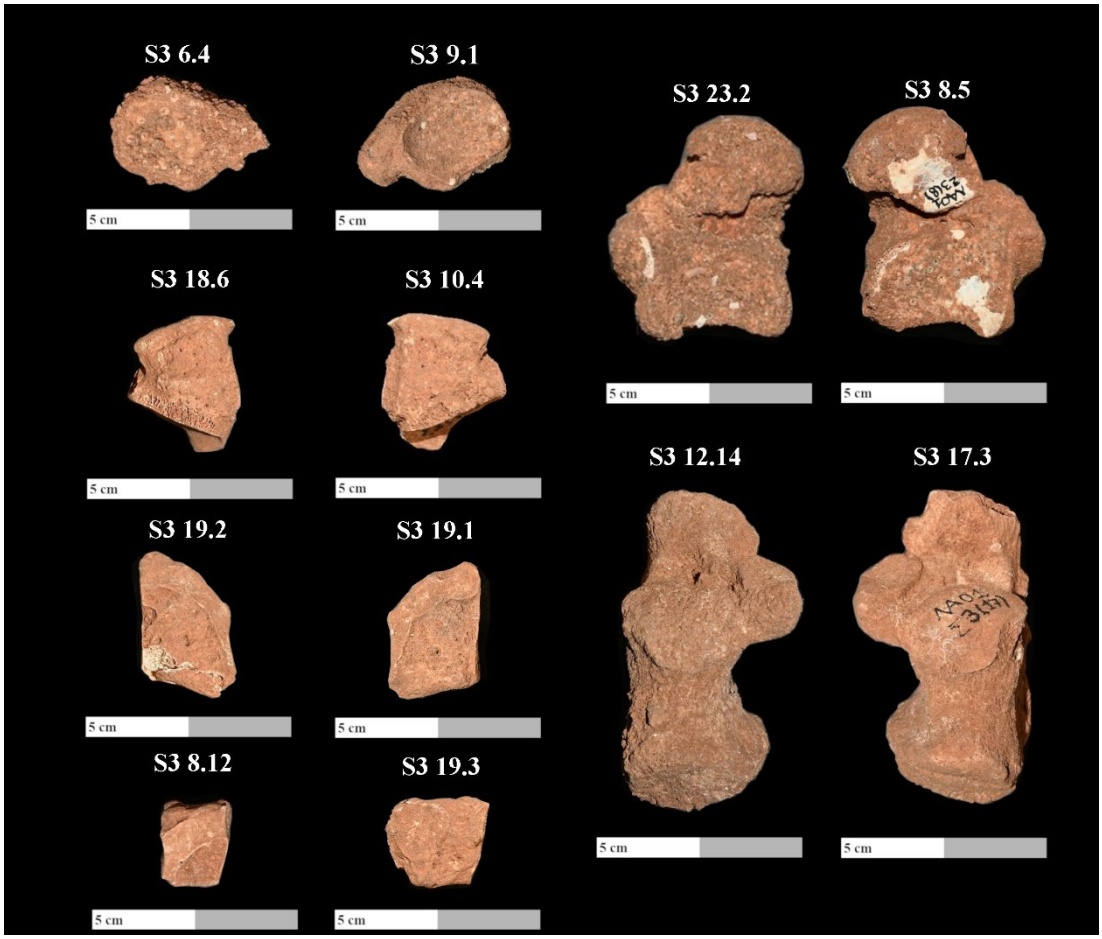

Metatarsals

SI-Figure 16 shows all metatarsalia from the Apidima 3 inventory.

S3 11.6: MT1 (l)

The left first metatarsus has a preserved maximum length: 38.38 mm. Preserved is a proximal fragment including the base and medial half of the proximal shaft portion. The distal bone half is not preserved, and the fracturing line occurred around the mid-shaft location. The lateral half of the proximal shaft is not preserved. On the proximal base, medially and inferiorly located is an oval-shaped lesion, but its formation was due to taphonomy. The bone fragmentation is, in general, of an older nature since the exposed internal bone structures are filled with solidified sediment.

S3 9.4 and S3 11.2: MT2 (r)

The right second metatarsus has a preserved maximum length of 29.31 mm for the proximal fragment and a maximum. length of 44.36 mm for the distal fragment. No visible signs of damage except for the oblique fracture line that separated the bone into two pieces and slight compact bone abrasions where the bone surface is not covered by sediment crust.

S3 6.2: MT2 (l)
The left second metatarsus has a preserved maximum length of 50.5 mm. Most of the proximal base morphology is preserved, but the inferior margin and the lateral inferior articular facet are not preserved. Distally, the shaft is broken into step fractures around the mid-shaft. The distal half is missing.

S3 9.3: MT3 (l)
The left third metatarsus has a preserved maximum length of 67.22 mm. The shaft and proximal base morphology are well preserved, but the distal end is missing. A compact bone fracture shows irregular edges, and the exposed trabecular architecture contains sediment fill.

S3 20.2: MT4 (l)
The left fourth metatarsus has a preserved maximum length of 35.96 mm. Only the proximal base and the most proximal shaft portion are preserved. Recent surface damage is present around the margins of the cuboid articular facet. The distal shaft fracture shows step-like and irregular edges and a vertical crack parallel to the shaft axis. The fracturing event is of older nature since the exposed internal bone structure shows filling with solidified sediment.

SI-Figure 16. Metatarsalia (MT) of Apidima 3. MT1 (l) in medial view; S3 6.2: MT2 (l) in dorsal view; S3 9.4 and S3 11.2: MT2 (r): lateral view; S3 9.3: MT3 (l) in dorsal view; S3 11.6: S3 20.2: MT4 (l) in lateral view.

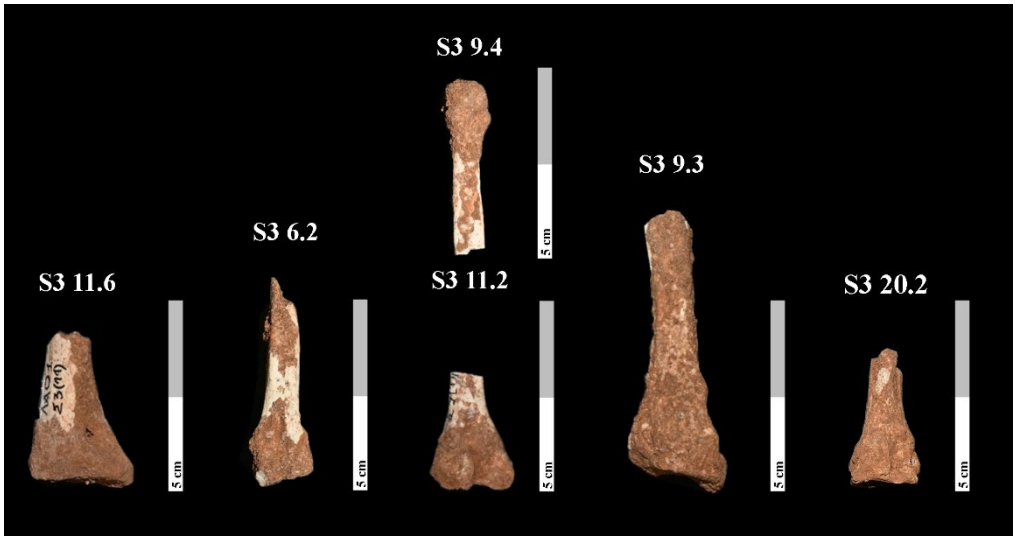

Phalanges
Mostly proximal phalanges were retrieved during the 1984 excavation, but one medial and one distal phalanx were also found. All foot phalanges of Apidima 3 are shown in SI-Figure 17. Complete proximal phalanges are recorded as S3 8.4, S3 12.4, S3 23.1, and S3 24.1. One medial phalanx was found and is recorded as S3 15.4, and one distal phalanx (right side, first row) has the ID S3 22.1. All phalanges were retrieved in very good condition, with only minimal visible surface damage. Only the distal phalanx S3 22.1 has minimal damage on the contours of the base and the distal tip, but the rest of the bone is also very well preserved. The surfaces are covered by a thin layer of sediment crust in all bones, but the thickness and granulation vary. The phalanges have no unusual characteristics, except for the distal phalanx S3 22.1, which is characterized by severe osteoarthritic changes (see "Paleopathology, Non-Metric Traits, and Skeletal Modifications" and Figure 7). Despite the osteoarthritic condition of S3 22.1, no signs of degenerative changes or pathologies were observed on the other phalanges.

SI-Figure 17. Phalanges pedis distalis of Apidima 3. All phalanges are shown in dorsal view with the distal end pointing up.

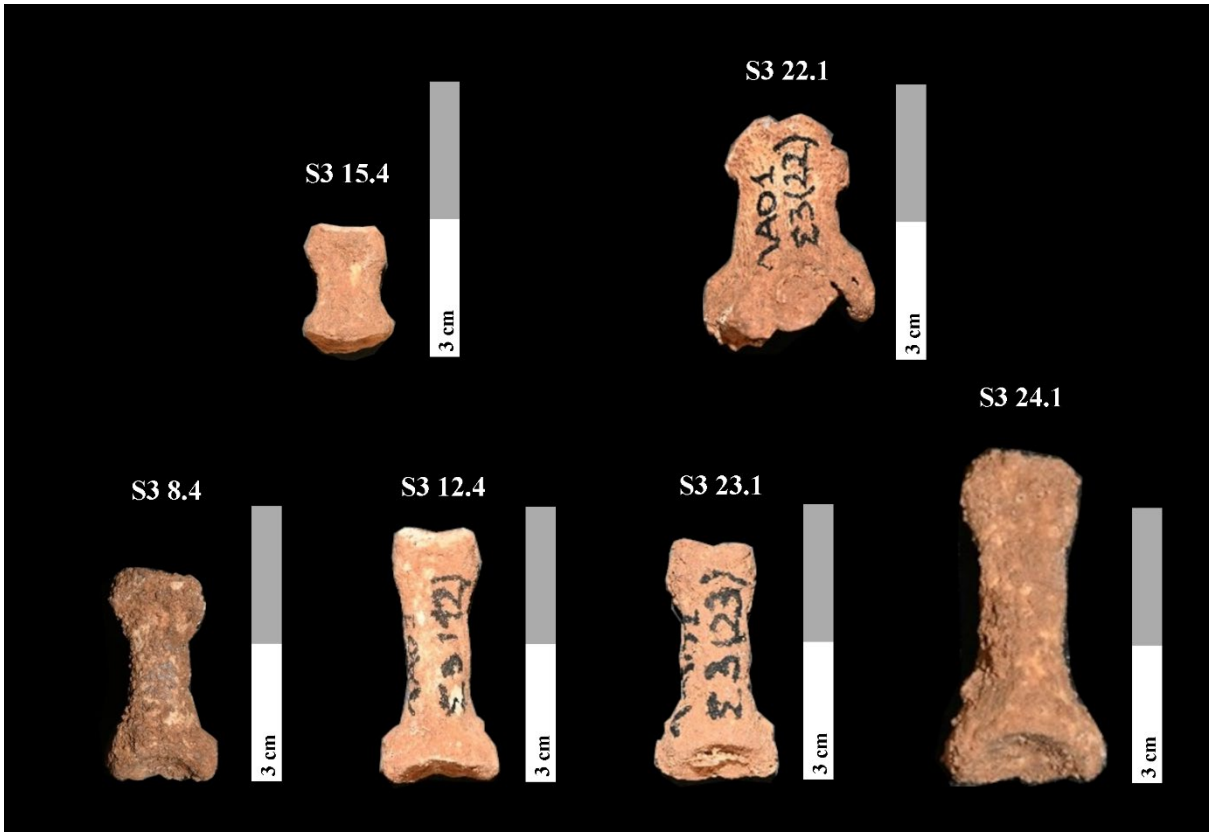

MORPHOLOGICAL DESCRIPTION OF APIDIMA 4

All skeletal elements that could be identified as not belonging to Apidima 3 and were therefore assigned to the second adult individual, Apidima 4, are presented in SI-Figure 18.

S9.1: Tibia (l)

The left tibia S9.1 is in an extreme state of fragmentation. All preserved morphological features are damaged. Represented is a distal end fragment with a maximum length of 54.58 mm that includes the lateral malleolus and a small portion of the anterior surface, as well as a small area of the distal articular surface. The distal half of the diaphysis, with a maximum length of 141.85 mm, is preserved as several small fragments that are agglomerated and connected by sediment but compressed into each other. The most distal area shows some exposed trabeculae, and it refits with the distal end fragment. The proximal half is preserved as a single, larger fragment with a maximum length of 229 mm. This fragment includes features like the tibial tuberosity, the soleal line, and a small portion of the medial condyle. Except for this remnant of the medial condyle, the tibial plateau is not preserved, and the proximal fragment shows two major vertical cracks along its diaphysis. One more diaphysis fragment with a maximum length of 51.17 mm is preserved and refits to the distal end of the posterior surface of the proximal half fragment. Attached to the distal articular joint surface is the proximal end of a small-sized mammal limb bone.

Due to the extreme fragmentary state of preservation and relatively thick sedimentary crust that covers most bone surfaces, it is not possible to provide a more detailed morphological description of the left tibia S9.1. This is unfortunate, especially because its association with the other human skeletal remains that are registered as Apidima 3 is unclear. More specific explanations about the relationship between the left tibia and the other lower limb remains are provided in the section “Burial

Taphonomy". Still, it can be noted that in the left tibia, the anterior squatting facet seems to be absent, while the presence of a very well pronounced squatting facet on the right tibia and the presence of squatting facets on the tali have been observed. The soleal line appears prominent, and the shaft generally seems to be very narrow compared to the right tibia. It is, however, difficult to provide a reliable description of the true nature of bone morphology due to the severe state of bone compression and fragmentation.

S26.1: Talus (r)

The second right talus is registered under the primary ID S26.1. Most morphological features are damaged. Only the posterior subtalar facet and the talar trochlea are vastly intact, but little damage around their margins is still present. The talar head is preserved only by a tiny remnant of the anterior articular surface and by some trabecular architecture. The lateral malleolar articular surface is also just partially represented. The lateral process and the entire medial aspect of the talus are not preserved. The exposed internal bone structures are filled with solidified sediments. Direct qualitative and quantitative comparisons to the tali of Apidima 3 were not possible due to high levels of bone damage.

S3 6.5: Lateral cuneiform (r)

We have identified S3 6.5 as a right lateral cuneiform that originated from the human remains of a second adult individual based on its mismatching articulation with the right cuboid S3 10.4. A closer look at the joint morphology revealed that S3 19.3 exhibits different outlines of its articular facets. The distal articular facet of S3 6.5 has an elongated shape and appears wider compared to S3 19.3. Its navicular articular facet, however, is shorter. Both the surface and the shape of the articular facet for the intermediate cuneiform are rounder in S3 6.5, and its transition to the body of the lateral cuneiform is less steep than in S3 19.3. The inferior aspect of the lateral cuneiform shows a narrow body that originates from the inferior rim of the distal articular facet and continues posteriorly, where its shape shows a step-like incision before the transition to the navicular articular facet. From the medial and lateral point of view, this narrow body is longer in S3 19.3, and its transition to the navicular articular facet is much more abrupt, whereas in S3 6.5, the transition begins more distally and appears more oblique.

Both lateral cuneiforms have excellent bone preservation, but S3 6.5 exhibits some surface damage on its medial aspect, particularly at the anterior and posterior margins.

It is interesting to note that the solidified sediment crust attached to the bone surfaces also exhibits slight color differences. Sediment attached to S3 6.5 is preserved as a thicker and more granular crust with a darker red-brown color than in S3 19.3.

SI-Figure 18. Skeletal elements of Apidima 4. S9.1 (l): Tibia in anteromedial view. S3 6.5 (r): lateral cuneiform in view from the cuboid. S26.1 (r): Talus in plantar view.

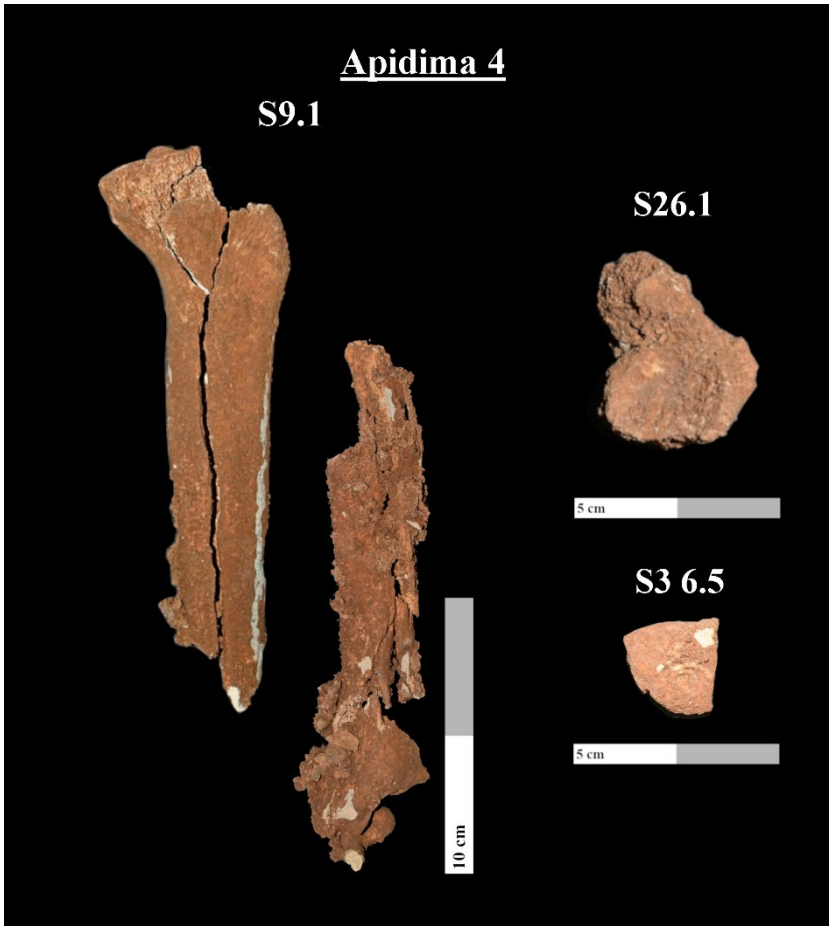

Supplementary Tables

SI-Table 1. List of Upper Palaeolithic specimens used as samples for the osteometric comparison with Apidima 3. The comparative data were obtained from the reference publication of the respective specimen. If measurement values were available bilaterally, the average value of right and left was used for the comparison with Apidima 3's measurements.

Specimen	Hu	Rad	Ul	Fem	Tib	Fib	Sex	Culture	Geography	Reference
Dolní Věstonice 13	x	x	x	x	x	x	Male	Gravettian	Czech Republic	Sládek et al. 2000; Fewlass et al. 2019; Mittnik et al. 2016
Dolní Věstonice 14	x	x	x	x	x	x	Male	Gravettian	Czech Republic	Sládek et al. 2000; Fewlass et al. 2019; Mittnik et al. 2016
Dolní Věstonice 15	x	x	x	x	x	x	Male	Gravettian	Czech Republic	Sládek et al. 2000; Fewlass et al. 2019; Mittnik et al. 2016
Dolní Věstonice 16	x	x	x	x	x	x	Male	Gravettian	Czech Republic	Sládek et al. 2000; Fewlass et al. 2019
Dolní Věstonice 3		x	x	x	x	x	Female	Gravettian	Czech Republic	Sládek et al. 2000
Pavlov 1	x	x	x	x			Male	Gravettian	Czech Republic	Sládek et al. 2000; Fewlass et al. 2019
Předmostí 1					x		Male	Gravettian	Czech Republic	Mallegni et al. 2000; Trinkaus and Ruff 2012
Předmostí 10				x	x		Female	Gravettian	Czech Republic	Mallegni et al. 2000; Trinkaus and Ruff 2012
Předmostí 14				x	x		Male	Gravettian	Czech Republic	Mallegni et al. 2000; Trinkaus and Ruff 2012
Předmostí 3				x	x	x	Male	Gravettian	Czech Republic	Mallegni et al. 2000; Trinkaus and Ruff 2012
Předmostí 4	x	x	x	x	x	x	Female	Gravettian	Czech Republic	Billy 1975; Mallegni et al. 2000; Trinkaus and Ruff 2012
Předmostí 9				x	x		Male	Gravettian	Czech Republic	Mallegni et al. 2000; Trinkaus and Ruff 2012

Specimen	Hu	Rad	Ul	Fem	Tib	Fib	Sex	Culture	Geography	Reference
Abri Pataud 8						x	Female	Gravettian	France	Billy 1975
Cap-Blanc	x	x	x	x	x		Female	Magdalenian	France	Billy 1975; Trinkaus and Ruff 2012
Chancelade	x		x				Male	Magdalenian	France	Billy 1975
Cro Magnon 4306		x					Male	Gravettian	France	Villotte et al. 2020; Trinkaus et al. 2022
Cro Magnon Alpha		x	x	x	x	x	Male	Gravettian	France	Villotte et al. 2020
Cro Magnon Beta	x	x		x			Female	Gravettian	France	Villotte et al. 2020
Cro Magnon Gamma	x	x	x	x	x	x	Male	Gravettian	France	Villotte et al. 2020
La Rochette		x	x	x			Male	Gravettian	France	Naumann and Harvati 2026
P3 - Abri Pataud 22	x	x	x				Female	Gravettian	France	Billy 1975
P5 - Abri Pataud 7		x	x				Male	Gravettian	France	Billy 1975
Parabita 1				x	x	x	Male	Gravettian	France	Mallegni et al. 2000; Trinkaus and Ruff 2012
Parabita 2				x	x	x	Female	Gravettian	France	Mallegni et al. 2000; Trinkaus and Ruff 2012
Saint-Germain-la-Rivière		x	x				Female	Magdalenian	France	Billy 1975
Oberkassel 1				x			Male	Magdalenian	Germany	Trinkaus and Ruff 2012; Orschiedt et al. 2017
Oberkassel 2	x		x	x	x	x	Female	Magdalenian	Germany	Trinkaus and Ruff 2012; Orschiedt et al. 2017
Arence Candide 1				x			Male	Gravettian	Italy	Trinkaus and Ruff 2012

Specimen	Hu	Rad	Ul	Fem	Tib	Fib	Sex	Culture	Geography	Reference
Baousso da Torre 1	x	x		x	x		Male	Gravettian	Italy	Villotte 2017
Baousso da Torre 2	x	x	x	x	x	x	Male	Gravettian	Italy	Villotte 2017
Barma Grande 1				x	x		Male	Gravettian	Italy	Mallegni et al. 2000; Trinkaus and Ruff 2012
Barma Grande 2	x	x		x	x		Male	Gravettian	Italy	Churchill and Formicola 1997; Mallegni et al. 2000; Trinkaus and Ruff 2012
Barma Grande 6				x			Male	Gravettian	Italy	Trinkaus and Ruff 2012
Caviglione 1				x			Female	Gravettian	Italy	Trinkaus and Ruff 2012
Grotte des Enfants 3					x		Female	Gravettian	Italy	Mallegni et al. 2000
Grotte des Enfants 4				x	x		Male	Gravettian	Italy	Mallegni et al. 2000; Trinkaus and Ruff 2012
Grotte des Enfants 5					x		Female	Gravettian	Italy	Mallegni et al. 2000
Grotte des Enfants 6					x		Male	Gravettian	Italy	Mallegni et al. 2000
Paglicci 25				x	x	x	Female	Gravettian	Italy	Mallegni et al. 2000
Romito 1	x	x	x	x			Female	Epigravettian	Italy	Mallegni and Fabbri 1995
Romito 3	x	x	x	x	x	x	Male	Epigravettian	Italy	Mallegni and Fabbri 1995
Romito 4	x	x	x	x	x	x	Female	Epigravettian	Italy	Mallegni and Fabbri 1995
Romito 5		x	x	x			Female	Epigravettian	Italy	Mallegni and Fabbri 1995
Romito 6		x	x	x	x	x	Male	Epigravettian	Italy	Mallegni and Fabbri 1995

Specimen	Hu	Rad	Ul	Fem	Tib	Fib	Sex	Culture	Geography	Reference
Villabruna 1	x	x	x		x		Male	Epigravettian	Italy	Vercellotti et al. 2008
Sunghir 1				x			Male	Gravettian	Russia	Trinkaus and Ruff 2012
Eel Point 1	x						Male	Gravettian	United Kingdom	Schulting et al. 2005
Paviland 1	x			x			Male	Gravettian	United Kingdom	Trinkaus and Holliday 2000; Trinkaus and Ruff 2012

SI-Table 2. List of Upper Palaeolithic specimens used for the comparison with the stature estimate of Apidima 3 presented in Figure 5. The comparative data were obtained from the listed reference publications.

Specimen	Sex	Chronological Group	Culture	Geography	Stature (cm)	Reference
Grotte des Enfants 5	Female	EUP	Gravettian	Italy	164	Trinkaus and Jelinek 1997
Abri Pataud 22	Female	EUP	Gravettian	France	160.5	Billy 1975
Dolní Věstonice 3	Female	EUP	Gravettian	Czech Republic	161.2	Trinkaus and Jelinek 1997
Předmostí 10	Female	EUP	Gravettian	Czech Republic	162.5	Billy 1975
Předmostí 4	Female	EUP	Gravettian	Czech Republic	165	Billy 1975
Cro-Magnon 2	Female	EUP	Gravettian	France	166	Billy 1975
Paglicci 3	Female	EUP	Gravettian	Italy	169.2	Trinkaus and Jelinek 1997
Caviglione 1	Female	EUP	Gravettian	Italy	172.7	Trinkaus and Jelinek 1997
Parabita 2	Female	EUP	Gravettian	France	172.4	Trinkaus and Ruff 2012
Oberkassel 2	Female	LUP	Magdalenian	Germany	147.1	Orschiedt et al. 2017
Saint-Germain-la-Rivière	Female	LUP	Magdalenian	France	155.3	Billy 1975
Cap-Blanc	Female	LUP	Magdalenian	France	157	Billy 1975
El Mirón	Female	LUP	Magdalenian	Spain	159.9	Carrero et al. 2015
Romito 4	Female	LUP	Epigravettian	Italy	161.04	Mallegni and Fabri 1995

SI-Table 3. List of Upper Palaeolithic specimens used for the comparison with the body mass estimate of Apidima 3 presented in Figure 6. The comparative data were obtained from the listed reference publications.

Specimen	Sex	Chronological Group	Culture	Geography	Body mass (kg)	Reference
Arene Candide (IP)	Male	EUP	Gravettian	Italy	73.1	Trinkaus and Ruff 2012
Baousso da Torre 1	Male	EUP	Gravettian	Italy	78.1	Villotte et al. 2017
Baousso da Torre 2	Male	EUP	Gravettian	Italy	73.1	Villotte et al. 2017
Barma Grande 2	Male	EUP	Gravettian	Italy	81.1	Trinkaus and Ruff 2012
Brno 2	Male	EUP	Gravettian	Czech Republic	67	Dočkalová and Vančata 2005
Cro Magnon 1	Male	EUP	Gravettian	France	67.3	Trinkaus and Ruff 2012
Cro Magnon Alpha	Male	EUP	Gravettian	France	69.1	Trinkaus et al. 2022
Cro Magnon Beta	Female	EUP	Gravettian	France	56.8	Trinkaus et al. 2022
Cro Magnon Gamma	Male	EUP	Gravettian	France	73	Trinkaus et al. 2022
Dolní Věstonice 13	Male	EUP	Gravettian	Czech Republic	69.5	Trinkaus and Ruff 2012
Dolní Věstonice 14	Male	EUP	Gravettian	Czech Republic	77.8	Trinkaus and Ruff 2012
Dolní Věstonice 16	Male	EUP	Gravettian	Czech Republic	76.6	Trinkaus and Ruff 2012
Dolní Věstonice 3	Female	EUP	Gravettian	Czech Republic	54.3	Trinkaus and Ruff 2012
Grotte-des-Enfants 4	Male	EUP	Gravettian	Italy	82.5	Trinkaus and Ruff 2012
Paglicci 25	Female	EUP	Gravettian	Italy	59.7	Trinkaus and Ruff 2012
Paviland 1	Male	EUP	Gravettian	United Kingdom	72.4	Trinkaus and Ruff 2012
Veneri 1	Male	EUP	Gravettian	France	75.7	Trinkaus and Ruff 2012
Veneri 2	Female	EUP	Gravettian	France	74.6	Trinkaus and Ruff 2012
La Rochette	Male	EUP	Gravettian	France	63.18	Naumann and Harvati 2026
El Mirón	Female	LUP	Magdalenian	Spain	59.6	Carrero et al. 2015
Šandalja 14050	Female	LUP	Epigravettian	Croatia	59.2	Jankovic et al. 2012
Villabrunna 1	Male	LUP	Epigravettian	Italy	66.2	Vercellotti et al. 2008
Oberkassel 1	Male	LUP	Magdalenian	Germany	71.01	Orschiedt et al. 2017
Romito 4	Female	LUP	Epigravettian	Italy	65.35	Mallegni and Fabri 1995

SI-Table 4. Osteometry of Apidima 3 – Bräuer (1988) measurements of scapulae. All measurements are in mm. Error (%) was calculated as 100*((X1-X2)/X2) with X1 being the larger value.

Measurement definitions by Bräuer (1988)	S3 13.2 L	S3 8.10 R	Difference (mm)	Error (%)
supraspinous fossa breadth (M6)	-	38.93	-	-
acromial length (M10)	-	43	-	-
max coracoid length (M11)	38.8	-	-	-
glenoid height (M12)	38.03	38.02	0.01	0.03

SI-Table 5. Osteometry of Apidima 3 – Bräuer (1988) measurements of humeri. All measurements are in mm. Error (%) was calculated as 100*((X1-X2)/X2) with X1 being the larger value.

Measurement definitions by Bräuer (1988)	S3 13.1 L	S3 8.1 R	Difference (mm)	Error (%)
maximum length (M1)	298.75	302.47	-3.72	1.25
total length (M2)	-	299.32	-	-
prox. epiphyseal breadth (M3)	-	46.5	-	-
epicondylar breadth (M4)	52.5	55.6	-3.1	5.90
humeral head anteroposterior diameter (M9)	-	38.7	-	-
humeral head superoinferior diameter (M10)	40.7	41.9	-1.2	2.95
mediolateral breadth of trochlea (M11)	22.5	22.55	-0.05	0.22
mediolateral breadth of capitulum (M12)	16.4	16.4	0	0.00
width of distal articular surface (M12a)	38.9	38.95	-0.05	0.13
capitular height (M12c)	19.2	19.33	-0.13	0.68
trochlear depth (M13)	21.65	23.1	-1.45	6.70
width of olecranon fossa (M14)	24.86	23.6	1.26	5.34
depth of olecranon fossa (M15)	7.89	8.13	-0.24	3.04

SI-Table 6. Osteometry of Apidima 3 – Bräuer (1988) measurements of radii. All measurements are in mm.

Measurement definitions by Bräuer (1988)	S3 17.2 L
maximum length (M1)	232
head-neck length (M1a)	31.43
parallel length (M1b)	227
height of articular circumference of radial head (M1d)	9.18
smallest circumference of the distal diaphyseal half (M3)	39
maximum mediolateral shaft diameter (M4)	15.19
breadth of carpal articular facet (M4b)	15.57
transverse head diameter (M4(1))	19.8
transverse neck diameter (M4(2))	10.05
smallest sagittal shaft diameter (M5)	10.5
sagittal head diameter (M5(1))	19.44
sagittal neck diameter (M5(2))	11.22
head circumference (M5(3))	62
neck circumference (M5(4))	40
mid-shaft circumference (M5(5))	42

SI-Table 7. Osteometry of Apidima 3 – Bräuer (1988) measurements of ulnae. All measurements are in mm.

Measurement definitions by Bräuer (1988)	S3 17.1 L
minimal circumference of distal diaphyseal portion (M3)	35
smallest circumference at the height of the ulnar tuberosity (M3b)	52
height of proximal articular surface (M5(1))	35.76
estimated height of humerus joint surface (M5 (2))	27.67
olecranon breadth (M6)	23
smallest olecranon breadth at the height of the trochlear notch (M6a)	15.26
depth of olecranon (M7)	23.5
greatest sagittal olecranon dimension (M7a)	21.6
smallest olecranon diameter (M7b)	17.87
anteroposterior distance from coronoid process to dorsal shaft (M7d)	30.65
trochlear-notch height (M7(1))	22.24
olecranon height (M8)	17
anterior breadth of radial articular surface on coronoid process (M9)	10.5
breadth of radial notch (M9a)	16.5
height of radial notch (M9b)	10.9
dorsoventral shaft diameter (M11)	14.57
mediolateral shaft diameter (M12)	12.04
transverse diameter (M13)	18.04
anteroposterior diameter (M14)	20.75

SI-Table 8. Osteometry of Apidima 3 – Bräuer (1988) measurements of capitates. All measurements are in mm.

Measurement definitions by Bräuer (1988)	S3 6.6 L
maximum length (M1)	24.2
maximum breadth (M2)	15.58
maximum height (M3)	17.54
maximum breadth of capitate head (M5)	14.63
maximum height of distal articular facet (M7)	15.81
maximum breadth of distal articular facet (M8)	12.92

SI-Table 9. Osteometry of Apidima 3 – Bräuer (1988) measurements of hamates. All measurements are in mm.

Measurement definitions by Bräuer (1988)	S3 8.24 L
maximum length (M1)	19.28
maximum height (M3)	20.78
hamate body height (M4)	13.68
hamulus height (M5)	7.1
height of distal articular facet (M7)	10.96

SI-Table 10. Osteometry of Apidima 3 – Bräuer (1988) measurements of femora. All measurements are in mm. Error (%) was calculated as 100*((X1-X2)/X2) with X1 being the larger value.

Measurement definitions by Bräuer (1988)	S3 12.16 L	S3 12.15 R	Difference (mm)	Error (%)
diaphyseal length (M5)	365	-	-	-
alternative diaphyseal length (M5a)	378	-	-	-
anteroposterior mid-shaft diameter (M6)	29.19	31.57	-2.38	8.15
mediolateral mid-shaft diameter (M7)	26.53	26.14	0.39	1.49
mid-shaft circumference (M8)	91	92	-1	1.10
mediolateral diameter of proximal shaft (M9)	34.29	33.67	0.62	1.84
anteroposterior diameter of proximal shaft (M10)	23.37	23.6	-0.23	0.98
dorsoventral diameter of the shaft just above the condyles (M11)	28.86	29.16	-0.3	1.04
mediolateral diameter of the shaft just above the condyles (M12)	32.3	32.47	-0.17	0.53
upper epiphyseal length (M13)	84.16	-	-	-
proximal width (M13a)	88.1	-	-	-
anterior head and neck length (M14)	61.55	-	-	-
head length (M14b)	31.88	-	-	-
neck length (M14c)	28.6	-	-	-
vertical diameter of neck (M15)	27.29	-	-	-
anteroposterior diameter of neck (M16)	23.51	-	-	-
neck circumference (M17)	90	-	-	-
superoinferior head diameter (M18)	42.87	-	-	-
anteroposterior head diameter (M19)	40.69	-	-	-
head circumference (M20)	135	-	-	-
mediolateral breadth of epicondyles (M21)	76.29	76.28	0.01	0.01
anterior breadth of medial condyle (M21a)	42.11	41.13	0.98	2.38
anterior breadth of lateral condyle (M21b)	37.49	36.32	1.17	3.22
posterior breadth of medial condyle (M21c)	26.04	23.26	2.78	11.95

Measurement definitions by Bräuer (1988)	S3 12.16 L	S3 12.15 R	Difference (mm)	Error (%)
condylar notch width (M21d)	19.48	19.07	0.41	2.15
posterior breadth of lateral condyle (M21e)	25.69	24.49	1.2	4.90
greatest dorsoventral length of lateral condyle (M23)	57.5	61.48	-3.98	6.92
greatest dorsoventral length of medial condyle (M24)	60.79	59.4	1.39	2.34
height of lateral condyle (M25)	35.58	36.16	-0.58	1.63
height of medial condyle (M26)	35.79	36.58	-0.79	2.21

SI-Table 11. Osteometry of Apidima 3 – Bräuer (1988) measurements of tibiae. All measurements are in mm.

Measurement definitions by Bräuer (1988)	**S3 11.1/ S3 12.13 R**
lateral condyle-malleolar length (M1)	347.95
maximum length (M1a)	353.6
medial condyle-malleolar length (M1b)	348
bicyondylar breadth (M3)	68.55
breadth of the medial condyle (M3a)	30.5
breadth of the lateral condyle (M3b)	33
maximum sagittal diameter at level of the tibial tuberosity (M4)	46.05
sagittal diameter of medial condyle (M4a)	48
sagittal diameter of lateral condyle (M4b)	41.5
minimum transverse diameter of tibia at level of the tibia tuberosity (M5)	-
mediolateral diameter of distal epiphysis (M6)	47.73
anteroposterior diameter of distal epiphysis (M7)	34.3
anteroposterior mid-shaft diameter (M8)	31.3
mediolateral mid-shaft diameter (M9)	18.75
mid-shaft circumference (M10)	-
smallest diaphysis circumference (M10b)	-

SI-Table 12. Osteometry of Apidima 3 – Bräuer (1988) measurements of fibulae. All measurements are in mm.

Measurement definitions by Bräuer (1988)	S3 9.2/ S3 12.18	S3 8.27/ S3 12.12
	L	R
maximum length (M1)	-	341.32
maximum mid-shaft diameter (M2)	-	16.5
minimum mid-shaft diameter (M3)	-	10.6
mediolateral diameter (M3(1))	-	15.32
anteroposterior diameter (M3(2))	-	16.1
maximum proximal diaphyseal breadth (M4(1))	28.43	-
maximum distal epiphyseal breadth (M4(2))	-	18.5

SI-Table 13. Osteometry of Apidima 3 – Bräuer (1988) measurements of patellae. All measurements are in mm. Error (%) was calculated as 100*((X1-X2)/X2) with X1 being the larger value.

Measurement definitions by Bräuer (1988)	S3 12.17 L	S3 12.9 R	Difference (mm)	Error (%)
patellar height (M1)	37.8	37.7	0.1	0.27
maximum patellar breadth (M2)	43.65	42.49	1.16	2.73
maximum thickness (M3)	-	22.75	-	-
articular height (M4)	-	29.45	-	-
breadth of medial articular facet (M5)	-	18.31	-	-
breadth of lateral articular facet (M6)	-	23.96	-	-

SI-Table 14. Osteometry of Apidima 3 – Bräuer (1988) measurements of calcanei. All measurements are in mm. Error (%) was calculated as 100*((X1-X2)/X2) with X1 being the larger value.

Measurement definitions by Bräuer (1988)	S3 12.14 L	S3 17.3 R	Difference (mm)	Error (%)
maximum length (M1)	72.25	72.43	-0.18	0.25
length between calcaneal tuberosity and the cuboid articular facet (M1a)	68.72	67.94	0.78	1.15
medial breadth across the talar sustentaculum (M2)	39.6	38.66	0.94	2.43
height of body (M4)	35.26	35.29	-0.03	0.09
maximum body height (M4a)	40.23	-	-	-
length of body (M5)	52.18	52.07	0.11	0.21
load arm length (M5a)	44.5	45.66	-1.16	2.61
height of the calcaneal tuberosity (M7)	38.54	39.7	-1.16	3.01
breadth of the calcaneal tuberosity (M8)	29.07	29.1	-0.03	0.10
length of the posterior articular surface for the talus (M9)	27	27.09	-0.09	0.33
breadth of the posterior articular surface of the talus (M10)	27.35	28.81	-1.46	5.34
cuboid articular breadth (M12)	25.71	25.91	-0.2	0.78

SI-Table 15. Osteometry of Apidima 3 – Bräuer (1988) measurements of tali. All measurements are in mm. Error (%) was calculated as 100*((X1-X2)/X2) with X1 being the larger value.

Measurement definitions by Bräuer (1988)	S3 23.2 L	S3 8.5 R	Difference (mm)	Error (%)
talar length (M1)	48.19	48.2	-0.01	0.02
maximum talar length (M1a)	54.76	55.1	-0.34	0.62
talar width (M2)	40.04	38.51	1.53	3.97
articular breadth (M2b)	39.34	39.39	-0.05	0.13
talar height (M3)	28.65	28	0.65	2.32
medial talar height (M3(1))	29.56	28.96	0.6	2.07
length of trochlea (M4)	32.1	31.55	0.55	1.74
breadth of trochlea (M5)	25.49	24.84	0.65	2.62
posterior breadth of trochlea (M5(1))	21.64	20.87	0.77	3.69
anterior breadth of trochlea (M5(2))	27.15	26.5	0.65	2.45
lateral malleolar oblique height (M7)	28.19	27.79	0.4	1.44
head breadth (M10)	28.04	28.19	-0.15	0.53
head height (M11)	28.27	28.11	0.16	0.57
length of posterior articular surface for calcaneus (M12)	28.8	-	-	-
breadth of posterior articular surface for calcaneus (M13)	32.69	32.39	0.3	0.93

SI-Table 16. Osteometry of Apidima 3 – Bräuer (1988) measurements of naviculares. All measurements are in mm. Error (%) was calculated as 100*((X1-X2)/X2) with X1 being the larger value.

Measurement definitions by Bräuer (1988)	S3 6.4 L	S3 9.1 R	Difference (mm)	Error (%)
navicular breadth (M1)	-	35.98	-	-
navicular height (M2)	26.83	26.8	0.03	0.11
talar articular length (M3)	21.63	22.56	-0.93	4.30
talar articular height (M4)	26.6	26.59	0.01	0.04
articular length for cuneiforms (M6)	-	33.13	-	-
minimum thickness (M7)	6.45	7.11	-0.66	10.23
maximum thickness (M8)	19.6	18.88	0.72	3.81

SI-Table 17. Osteometry of Apidima 3 – Bräuer (1988) measurements of cuboidea. All measurements are in mm. Error (%) was calculated as 100*((X1-X2)/X2) with X1 being the larger value.

Measurement definitions by Bräuer (1988)	S3 18.6 L	S3 10.4 R	Difference (mm)	Error (%)
medial length (M1)	30.74	30.97	-0.23	0.75
lateral length (M2)	14.13	14.92	-0.79	5.59
cuboid height (M3)	22.43	22.45	-0.02	0.09

SI-Table 18. Osteometry of Apidima 3 – Bräuer (1988) measurements of medial cuneiformia. All measurements are in mm. Error (%) was calculated as 100*((X1-X2)/X2) with X1 being the larger value.

Measurement definitions by Bräuer (1988)	S3 19.2 L	S3 19.1 R	Difference (mm)	Error (%)
inferior length (M1)	21.76	21.62	0.14	0.65
middle length (M2)	18.71	18.68	0.03	0.16
superior length (M3)	24.36	24.55	-0.19	0.78
proximal articular height (M4)	17.45	17.88	-0.43	2.46
distal articular height (M5)	-	28.43	-	-
proximal height (M6)	21.15	21.66	-0.51	2.41
distal height (M7)	29.75	29.59	0.16	0.54
medial cuneiform breadth (M8)	-	16.68	-	-

SI-Table 19. Osteometry of Apidima 3 – Bräuer (1988) measurements of intermediate and lateral cuneiformia. All measurements are in mm.

Measurement definitions by Bräuer (1988)	S3 19.3 lateral - R	S3 6.5 lateral - R	S3 8.12 intermediate - L
superior length (M1)	20.6	21	15.47
superior middle breadth (M2)	12.73	13.45	16.06
distal breadth - lateral cuneiform only (M3)	13.48	14.05	-
proximal breadth - lateral cuneiform only (M4)	12.44	12.24	-

SI-Table 20. Osteometry of Apidima 3 – Bräuer (1988) measurements of metatarsalia. All measurements are in mm.

Measurement definitions by Bräuer (1988)	S3 9.4/S3 11.2 MT 2 - R	S3 9.3 MT 3 - L	S3 6.2 MT 2 - L	S3 20.2 MT 4 - L	S3 11.6 MT 1 - L
metatarsal length (M2)	70.75	-	-	-	-
mid-shaft breadth (M3)	7.72	6.56	-	-	-
mid-shaft height (M4)	7.92	8.14	-	-	-
proximal breadth (M6a)	13.69	12.21	14.23	11.62	-
height of MT 1 (M7)	-	-	-	-	26.52
maximum height (M7a)	21.5	19.21	-	17.14	-
proximal articular height (M7b)	20.44	18.93	-	16.87	25.46
distal epiphyseal breadth (M8a)	11.75	-	-	-	-
distal articular breadth (M8b)	10.29	-	-	-	-
distal height (M9a)	14.3	-	-	-	-

SI-Table 21. Osteometry of Apidima 3 – Bräuer (1988) measurements of phalanges pedis. All measurements are in mm.

Measurement definitions by Bräuer (1988)	S3 12.4 prox., R	S3 24.1 prox., R	S3 8.4 prox., R	S3 15.4 intermediate, R	S3 23.1 prox., R	S3 22.1 distal, R
phalanx length (M1)	24.1	21.09	18.93	12.3	22.08	-
articular length (M1a)	24.6	21.34	19.77	12.06	22.8	-
mid-shaft breadth (M2)	6.8	5.92	6.09	6.56	7.15	-
proximal max breadth (M2a)	12.62	11.52	11.67	9.52	13	-
distal max breadth (M2b)	9.1	8.31	9.82	8.51	9.69	-
mid-shaft height (M3)	6.2	5.74	5.5	4.42	6.96	-
proximal height (M3a)	11.63	10.24	10.03	8.51	11.56	-
distal height (M3b)	5.57	5.76	6.12	4.76	6.93	-

SI-Table 22. Osteometry of Apidima 3 – Bräuer (1988) measurements of metacarpalia and phalanges manus. All measurements are in mm.

Measurement definitions by Bräuer (1988)	O302.1 prox., pos. 1, R	S12.1 prox., R	S10.1 prox., R	S3 1.1 prox., R
metacarpal length (M2)	-	-	-	-
phalanx length (M3)	-	-	30.22	37.22
mid-shaft breadth (M6)	-	8.57	7.61	8.55
proximal breadth (M8)	-	-	13.48	13.54
distal breadth (M9)	13.1	11.01	9.25	10.94
mid-shaft height (M7)	-	6.01	5.23	6.22
proximal height (M10)	-	-	9.18	10.21
distal height (M11)	8.68	6.83	5.82	6.88

Measurement definitions by Bräuer (1988)	S3 6.3 prox., L	S3 11.3 prox.	S3 19.4 prox.	S13.1 intermediate, L
metacarpal length (M2)	-	-	-	-
phalanx length (M3)	36.14	40.24	-	26.5
mid-shaft breadth (M6)	9.08	9.13	-	8.59
proximal breadth (M8)	15.96	14.95	15.28	12.06
distal breadth (M9)	11.75	11.73	-	9.98
mid-shaft height (M7)	6.25	6.43	-	4.74
proximal height (M10)	10.79	10.8	10.76	9.38
distal height (M11)	7.41	6.82	-	6.06

Measurement definitions by Bräuer (1988)	S3 12.5 intermediate, L	S3 12.6 intermediate, L	S3 12.7 distal, R	S3 14.1 distal
metacarpal length (M2)	-	-	-	-
phalanx length (M3)	24.17	26.45	17.28	16.56
mid-shaft breadth (M6)	7.3	8.45	5.18	4.12
proximal breadth (M8)	12.89	12.39	10.75	9.82
distal breadth (M9)	9.36	10.17	7.14	5.97
mid-shaft height (M7)	4.98	5.06	4.28	3.7
proximal height (M10)	8.86	8.89	6.24	6.41
distal height (M11)	5.5	5.29	3.36	3.6

Measurement definitions by Bräuer (1988)	S10a.1 distal	S16.1 distal	S3 6.1 MC 3 - L	S3 25.1 MC 1 - L
metacarpal length (M2)	-	-	63	41.76
phalanx length (M3)	17.81	17.09	-	-
mid-shaft breadth (M6)	5.44	4.74	7.79	11.43
proximal breadth (M8)	11.49	10.87	12.6	15.22
distal breadth (M9)	8.14	7.03	14.35	14.89
mid-shaft height (M7)	4.34	3.7	7.86	6.8
proximal height (M10)	6.9	6.78	15.51	14.65
distal height (M11)	3.82	3.48	12.9	12.66

Measurement definitions by Bräuer (1988)	S3 20.3 MC 2 - R	S3 8.14 MC 4 - L	S3 8.13 MC 2 - L
metacarpal length (M2)	-	-	-
phalanx length (M3)	-	-	-
mid-shaft breadth (M6)	8.01	6.83	7.33
proximal breadth (M8)	-	9.88	13.89
distal breadth (M9)	-	-	-
mid-shaft height (M7)	7.22	5.91	7.68
proximal height (M10)	-	12.14	13.17
distal height (M11)	-	-	-

SI-Table 23. Osteometry of Apidima 3 – Bräuer (1988) measurements of vertebrae. All measurements are in mm.

Measurement definitions by Bräuer (1988)	S3 7.3	S3 8.3	S3 8.15	S3 18.5	S3 8.9	S3 8.6
anterior height (M1)	11.1	11	12.78	-	17.86	14.42
posterior height (M2)	11.82	12.34	13.6	-	-	16
superior anteroposterior diameter (M4)	14.87	16.66	16.92	-	21.92	17.66
inferior anteroposterior diameter (M5)	14.76	17.64	17.3	-	22.72	18
superior transverse diameter (M7)	23.12	-	30.32	24.44	25.22	-
inferior transverse diameter (M8)	19.32	-	29.29	-	26.34	-
middle transverse diameter (M9)	-	-	-	-	23.9	-

Measurement definitions by Bräuer (1988)	S3 8.7	S3 8.8	S3 8.16	S3 12.1
anterior height (M1)	16.18	16.95	-	-
posterior height (M2)	-	-	-	-
superior anteroposterior diameter (M4)	18.46	-	-	-
inferior anteroposterior diameter (M5)	-	20.99	-	-
superior transverse diameter (M7)	-	-	-	-
inferior transverse diameter (M8)	-	-	-	-
middle transverse diameter (M9)	-	-	-	-

Additional Supplementary Figures

SI-Figure 19. Comparative osteometry of Apidima 3's humerus length measurements. Information and references about the comparative data used in this figure are provided in SI-Table 1.

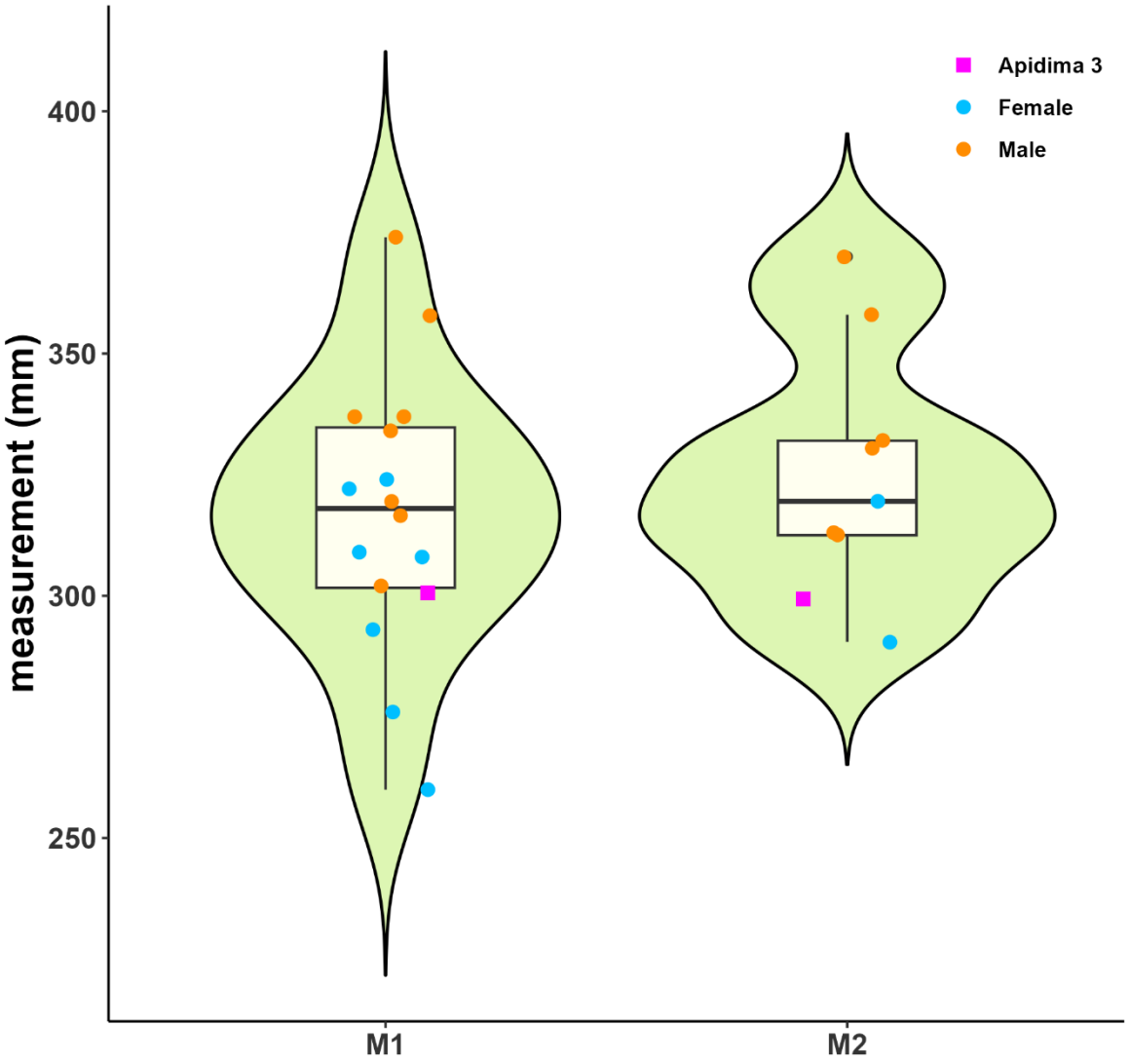

SI-Figure 20. Comparative osteometry of Apidima 3's humerus measurements. Information and references about the comparative data used in this figure are provided in SI-Table 1.

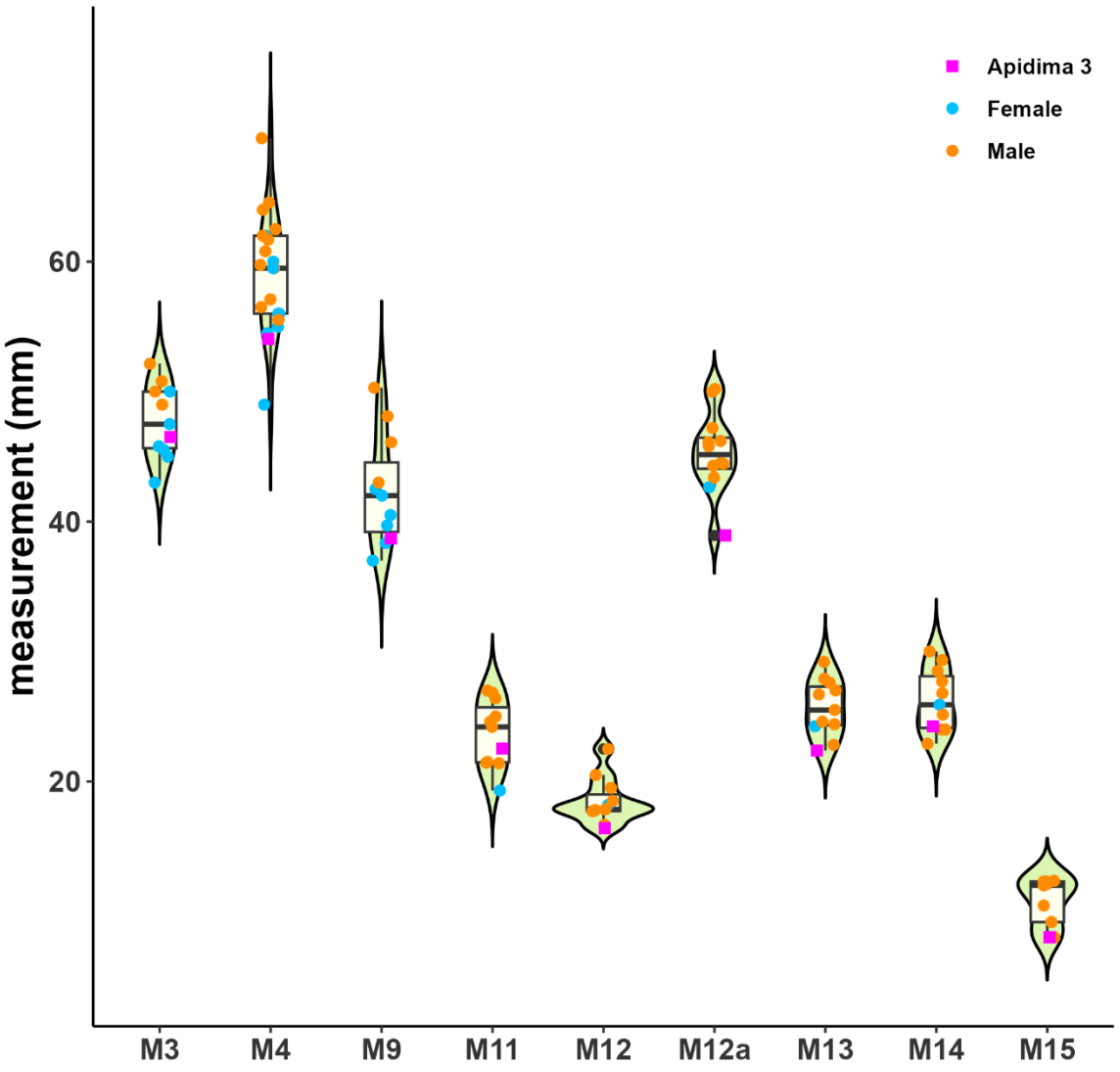

SI-Figure 21. Comparative osteometry of Apidima 3's radius length. Information and references about the comparative data used in this figure are provided in SI-Table 1.

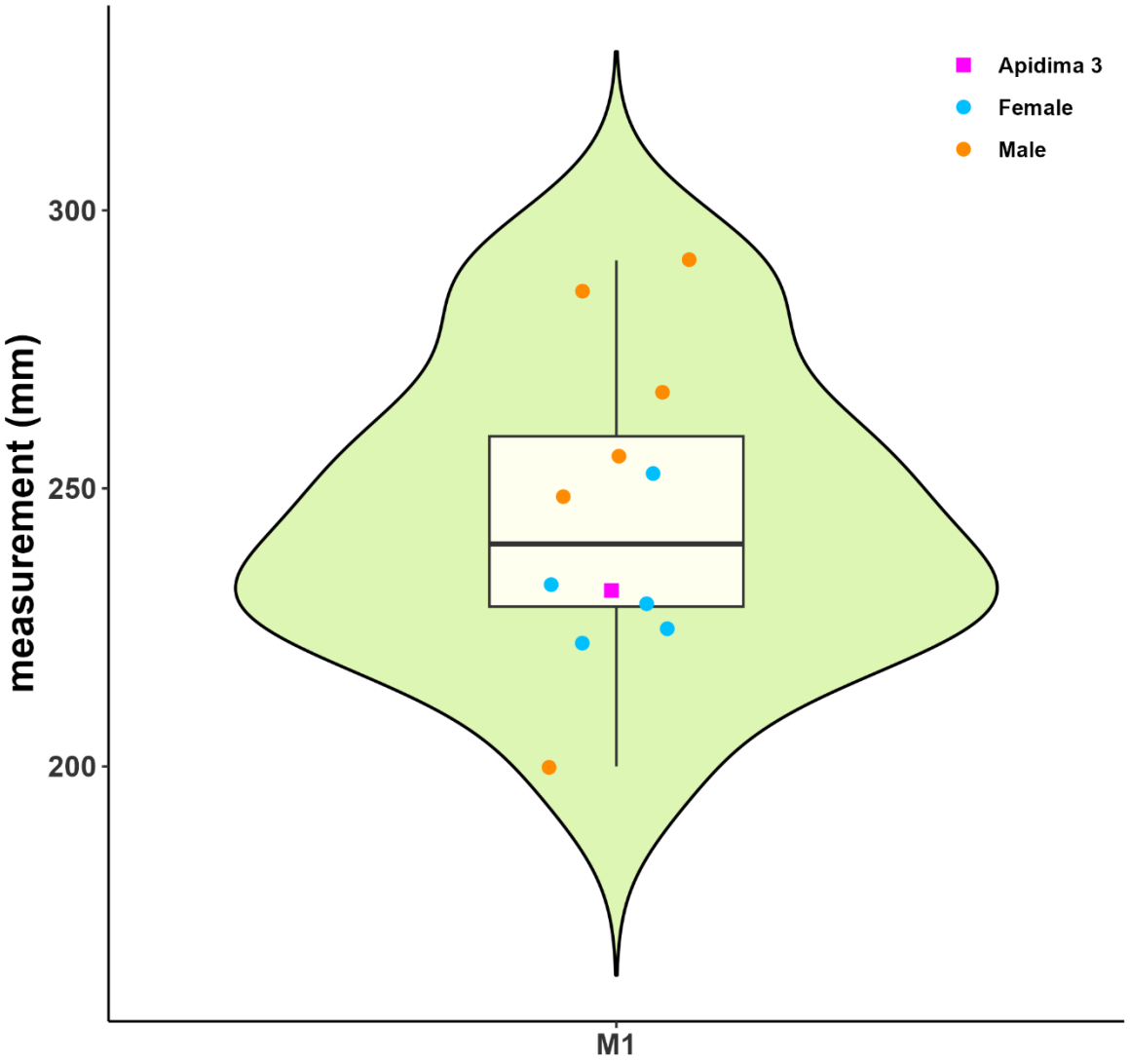

SI-Figure 22. Comparative osteometry of Apidima 3's radius measurements. Information and references about the comparative data used in this figure are provided in SI-Table 1.

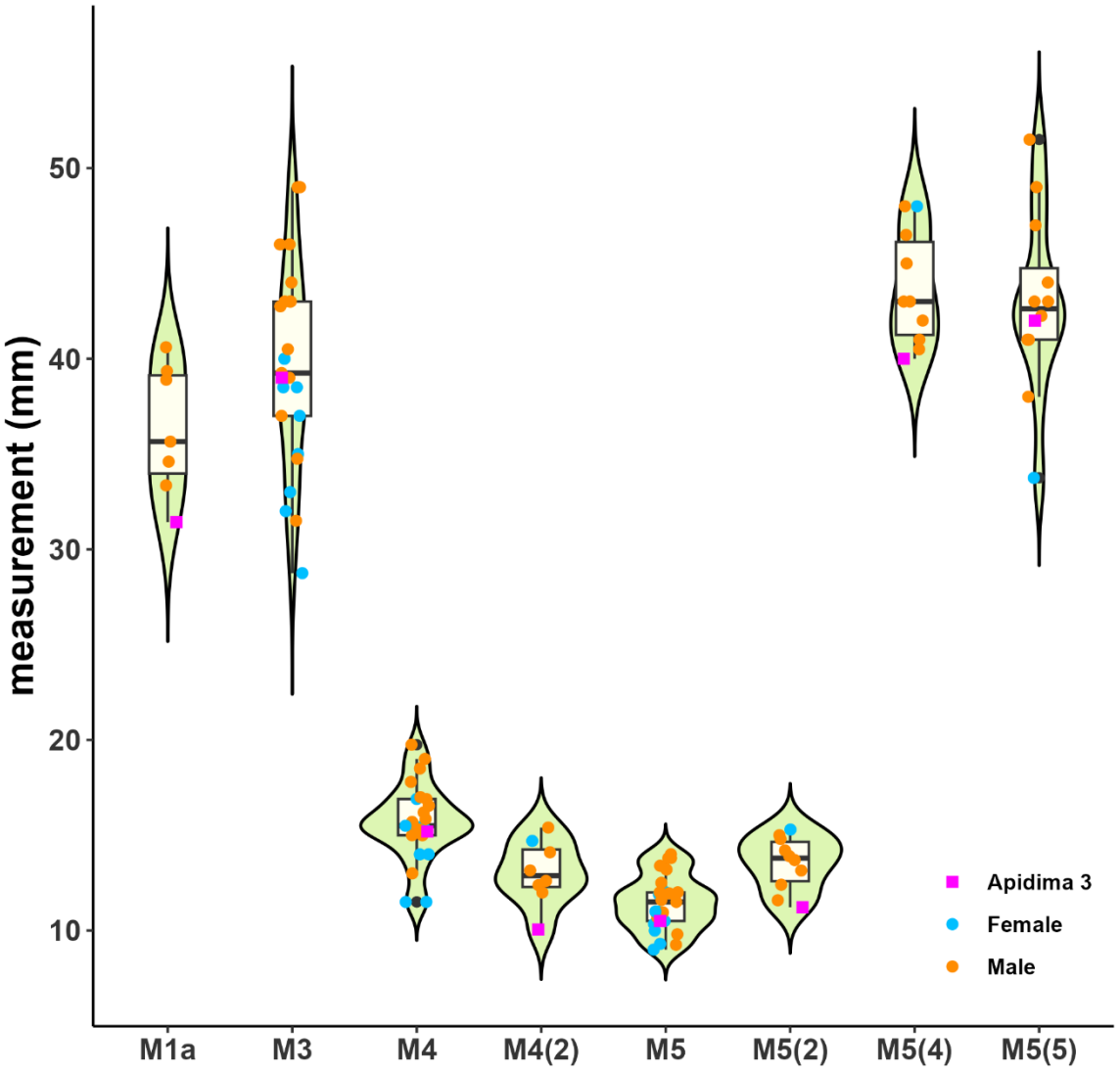

SI-Figure 23. Comparative osteometry of Apidima 3's ulna measurements. Information and references about the comparative data used in this figure are provided in SI-Table 1.

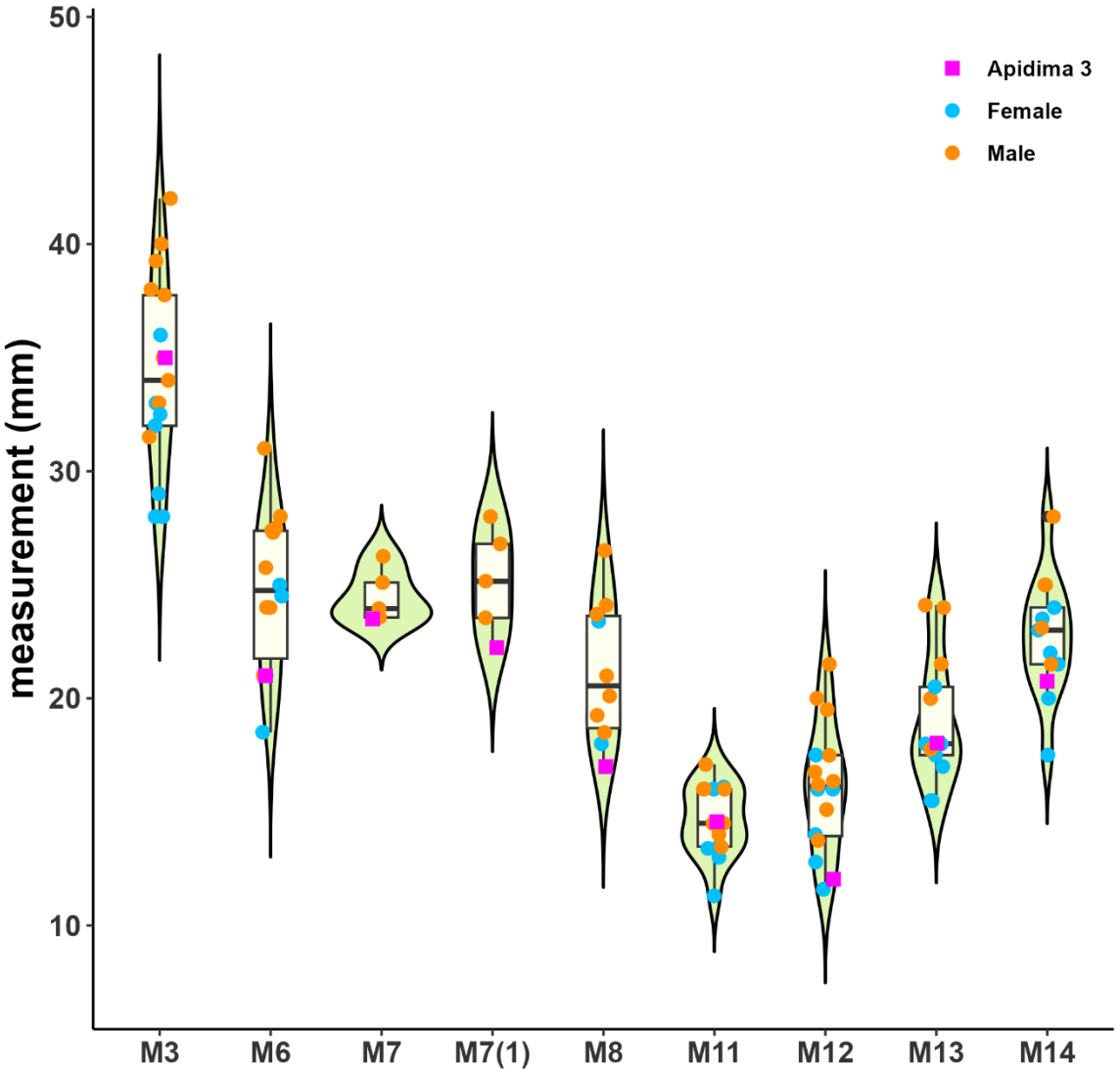

SI-Figure 24. Comparative osteometry of Apidima 3's femur measurements. Information and references about the comparative data used in this figure are provided in SI-Table 1.

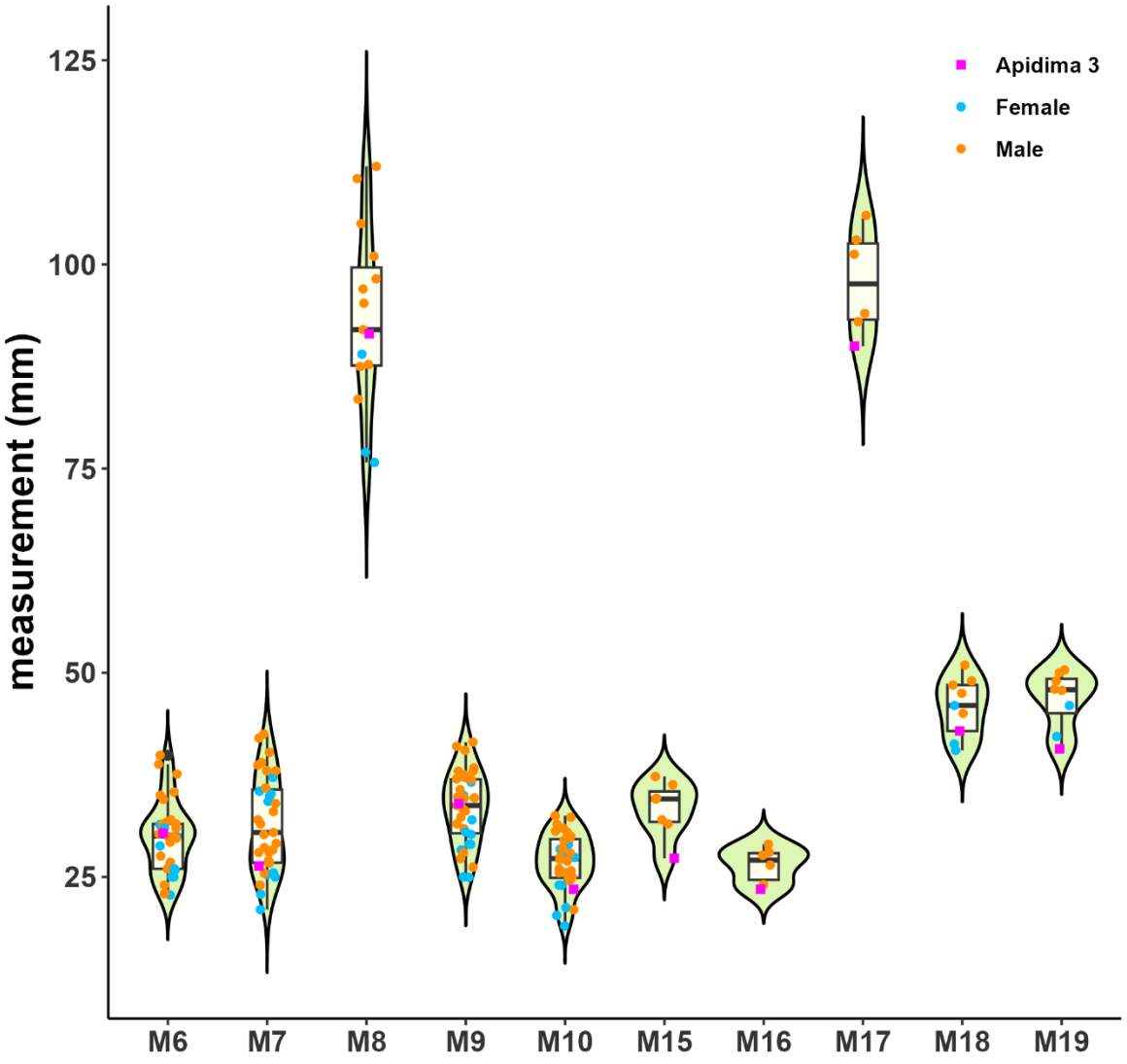

SI-Figure 25. Comparative osteometry of Apidima 3's tibia length measurements. Information and references about the comparative data used in this figure are provided in SI-Table 1.

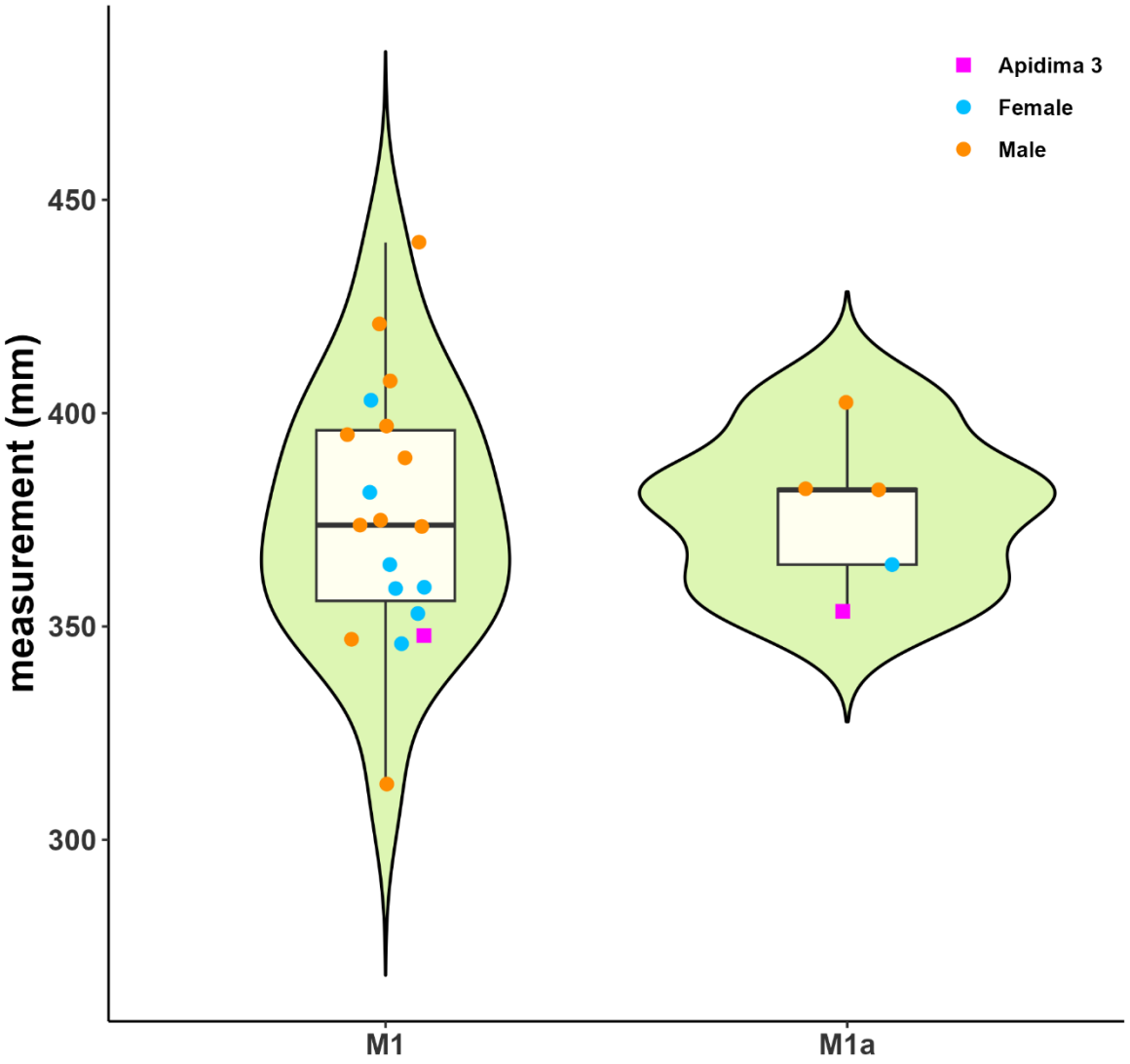

SI-Figure 26. Comparative osteometry of Apidima 3's tibia measurements. Information and references about the comparative data used in this figure are provided in SI-Table 1.

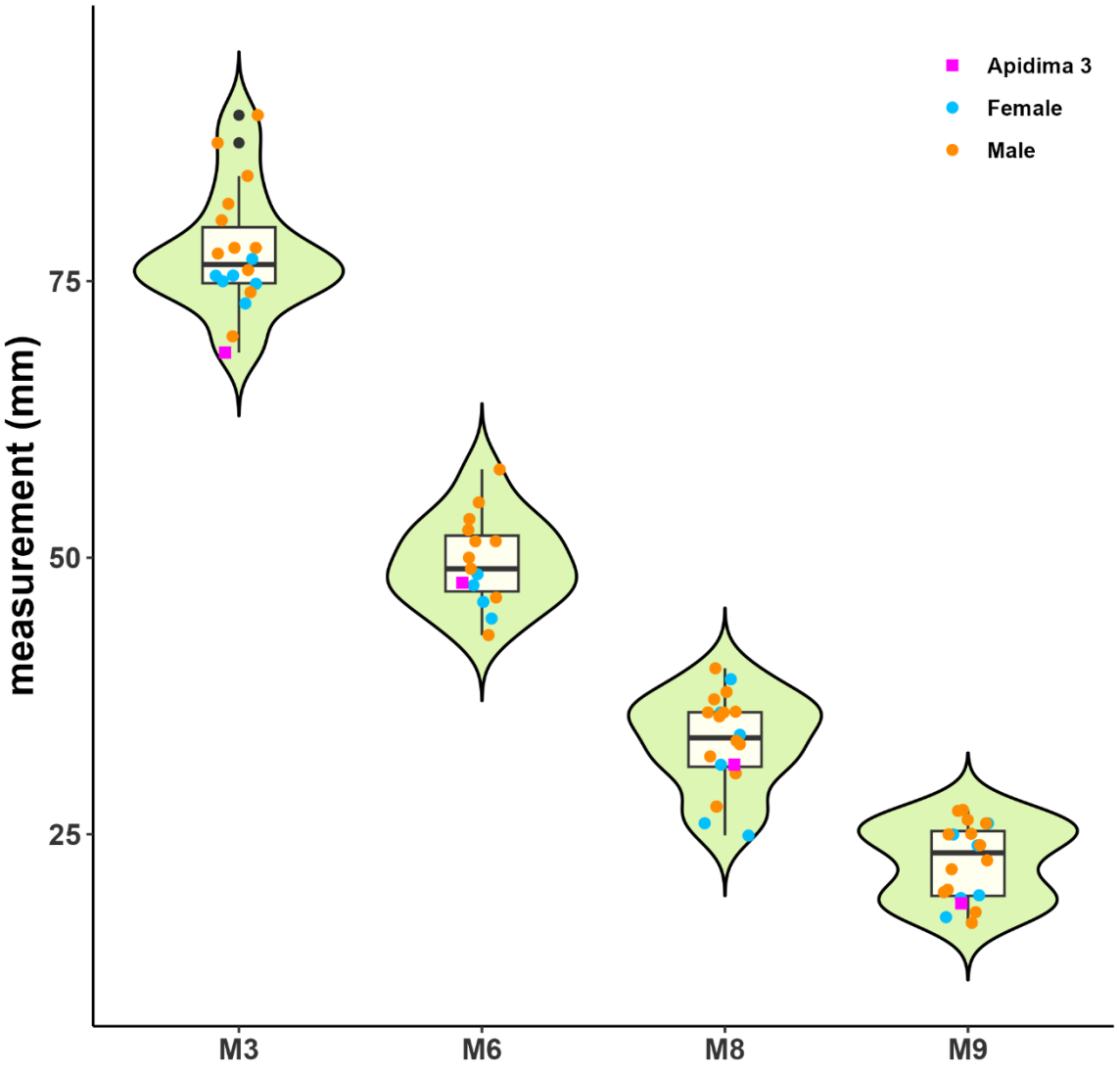

SI-Figure 27. Comparative osteometry of Apidima 3's fibula length measurements. Information and references about the comparative data used in this figure are provided in SI-Table 1.

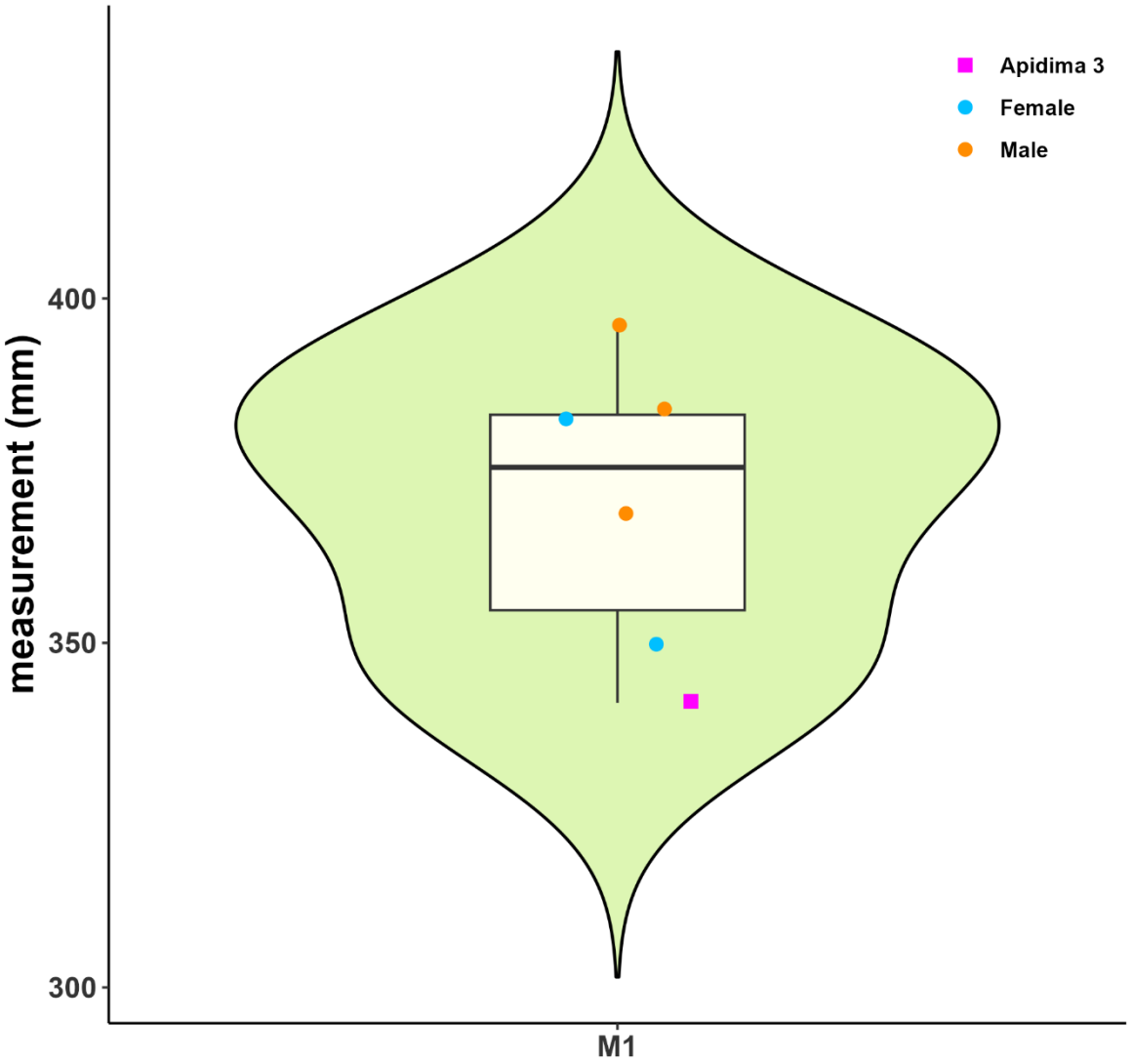

SI-Figure 28. Comparative osteometry of Apidima 3's fibula measurements. Information and references about the comparative data used in this figure are provided in SI-Table 1.

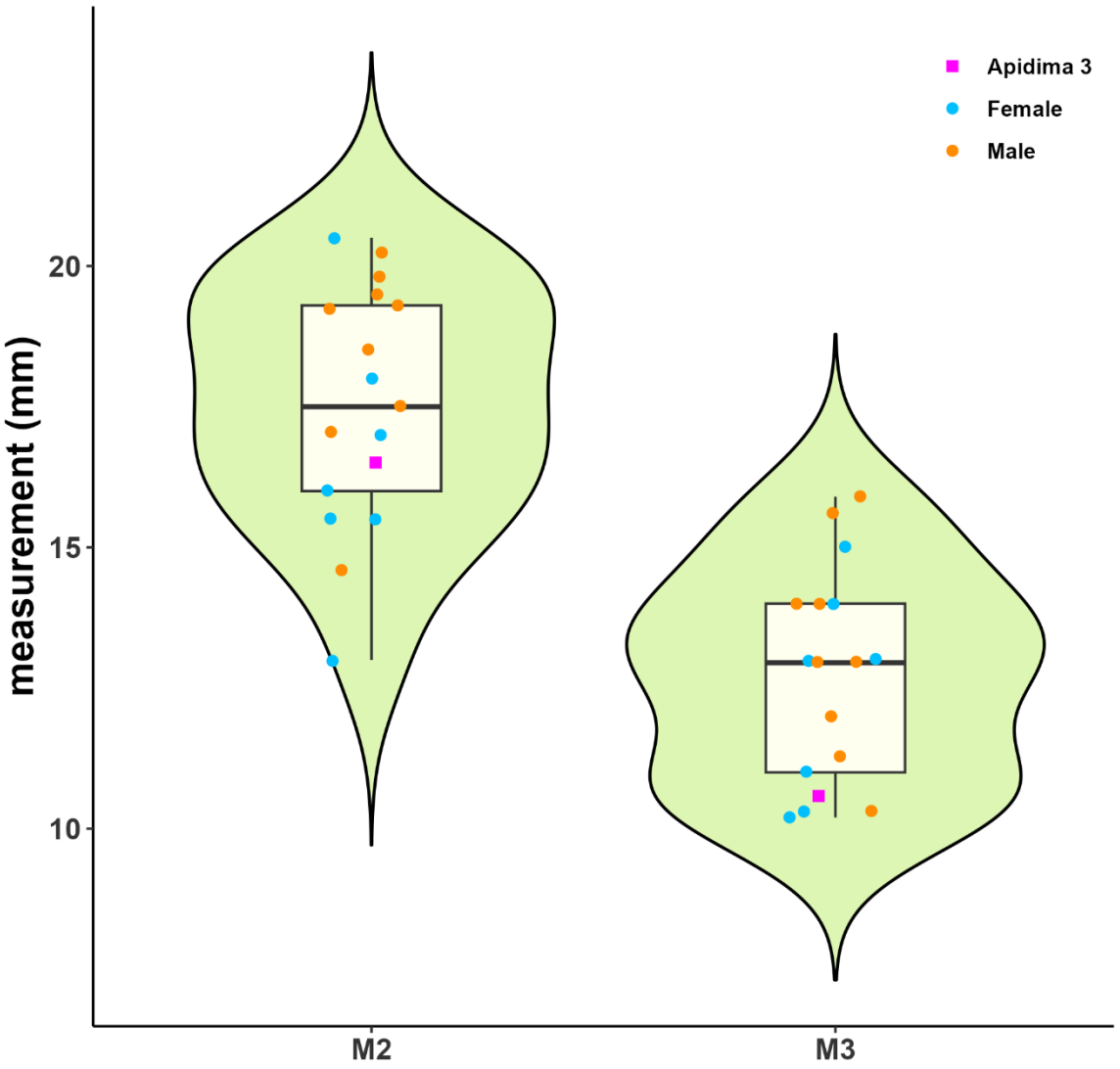

REFERENCES

Billy, G., 1975. Etude anthropologique des restes humains de l'Abri Pataud. In: Movius, Jr., H.L. (Ed.), Excavation of the Abri Pataud, Les Eyzies (Dordogne). American School of Prehistoric Research, Peabody Museum, Harvard University, Cambridge, MA, pp. 201–261.

Bräuer, G., 1988. Osteometrie. In: Knußmann, R. (Ed.), Wesen und Methoden der Anthropologie. 1. Teil Wissenschaftstheorie, Geschichte, morphologische Methoden. Gustav Fischer Verlag, Stuttgart, New York, pp. 160–231.

Carrero, J.M., Quam, R.M., Gomez-Olivencia, A., Castilla, M., Rodríguez, L., García-González, R., 2015. The Magdalenian human remains from El Miron Cave, Cantabria (Spain). J. Archaeol. Sci. 60, 10–27.

Churchill, S.E., Formicola, V., 1997. A case of marked bilateral asymmetry in the upper limbs of an Upper Paleolithic male from Barma Grande (Liguria), Italy. Int. J. Osteoarchaeol. 7, 18–38.

Dočkalová, M., Vančata, V., 2005. Gravettian Human Remains Brno II: Postcranial Skeleton. Anthropologie 43 (2/3), 295–304.

Fewlass, H., Talamo, S., Kromer, B., Bard, E., Tuna, T., Fagault, Y., Sponheimer, M., Ryder, C., Hublin, J.-J., Perri, A., Sázelova, S., Svoboda, J., 2019. Direct radiocarbon dates of mid Upper Palaeolithic human remains from Dolní Věstonice II and Pavlov I, Czech Republic. Journal of Archaeological Science: Reports 27, 102000.

Janković, I., Aherm, J. C. M., Karavanić, I., Stockton, T., Smith, F. H., 2012. Epigravetian Human Remains and Artifacts from Šandalja II, Istria, Croatia. PaleoAnthropology 2012, 87–122.

Mallegni, F., Fabbri, P. F., 1995. The human skeletal remains from the upper palaeolithic burials found in Romito cave (Papasidero, Cosenza, Italy). Bulletins et Mémoires de la Société d'anthropologie de Paris 7 (3-4), 99–137.

Mallegni, F., Bertoldi, F., Manolis, S., 2000. Palaeobiology of two Gravettian skeletons from Veneri cave (Parabita, Puglia, Italy). Homo 51(2–3), 235–257.

Mittnik, A., Wang, C.-C., Svoboda, J., Krause, J., 2016. A Molecular Approach to the Sexing of the Triple Burial at the Upper Paleolithic Site of Dolní Věstonice. PLoS ONE 11(10), e0163019. DOI:10.1371/journal.pone.0163019

Naumann, D., Harvati, K., 2026. A Reinvestigation of the Upper Paleolithic Postcranial Human Remains from the La Rochette Rock Shelter (Saint-Léon-sur-Vézère, France)- PaleoAnthropology 2026(1), 1–27.

Orschiedt, J., Kierdorf, U., Schultz, M., Baales, M., von Berg, A., Flohr, S., 2017. The Late Upper Palaeolithic human remains from Neuwied-Irlich, Germany. A rare find from the Late Glacial of Central Europe. Quartär 64, 203–216.

Schulting, R. J., Trinkaus, E., Higham, T., Hedges, R., Richards, M., Cardy, B., 2005. A Mid-Upper Palaeolithic human humerus from Eel Point, South Wales, UK. J. Hum. Evol. 48, 493-505.

Sládek, V., Trinkaus, E., Hillson, S. W., Holliday, T. W., 2000. The Dolní Věstonice Studies, Vol. 5: The People of the Pavlovian. Skeletal Catalogue and Osteometrics of the Gravettian Fossil Hominids from Dolní Věstonice and Pavlov. Archaeological Institute of the Czech Academy of Sciences, Brno.

Trinkaus, E., Jelinek, J., 1997. Human remains from the Moravian Gravettian: the Dolní Věstonice 3 postcrania. J. Hum. Evol. 33, 33–82.

Trinkaus, E., Holliday, T.W., 2000. The human remains from Paviland Cave. In: Aldhouse-Green, S. (Ed.), Paviland Cave and the "Red Lady": A Definitive Report. Western Academic & Specialist Press Limited, Bristol, pp. 141–204.

Trinkaus, E., Ruff, C.B., 2012. Femoral and tibial diaphyseal cross-sectional geometry in Pleistocene Homo. PaleoAnthropology 2012, 13–62.

Trinkaus, E., Sparacello, V.S., Xing, S., Thibeault, A., Villotte, S., 2022. Describing Cro-Magnon: the femora, tibiae and fibulae. J. Archaeol. Sci. Rep. 42, 103418.

Vercellotti, G., Alciati, G., Richards, M.P., Formicola, V.,2008. The Late Upper Paleolithic skeleton Villabruna 1 (Italy): a source of data on biology and behavior of a 14.000 year-old hunter. J. Anthropol. Sci. 86, 143–163.

Villotte, S., Samsel, M., Zamolli, C., 2017. The paleobiology of two adult skeletons from Baousso da Torre (Bausu da Ture) (Liguria, Italy): implications for Gravettian lifestyle. C. R. Palevol. 16(4), 462–473. DOI: 10.1016/j.crpv.2016.09.004

Villotte, S., Thibeault, A., Sparacello, V., Trinkaus, E., 2020. Disentangling Cro-Magnon: the adult upper limb skeleton. J. Archaeol. Sci. Rep. 33, 102475.